INSTITUTO
UNIVERSITÁRIO
DE LISBOA

Study and implementation of a low complexity receiver using TCH Codes

João André Calado de Oliveira

Master Degree in,
Telecommunications and Computer Engineering

Supervisor:
PhD Francisco António Bucho Cercas, Full Professor,
ISCTE-IUL

Co-Supervisor:
PhD Tiago Manuel Ferreira Alves, Assistant Professor,
ISCTE-IUL

October, 2021

TECNOLOGIAS
E ARQUITETURA

Department of Information Science and Technology

Study and implementation of a low complexity receiver using TCH Codes

João André Calado de Oliveira

Master Degree in,
Telecommunications and Computer Engineering

Supervisor:
PhD Francisco António Bucho Cercas, Full Professor,
ISCTE-IUL

Co-Supervisor:
PhD Tiago Manuel Ferreira Alves, Assistant Professor,
ISCTE-IUL

October, 2021

Acknowledgements

I would like to express my gratitude towards my supervisors, Professor Francisco Cercas and Professor Tiago Alves for all the orientation that they provided and all the patience they had with me throughout this work. I can't thank them enough for not giving up on me despite all the hardships and mistakes that I made and for always be willing to provide me with support whenever I needed the most.

Secondly, I would like to thank my family, especially, my father, my mother, and my grandmother for all their support. They always believed in my capabilities, even during the hardest moments, and that means a lot to me.

Lastly, I want to thank my friends. Throughout the years they inspired me to challenge myself and to aim for higher goals. They always believed in me, even when I didn't, and kept me motivated to face my problems head on and to strive to become a better person. I owe them a lot and if not for them I wouldn't be here.

To each person that I mentioned here I would like to say, from the bottom of my heart: "Thank you".

Resumo

O uso de codificação em sistemas de telecomunicações revela-se uma técnica com um contributo essencial na melhoria da recuperação de sinais transmitidos. Dependendo das circunstâncias às quais um sinal é submetido aquando a sua transmissão, com recurso à codificação, é possível atenuar os efeitos adversos resultantes deste processo, obtendo uma qualidade no sinal recebido superior face a um cenário com ausência da mesma.

Este estudo tem como objetivo testar a exequibilidade de um sistema de comunicações sem fios para alto débito usando códigos TCH e aplicando-os a um sinal OFDM, sujeito a componentes de ruído introduzidos por um canal sem fios AWGN, considerando um modelo de propagação em espaço livre. Devido às propriedades de correlação destes códigos, a sua utilização revela-se adequada pois permite que as mesmas palavras de código sejam utilizadas para efetuar correção de erros, minimizando os efeitos do canal, possibilitando o desenvolvimento de um recetor com menor complexidade.

Visando efetuar uma análise qualitativa do sistema, é realizada uma simulação simples em MATLAB onde é gerado um sinal OFDM ao qual são aplicados diversos códigos TCH, realizando estimação de canal com a finalidade de obter o BER para os diferentes comprimentos dos códigos e, consequentemente, ganhos de codificação relativos aos mesmos.

Os resultados obtidos foram realizados para os índices de modulação 16, 64 e 256-QAM. Estes demonstram que o uso destes códigos é uma opção viável para reduzir os erros detetados, permitindo recuperar o sinal com maior fiabilidade, especialmente para comprimentos de código e índices de modulação elevados.

Palavras-Chave: códigos TCH; OFDM; AWGN; estimação de canal; BER; QAM.

Abstract

The use of coding in telecommunications systems reveals to be a technique with an essential contribution to the improvement of the recovery of transmitted signals. Depending on the circumstances to which a signal is subjected at transmission, by recurring to coding, it is possible to attenuate the unfavorable effects that result from this process, obtaining a signal with superior quality in comparison with a scenario where the presence of coding is absent.

This study aims to test the feasibility of a high-rate wireless communications system using TCH codes being applied to an OFDM signal, subjected to noise components introduced by a wireless AWGN channel, considering a free path propagation model. Due to their correlation properties, the use of TCH codes reveals to be adequate since they allow the same codewords to be used to realize both error correction and channel estimation, mitigating the channels effects, leading to the realization of a receiver with lower complexity.

With the intent of performing a qualitative analysis to this system, a simple simulation is executed in MATLAB where an OFDM signal is generated, being therefore applied various TCH codes and, through channel estimation, obtain the BER for their respective code lengths and, consequently, coding gains.

The results were obtained for the modulation indexes of 16, 64 and 256-QAM. These demonstrate that the implementation of TCH codes is a viable option to reduce the rate of recovered errors, enabling the reception of a signal with better reliability, especially for higher code lengths and modulation indexes.

Keywords: TCH codes; OFDM; AWGN; channel estimation; BER; QAM.

Contents

Acknowledgements 2
Resumo iii
Abstract v
List of Tables ix
List of Figures xi
List of Acronyms xiii
List of Symbols xv
CHAPTER 1 1
Introduction 1
1.1. Motivation 1
1.2. Context 1
1.3. Investigation Questions 2
1.4. Objectives 2
1.5. Investigation Method 2
CHAPTER 2 5
State of the Art/Literature Review 5
2.1. Modern Wireless Communication Networks 5
2.2. TCH Codes 6
2.2.1. Generation of TCH Sequences and Main Properties 6
2.2.2. Coding Gain 12
2.2.3. Conclusion 18
2.3. Orthogonal Frequency Division Multiplexing 19
2.3.1. Mathematical Arrangement for an OFDM Signal 19
2.3.2. Implementation of the Discrete Fourier Transform in OFDM 20
2.3.3. Cyclic Prefix 22
2.3.4. Conclusions 25
2.4. AWGN Channel and Channel Estimation 26
CHAPTER 3 29
Methodology 29
3.1. Transmitter 29
3.1.1. TCH Coding 30
3.1.2. OFDM Modulation 31
3.1.2.1. QAM Mapping and Sampling 32

3.1.2.2. OFDM Modulation Steps 34
3.2. Wireless Channel 39
3.3. Receiver 41
3.3.1. OFDM Demodulation 41
3.3.1.1. OFDM Demodulation Steps 42
3.3.1.2. Channel Estimation 45
3.3.1.3. TCH Decoding 48
3.4. BER Estimation 50
CHAPTER 4 53
Analysis and Discussion of the Results 53
4.1. Simulation Parameters 53
4.2. Coding Results 54
4.3. Modulation Results 57
4.4. Coding and Modulation Results 58
CHAPTER 5 63
Conclusions 63
5.1. Main conclusions 63
5.2. Limitations of the study 64
5.3. Proposals for future investigation 64
Bibliography 67
Appendix A 69

List of Tables

Table 2.1 - Fermat numbers for generating TCH Codes. 8

Table 3.1 - TCH codes for various lengths and subsequent designation. 30
Table 3.2 – Pilot subcarriers (yellow) distribution in each OFDM symbol throughout the totality of the information subcarriers (blue). 46

Table 4.1 - Simulation Parameters. 53
Table 4.2 - EbN0 values obtained for various nTCH code lengths with BPSK modulation. 56
Table 4.3 - EbN0 values obtained for various modulation indexes. 58
Table 4.4 - Simulated coding gains for each TCH code length for 16-QAM. 60
Table 4.5 - Simulated coding gains for each TCH code length for 64-QAM. 61
Table 4.6 - Simulated coding gains for each TCH code length for 256-QAM. 62

List of Figures

Figure 2.1 - Autocorrelation of B-TCH Polynomial of length nTCH=16. Source: [3, p. 69]. 9
Figure 2.2 - Autocorrelation of B-TCH Polynomial of length nTCH=256. Source:[3, p. 71]. 9
Figure 2.3 - TCH receiver simple implementation. Source: [3, p. 198].....11
Figure 2.4 - Simple TCH decoder of maximum likelihood. Source: [3, p. 204]. 11
Figure 2.5 - BER of TCH codes length 16. Source: [3, p. 173]. 13
Figure 2.6 - Coding gain of TCH codes length 16. Source: [3, p. 174]. 13
Figure 2.7 - BER of TCH codes length 32. Source: [3, p. 174]. 14
Figure 2.8 - Coding gain of TCH codes length 32. Source: [3, p. 175]. 14
Figure 2.9 - BER of TCH codes length 64. Source: [3, p. 175]. 15
Figure 2.10 - Coding gain of TCH codes length 64. Source: [3, p. 176]. 15
Figure 2.11 - BER of TCH codes length 128. Source: [3, p. 176]. 16
Figure 2.12 - Coding gain of TCH codes length 128. Source: [3, p. 177]. 16
Figure 2.13 - BER of TCH codes length 256 and 512. Source: [3, p. 177]. 17
Figure 2.14 - Coding gain of TCH codes length 256 and 512. Source: [3, p. 178]. 17
Figure 2.15 - Generic multicarrier modulation diagram. Source: [5, p. 33]. 18
Figure 2.16 - OFDM transmitter (A) and Receiver (B) diagrams. Source: [5, p. 35].....21
Figure 2.17 - OFDM signal without cyclic prefix at the transmitter (A) and the receiver (B). Source: [5, p. 37]. 22
Figure 2.18 - OFDM signal with cyclic prefix at the transmitter (C) and the receiver (D). Source: [5, p.37]. 22
Figure 2.19 - Time domain representation of an OFDM symbol. Source: [5, p. 38]. ….23
Figure 2.20 - BER variance in function of EbN0 for the QAM modulation indexes M=4, 16, 64, 256 and 1024. Source: [19, p.320]. ..……..25
Figure 2.21 - Frame structure of an OFDM signal using PSAM. Source: [24]. ……...26

Figure 3.1 - Constellations for 16 and 64-QAM utilizing Gray mapping. 33
Figure 3.2 - Power spectral density of the signal after going through the modulation steps. 35
Figure 3.3 - Power spectral density of the signal after filtering with filter bandwidth B.37
Figure 3.4 - Power spectral density of the signal after up-conversion. 38
Figure 3.5 - AWGN power spectral density. 40
Figure 3.6 - Power spectral density of the signal after passing through the wireless channel. 41
Figure 3.7 - Power spectral density of the down converted signal. 43
Figure 3.8 - Demodulated constellations for 4-QAM and 16-QAM before equalization.44
Figure 3.9 – Amplitude and phase responses of the channel. 47
Figure 3.10 – Interpolated amplitude and phase responses of the inverse of the channel.47
Figure 3.11 - Recovered demodulated constellations for 4-QAM and 16-QAM after equalization. 48
Figure 3.12 – Output of the FFT correlator for a TCH code length 64. 49
Figure 3.13 - Output of the FFT correlator for a TCH code length 256. 49

Figure 4.1 - BER results obtained from the coding process for various TCH codes. 55
Figure 4.2 - Coding gains obtained from the coding process for various TCH codes. ...55
Figure 4.3 - BER results in function of EbN0 for the QAM modulation indexes M=4, 16, 64 and 256. 57
Figure 4.4 - BER results in function of EbN0 for 16-QAM with TCH codes. 59
Figure 4.5 - Coding gain results in function of EbN0 for 16-QAM with TCH codes. ..59
Figure 4.6 - BER results in function of EbN0 for 64-QAM with TCH codes. 60
Figure 4.7 - Coding gain results in function of EbN0 for 64-QAM with TCH codes. ..60
Figure 4.8 - BER results in function of EbN0 for 256-QAM with TCH codes. 61
Figure 4.9 - Coding gain results in function of EbN0 for 256-QAM with TCH codes. 61

List of Acronyms

5G – Fifth Generation

ADC – Analog-to-Digital Converter

AWGN – Additive White Gaussian Noise

B-TCH – Base TCH

BER – Bit Error Rate

BPSK – Binary Phase-Shift Keying

CW – Constant Weight

DAC – Digital-to-Analog Converter

DEC – Direct Error Counting

DFT – Discrete Fourier Transform

DSP – Digital Signal Processing

FFT – Fast Fourier Transform

GF – Galois Field

ICI – Intercarrier Interference

IDFT – Inverse Discrete Fourier Transform

IFFT – Inverse Fast Fourier Transform

IoT – Internet of Things

IQ – In-phase/Quadrature

ISI – Inter-symbol Interference

LPE – Low Pass Equivalent

LPF – Low Pass Filter

MCM – Multicarrier Modulation

MIMO – Multiple Input Multiple Output

MMSE – Minimum Mean-Square Error

NGMN – Next Generation Mobile Networks

NCW – Non-Constant Weight

OFDM – Orthogonal Frequency Division Multiplexing

PAPR – Peak-to-Average Power Ratio

PSAM – Pilot Symbol Aided Modulation

PSD – Power Spectral Density

QAM – Quadrature Amplitude Modulation

RF – Radiofrequency

SNR – Signal-to-Noise Ratio

TCH – Tomlinson, Cercas and Hughes

WRAN – Wireless Regional Area Network

ZF – Zero Forcing

List of Symbols

$\prod(t)$	Pulse shaping function
α	Primitive root of a Galois Field
Δ_G	Guard interval
ΔN_F	Frequency domain spacing
ΔN_T	Time domain spacing
δ_{ki}	Orthogonal signal set
λ	Signal wavelength
a_i	Coefficients used for the generation of TCH codes
B	Maximum bandwidth of the signal
B_{en}	Equivalent noise bandwidth
B_{LPF}	Low pass filter bandwidth
BER_{teo}	Theoretical BER
$bits_{symbol}$	Number of bits within one QAM symbol
c	Speed of light in vacuum
C_{ch}	Channel capacity
C_g	Coding gain
c_{ki}	i^{th} information symbol at the k^{th} subcarrier
d	Distance between antennas
D	Data symbols
d_{min}	Code minimum distance
D_r	Receiving antenna directivity
D_t	Transmitting antenna directivity
E_b	Energy per information bit

f	Frequency domain/axis
$\mathfrak{F}$	Fourier transform
F_i	Fermat numbers used for the generation of TCH codes
f_k	Subcarrier frequency
$f_{model}(d)$	Function of the distance between antennas
f_p	Central frequency
f_{p_up}	Accommodated frequency used in up-conversion
f_s	Nyquist frequency
h	Number of polynomials in a TCH code
$H(f)$	Channel impulse response
$H_{amplitude}(f)$	Amplitude response of the equalized channel
H_d	Hamming distance between two polynomials
$H_{ch}(f)$	Channel transfer function
$H_{interp}(f)$	Interpolation of the amplitude and phase responses of the equalized channel
$H_{phase}(f)$	Phase response of the equalized channel
H_{rect}	Filter transfer function
$H_{ZF}(f)$	Inverse of the channel transfer function
k_{TCH}	Number of data bits
K_i	Exponent
M	Modulation index
$n_{AWGN}(t)$	Noise component added to the signal in time domain
N_b	Number of OFDM symbols/blocks
N_{bits}	Number of bits

$N_{bitstream}$	Length of the randomly generated binary bitstream
n_{code}	Code length
N_{coding}	Total number of output chips
N_{CP}	Number of chips in the cyclic prefix
N_{CW}	Total number of codewords
N_{err}	Number of erred bits recovered
N_0	Unilateral noise power spectral density
N_{OFDM}	Number of subcarriers in an OFDM symbol
N_p	Number of periods
N_s	Number of samples per tone
N_{s_OFDM}	Number of samples in an OFDM symbol
N_{s_total}	Number of samples in an OFDM signal
N_{sc}	Number of subcarriers in an OFDM symbol
N_T	Total number of subcarriers in an OFDM signal
n_{TCH}	Length of a TCH code
N_{tx}	Number of transmitted bits
p	Prime number
P	Pilot symbols
$P_i(x)$	Base polynomials
p_{noise}	Mean noise power
P_r	Received signal power
p_{signal}	Mean power of the baseband signal
P_t	Transmitted signal power
$plt_{interval}$	Interval that defines the pilot subcarriers

q	Galois Field element
R_b	Information bit rate
R_c	Code rate
R_s	Symbol rate
$r(t)$	Received signal in time domain
r_m	Received sampled signal
$rand_{coeff}$	Vector of random coefficients
$s(t)$	MCM transmitted signal
$S_{AWGN}(t)$	Transmitted signal affected by AWGN in time domain
$S_d(t)$	Received signal in time domain
S_{dem}	Demodulated QAM symbols
S_{dem_pilots}	Pilots recovered after demodulation
S_{final}	Estimated QAM symbols
S_g	Code speed gain
$S_{I\_down}(t)$	Real component of the down-converted signal in time domain
$S_{I\_down\_filt}(t)$	Real component of the filtered down-converted signal in time domain
$S_{I\_up}(t)$	Real component of the upconverted signal in time domain
s_k	k^{th} subcarrier waveform
S_{pilots}	Pilot subcarriers
$S_{Q\_down}(t)$	Imaginary component of the down-converted signal in time domain
$S_{Q\_down\_filt}(t)$	Imaginary component of the filtered down-converted signal in time domain
$S_{Q\_up}(t)$	Imaginary component of the upconverted signal in time domain
$S_{rx}(t)$	Received down-converted signal

$S_{tx}(t)$	Transmitted Signal in time domain
snr	Signal-to-Noise ratio
t	Time domain/axis
T_c	Chip time
t_{cap}	Correcting capacity
t_d	Delay spread of a dispersive channel
T_0	Bit duration/Information block length
T_P	Duration of the cyclic prefix
t_s	DFT window observation period
T_s	OFDM symbol period
T_{samp}	Sampling time/period
x_{DAC}	Signal in time domain
$x_{LPE}(t)$	Low pass equivalent of the signal
$x_{LPF}(t)$	Filtered signal in time domain

CHAPTER 1

Introduction

This chapter presents an initial explanation of the work realized in this dissertation, with the purpose of introducing its motivation and context, as well as some investigation questions that are uplifted by its development. The objectives and investigation methods are also presented.

1.1. Motivation

The focus of this work is to implement the simulation of the transmission of a signal, including an explanation of all the respective modules and procedures. The coding process makes use of Tomlinson, Cercas and Hughes (TCH) codes while Orthogonal Frequency Division Multiplexing (OFDM) is the modulation format. The channel is modelled as an Additive White Gaussian Noise (AWGN) channel.

The focus of this work is to take advantage of these codes by applying them to an OFDM signal, determining the system performance and whether it is a viable solution for broadband applications and Internet of Things (IoT) environments and comprehend what are the limitations of the simulation.

1.2. Context

In the rapidly evolving environment that is IoT and modern digital cellular networks, it is imperative that studies revolving those areas achieve satisfactory results and the demand for improvements in these are ever so welcome. These studies serve as a foothold for the generations to come, resulting in the development of better equipment and infrastructures that allow progress towards enhanced technologies that provide better services for society.

This dissertation intends to comprehend the effectiveness of the usage of TCH codes in tandem with OFDM technologies to study their feasibility in obtaining viable telecommunications systems taking into consideration IoT based environments, all the while analyzing the issues that arise during the simulation of said systems and study effective solutions to mitigate them.

1.3. Investigation Questions

This work seeks to explain certain questions such as:

- Are TCH codes appropriate for broadband and IoT applications?
- Do TCH codes prove to be beneficial when applied to OFDM signals?
- Is the simplification of the receiver with TCH codes viable for future mobile networks?

1.4. Objectives

The main objective of this work is to simulate a communications system applying TCH codes with different sizes to OFDM signals, considering an AWGN channel implementation to study the advantages of the receiver and its limitations and possible applications.

The work is focused on: coded radio communication systems; conception and simulation of an optimized TCH receiver through channel estimation and determination of the receiver performance according to the different tested sequences.

1.5. Investigation Method

This work is to be analyzed through computer simulation, making use of Monte Carlo simulation to obtain the Bit Error Rate (BER) for the different TCH codes sequences, implemented in MATLAB.

This dissertation presents: a literature review of the state of art; analysis of the associated requirements to develop the intended system; the method to implement such system to proceed with its channel estimation; performing various simulations and collecting its data to evaluate the practicability of the system.

This work is divided into five chapters.

The first chapter serves as an introduction to the covered theme and to present the objectives and the dissertation layout.

The second chapter presents the literature review to understand the fundamental theory behind the presented work.

The third chapter is dedicated to the methodology used during the research and simulation steps.

The fourth chapter pretends to present and analyze the results obtained from the various simulations realized.

Finally, the fifth chapter reveals the main conclusions, observations and limitations of the present work and provides suggestions for future work.

CHAPTER 2

State of the Art/Literature Review

This chapter presents a literature review of the concepts that are used in this work. This is needed to understand the basis of the topics that serve as the foundation to this dissertation, as well as a starting point to give some insight to these concepts.

2.1. Modern Wireless Communication Networks

Modern wireless communication systems, such as Fifth Generation (5G), were developed in order to cope with several challenges imposed by a wide range of aspects, such as: "(…) services (mobile broadband, massive machine and mission critical communications, broad-/multicast services and vehicular communications); device classes (low-end sensors to high-end tablets); deployment types (macro and small cells); environments (low-density to ultra-dense urban); mobility levels (static to high-speed transport)." [1, p. 3323] proposing some improvements in capacity/user-rates, latency, reliability, coverage, mobility, massive number of devices and cost/energy consumption [1].

These aspects mentioned above are further developed in Next Generation Mobile Networks (NGMN) and their use and application can be categorized into the following scenarios: Bitpipe communications; IoT Tactile Internet; Wireless Regional Area Network (WRAN) [1].

This dissertation focuses mainly on the IoT scenario that features "(…) small data packets, massive connections of devices with limited power source, and delay tolerant communication." [1, p. 3323]. Since these packets are transmitted using burst techniques, IoT devices do not require large channel bandwidths, in addition, narrow band system designs can improve coverage, power consumption, and reduce terminal costs [1]. With that in mind, a great number of subcarriers are considered in this study, aiming to uphold broadband applications common to this technology.

In short, modern wireless communication networks fulfill several pre-requisites, such as higher data rates, lower latency and massive connectivity that address various problems related to radiofrequency (RF) spectrum exhaustion. This leads to the development of new techniques such as massive multiple input multiple output (MIMO) systems in order

to improve spectral efficiency at the link and network layers and to better utilize the unregulated bandwidth [2].

2.2. TCH Codes

The codes being employed in this work were created by M. Tomlinson, F. Cercas and C. Hughes, hence their designation TCH.

TCH codes provide a performance like other existing codes, however they have lesser complexity on the receiver. Due to their correlation properties and good coding gain, the same code words can be used to simultaneously correct errors in the channel, perform its estimation and to warrant synchronism. These codes seek to improve performance through a simplified structure to aid the development of robust applications with low latency in various domains, such as IoT and modern networks.

Some of these characteristics these codes are appropriateness for communications, mainly when those are performed in environments with unfavorable conditions, such as Doppler effects and reflections; nonlinear, non-systematic cyclic properties; use of transform techniques like Fast Fourier Transform (FFT); solid sizes, correcting and correlation performance [3].

2.2.1. Generation of TCH Sequences and Main Properties

TCH codes are a class of cyclic block codes with length n_{TCH}, where $n_{TCH}=2^m$, with $m \in \mathbb{N}$, that were found based on finite field theory. These codes have the advantage of being easy to implement on the receiver and can be used in various applications, being particularly useful in adverse environments, such as fading, Doppler effects and reflections [3].

The TCH decoder implements maximum likelihood decoding with banks of correlators that use transform techniques like FFT, which increases its efficiency. These codes are also nonlinear, since the linear addition modulo 2 of two codewords does not necessarily creates a valid codeword, and each of these is a block code undergoing continuous cyclic shifts, excluding the all-zero codeword [3].

Considering AWGN channels, the BER of TCH codes can be determined using the Union Bound approach.

According to [3], these codes are defined by Base Polynomials $P_i(x)$, with input blocks with a given number of data bits, k_{TCH}, and a correcting capacity, t_{cap}, further described as:

$$TCH(n_{TCH},k_{TCH},t_{cap})=\sum_{i=1}^{h} Pi(x) \tag{2.1}$$

$$k_{TCH}=m+\log_2 h+1 \tag{2.2}$$

$$P_i(x)\neq P_j(x)^r \bmod n_{TCH},\ i\neq j\ \forall t_{cap}\in\mathbb{N} \tag{2.3}$$

where h represents the number of TCH polynomials for a particular code.

Its error correcting capacity, t_{cap}, is dependent on the minimum distance of a code, d_{min}, between any two polynomials.

So, with H_d being the Hamming distance between two polynomials.

$$d_{min}\geq 2t_{cap}+1 \tag{2.4}$$

$$d_{min}\leq H_d[P_i(x),\ \{P_j(x)^r\} \bmod n_{code}]\leq n_{code}-d_{min} \tag{2.5}$$

In order to generate TCH codes it is required to find polynomials $P_i(x)$ with length n_{TCH} whose coefficients a_i, $i=0, 1, \ldots, n_{TCH}-1$, are from a Galois Field, GF(2). Finite field theory allege that polynomials of degree n_{code} and coefficients of a Galois Field GF(q), where q is related to a prime number p through the equation, $q=p^{k_{TCH}}$, being x a positive integer, can be field elements of GF(q) [3] by restricting the coefficients to GF(2). B-TCH polynomials can be generated for all prime numbers p that obey this condition:

$$p=n_{TCH}+1=2^m+1 \tag{2.6}$$

As stated in [3], basic TCH polynomials can be described as:

$$P_i(x)=\sum_{i=0}^{\left(\frac{p-1}{2}\right)-1} a_i x^{K_i} \tag{2.7}$$

The exponent values of K_i verify that:

$$\alpha^{K_i}=1+\alpha^{2i+1},\ i=0,1,\ldots,\ \left(\frac{p-1}{2}\right)-1 \tag{2.8}$$

for any primitive root α of GF(q). Each of the existing α generates a different polynomial with $2n_{TCH}$ codewords, being the foundation ($h=1$) for new TCH codes.

When established, the total number of polynomials used in a code allows the determination of the total resulting number of codewords:

$$N_{CW}=2h\cdot n_{TCH} \tag{2.9}$$

being N_{CW} the total number of resulting codewords, and h the number of polynomials present in each code.

If the number of information bits in an input block that are coded into n_{TCH} length codewords is not known, it can be calculated using:

$$k_{TCH}=\log_2 N_{CW} \tag{2.10}$$

It can be seen, from Equation (2.6) that the only prime numbers obeying that condition are Fermat numbers.

$$F_i=2^{2^i}+1,\ i\in\mathbb{N} \tag{2.11}$$

It was verified that there is a total of five values that comply with (2.11):

Table 2.1 - Fermat numbers for generating TCH Codes.

i	p	n_{TCH}
0	3	2
1	5	4
2	17	16
3	257	256
4	65537	65536

Source: [3, p. 54].

In Table 2.1 it is noticeable that there are five values in total, these values represent the five possible lengths of TCH Polynomials that can be created using the generator equation (2.11). These polynomials were named Basic TCH Base Polynomials (B-TCH Polynomials for short).

[3] explains that TCH codes originated from B-TCH polynomials have good cross and auto-correlation, where the latter can assume one of three values: n_{TCH}, 0 and -4. This

proves to be a great advantage when using TCH codes of great size, for example, code length of $n_{TCH} \geq 256$. When using such elevated code lengths, the correlation between sequences tends to resemble a Dirac impulse for larger values of n_{TCH}.

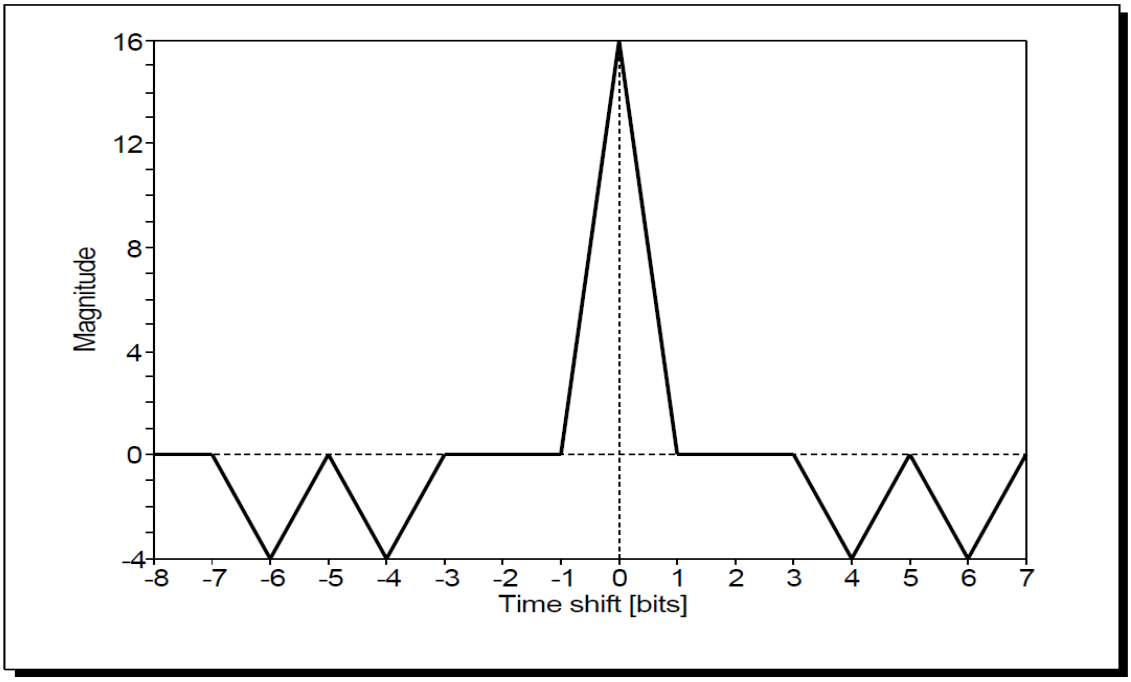

Figure 2.1 - Autocorrelation of B-TCH Polynomial of length n_{TCH}=16. Source: [3, p. 69].

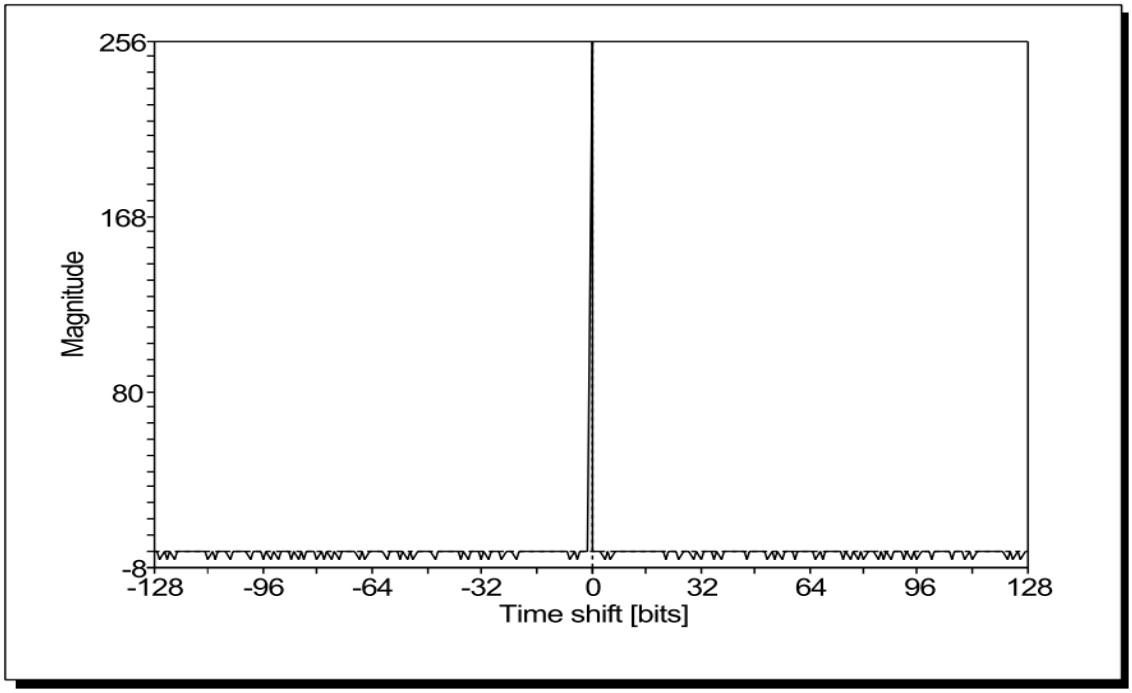

Figure 2.2 - Autocorrelation of B-TCH Polynomial of length n_{TCH}=256. Source:[3, p. 71].

Figure 2.1 shows the autocorrelation of a B-TCH Polynomial with length n_{TCH}=16 while Figure 2.2 shows the autocorrelation of a B-TCH Polynomial length n_{TCH}=256.

Considering the architecture of the TCH receiver employed in [3], the speed gain, the ratio between the total number of operations needed to perform maximum likelihood decoding and the number of operations needed by a TCH decoder, is calculated in (2.12):

$$S_g = \frac{h2^m}{h+2^m} = \frac{h}{1+\frac{h}{n_{TCH}}} = \frac{n_{TCH}2^{k_{TCH}}}{n_{TCH}2^2+2^{k_{TCH}}} \tag{2.12}$$

Keeping these characteristics in mind, while not exclusive to these codes, it is conceivable the determination of the code rate:

$$R_c = \frac{k_{TCH}}{n_{TCH}} \tag{2.13}$$

It can be noted that the condition, $R_c<1$, is always verified due to the introduction of redundancies, since $n_{TCH}>k_{TCH}$. To these redundancies, the difference between coded bits and information bits ($n_{TCH} - k_{TCH}$), are given the designation of parity check bits. If k_{TCH} information bits are unmodified together with the parity check bits in a codeword of length n_{TCH}, the code is systematic [3].

When considering a given codeword, the weight of said codeword can be determined by counting the number of nonzero elements contained in it. When all the codewords that compose a coded signal share the same weight, this code is designated as fixed or constant weight.

On this prospect, [3] affirms that the weight of any TCH polynomial is always half the sequence length n_{TCH}. Knowing that TCH codes can be derived from B-TCH polynomials, it is possible to generate two kinds of codes:

- Constant weight (CW) TCH codes. Like mentioned before, these all have codewords sharing the same weight, that weight being half the code length.
- Non constant weight (NCW) TCH codes. These codes can have any weight besides 0 and n_{TCH}, albeit keeping other previously discussed properties, such as cross-correlation.

There is a parameter that is useful to evaluate the performance of a code:

$$C_g = \lim_{\frac{E_b}{N_0} \to \infty} C_{gain} = R_c d_{min} \tag{2.14}$$

This parameter is called the asymptotic gain.

In [3], TCH codes have been used in a simple receiver implementation, based on a group of correlators, each of them comparing the received codeword. In a TCH (n_{TCH},k_{TCH}) code, the total number of codewords is $2^{k_{TCH}} = 2n_{TCH} \cdot h$, where h is the number of correlators that can be implemented to verify the maximum likelihood. The sequence with higher correlation is the selected one.

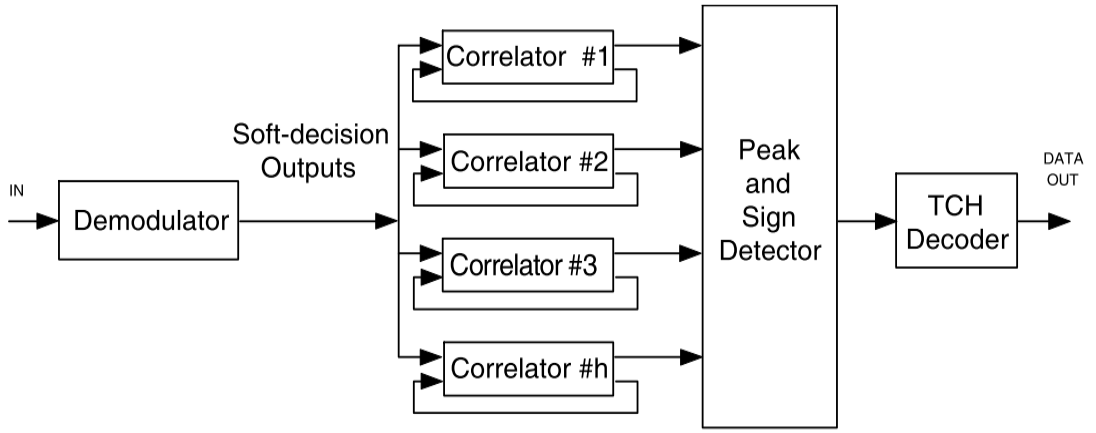

Figure 2.3 - TCH receiver simple implementation. Source: [3, p. 198].

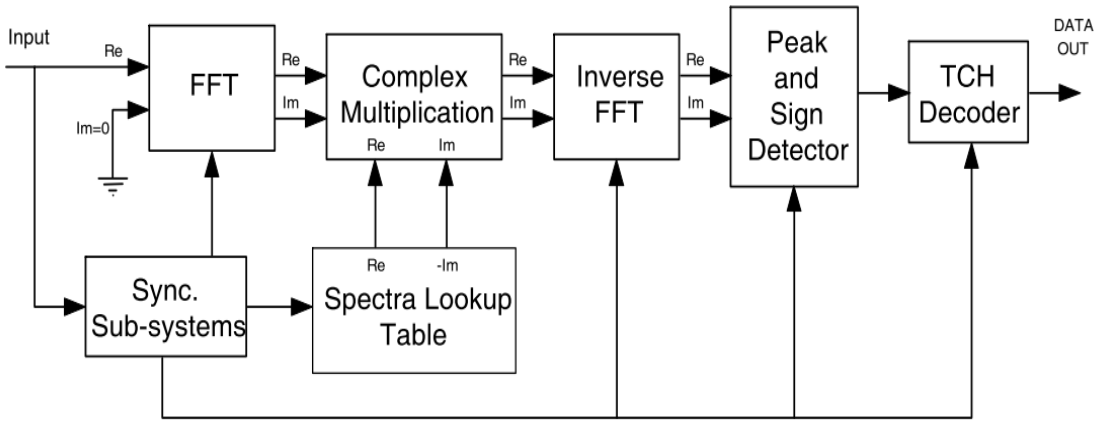

Figure 2.4 - Simple TCH decoder of maximum likelihood. Source: [3, p. 204].

The correlators in Figure 2.3 can be replaced by a FFT, a complex multiplication and an Inverse Fast Fourier Transform (IFFT) as shown in Figure 2.4.

2.2.2. Coding Gain

In the works of [4], when considering an AWGN channel, the resulting erred information introduced by it can be mitigated without compromising the information rate, minding all the while the channel capacity given by:

$$C_{ch}=B_{en}log_2(1+snr) \tag{2.15}$$

where B_{en} [Hz] is the equivalent noise bandwidth and *snr* the Signal-to-Noise Ratio.

Being the SNR a way to measure the quality of a link, this parameter compares the power of a given signal to the power of the noise present in the channel in which the signal is being transmitted.

The quality of a link can also be measured by the information BER using:

$$\frac{E_b}{N_0} \tag{2.16}$$

Being the major factors here represented the unilateral noise power spectral noise density N_0 [W/Hz] and the received energy per information bit E_b [J].

To reduce the errors that occur during the transmission of a signal, the use of coding is of great importance.

When assuming distinct scenarios, when coding is and is not performed, it is expected to note changes to the resulting BER values obtained. This difference, or rather, margin, that can be observed when comparing the uncoded system to the one containing coding schemes implemented is called coding gain, C_{gain}.

[3] provides good examples of the use of TCH codes to ascertain the importance and utility of said codes and obtention of their coding gain to improve communication systems.

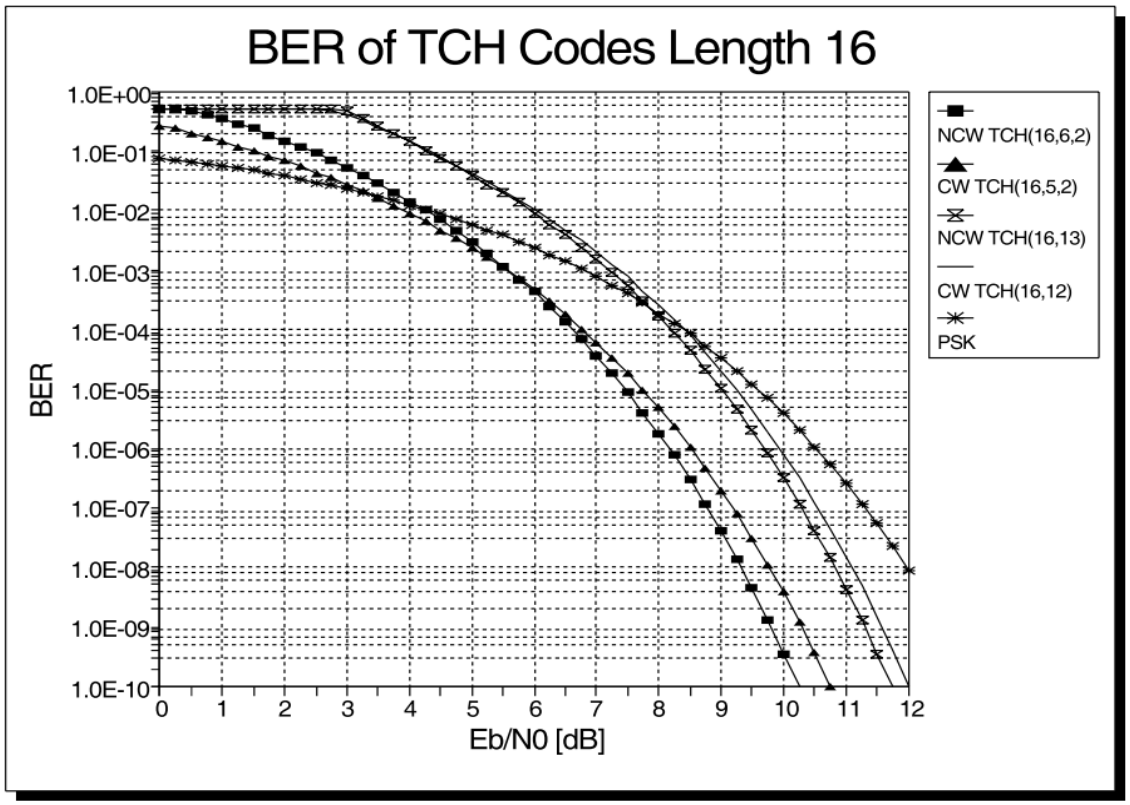

Figure 2.5 - BER of TCH codes length 16. Source: [3, p. 173].

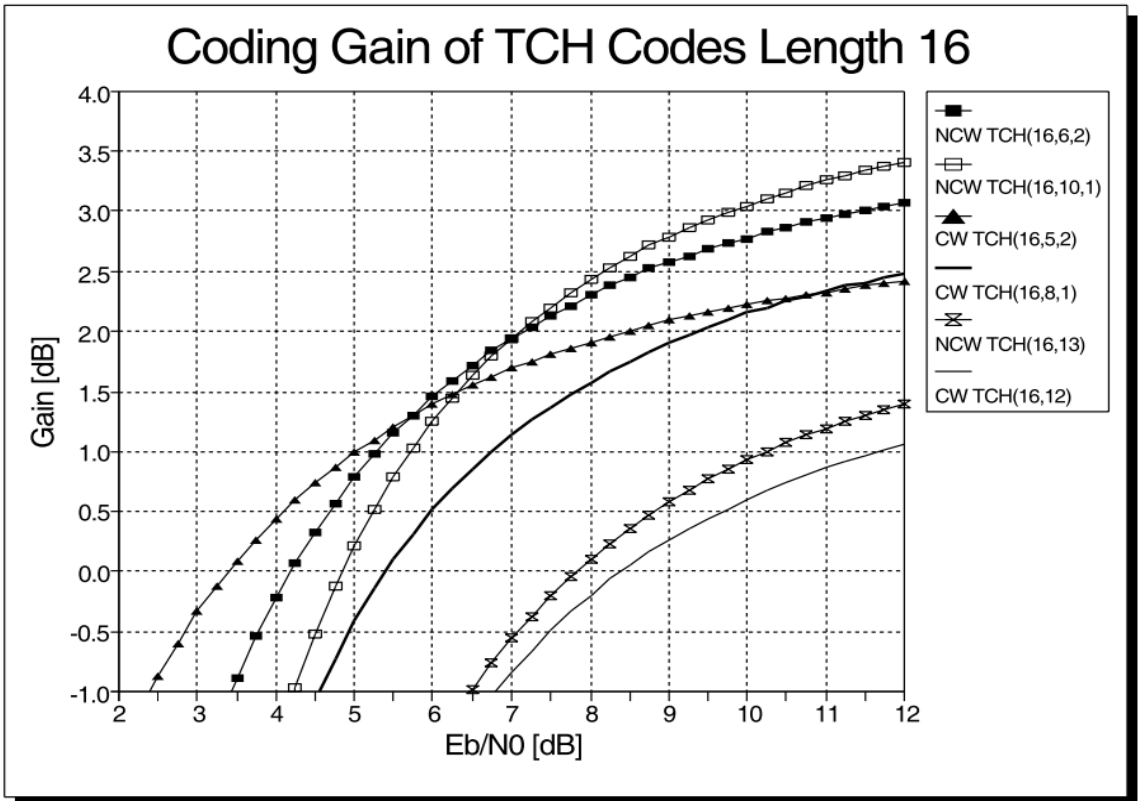

Figure 2.6 - Coding gain of TCH codes length 16. Source: [3, p. 174].

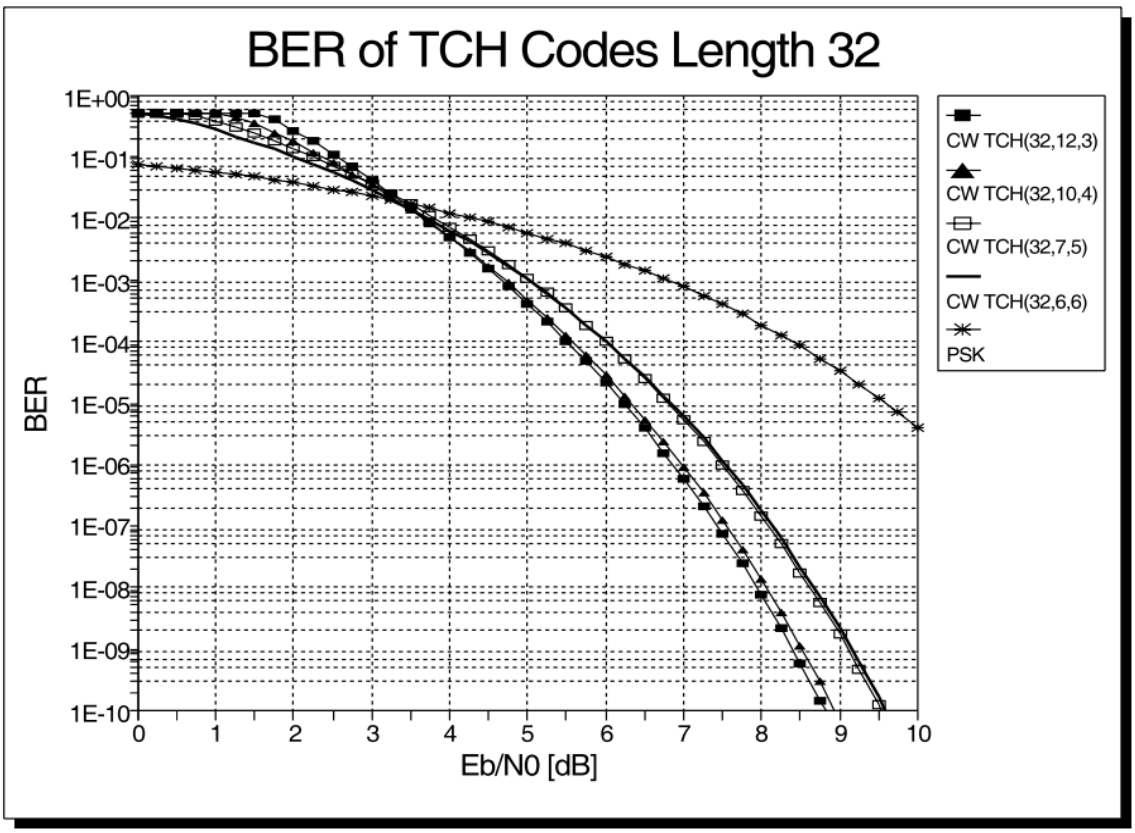

Figure 2.7 - BER of TCH codes length 32. Source: [3, p. 174].

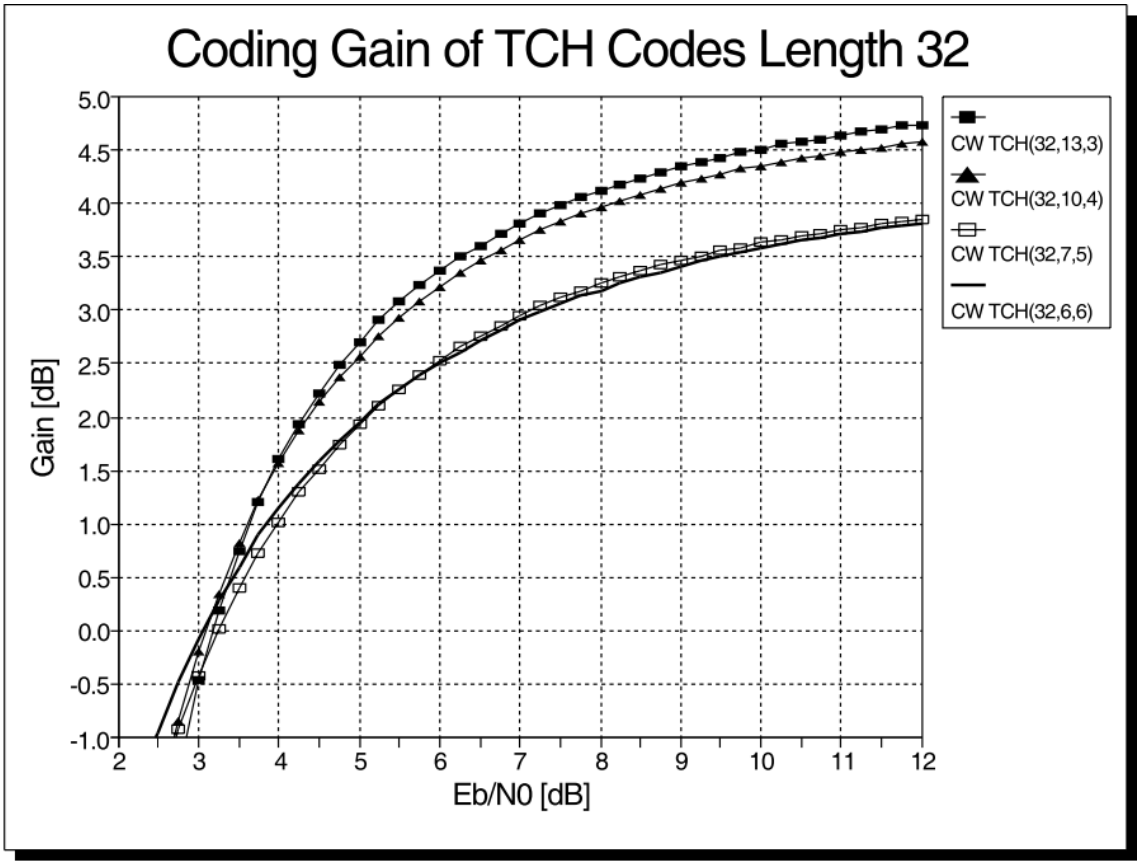

Figure 2.8 - Coding gain of TCH codes length 32. Source: [3, p. 175].

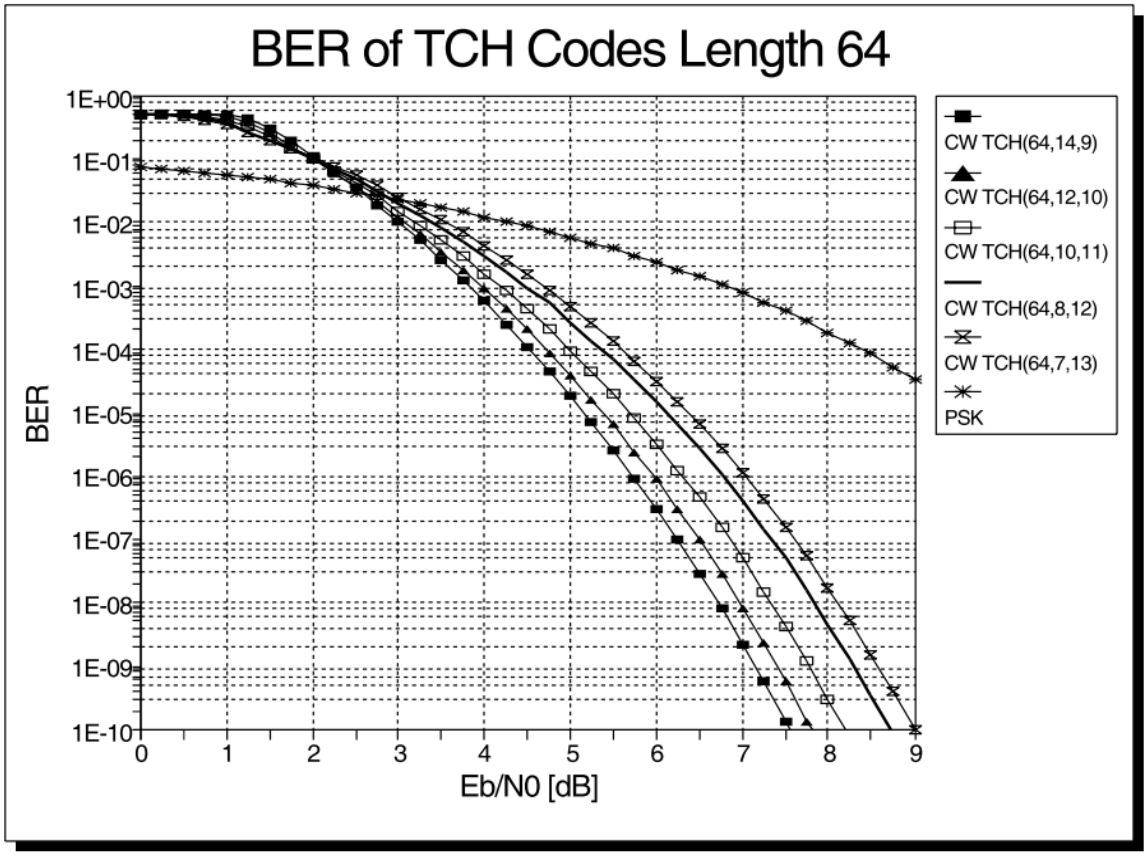

Figure 2.9 - BER of TCH codes length 64. Source: [3, p. 175].

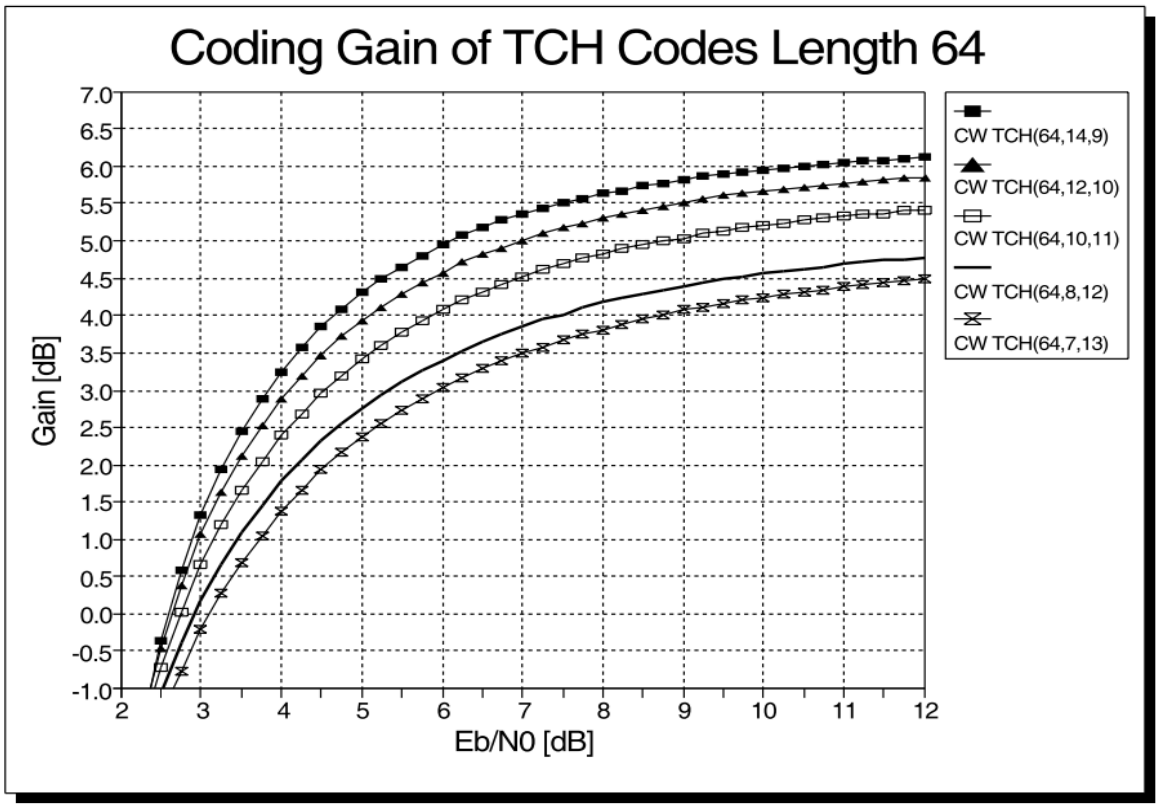

Figure 2.10 - Coding gain of TCH codes length 64. Source: [3, p. 176].

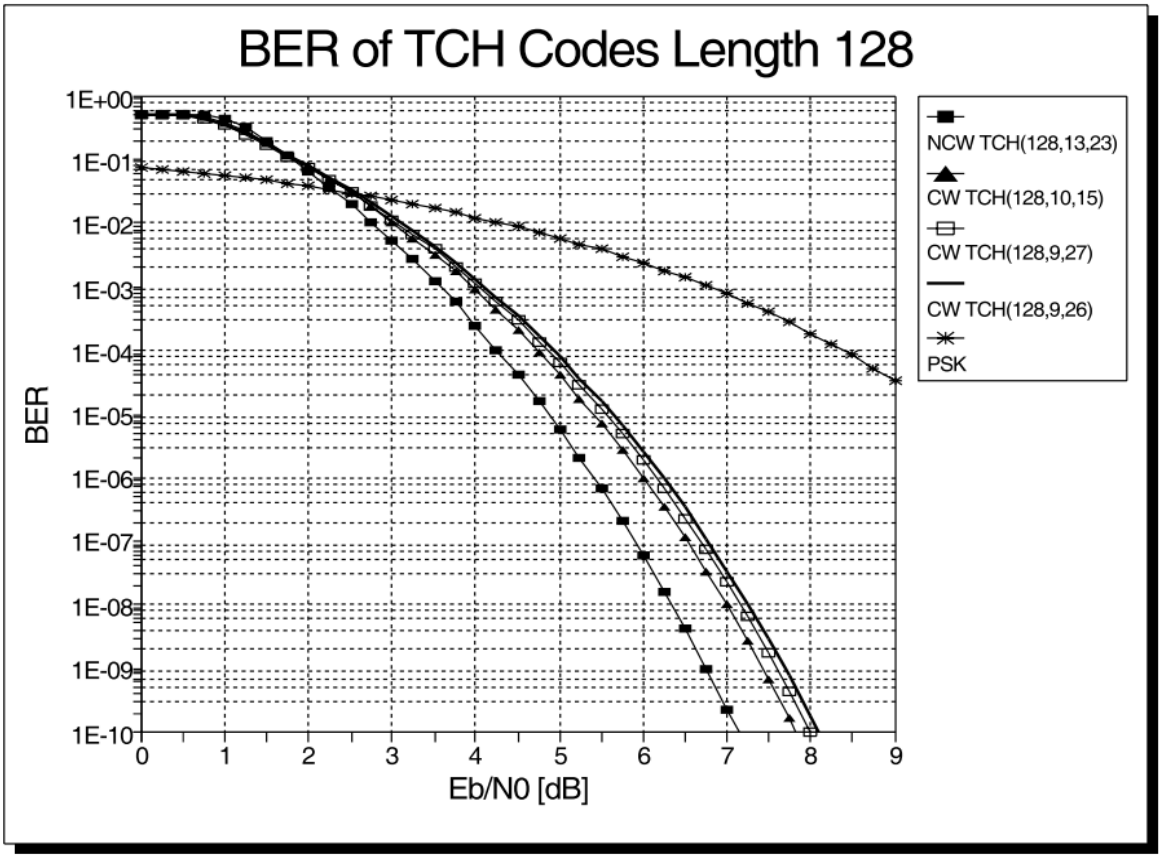

Figure 2.11 - BER of TCH codes length 128. Source: [3, p. 176].

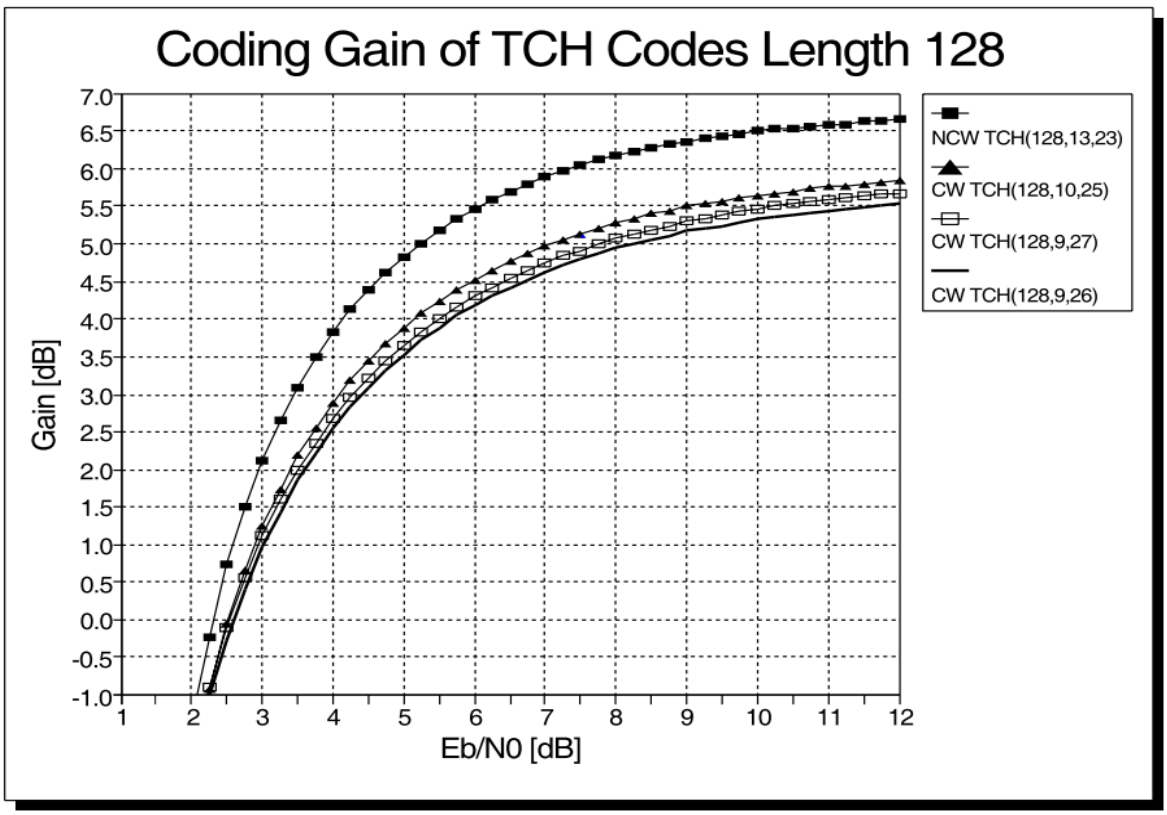

Figure 2.12 - Coding gain of TCH codes length 128. Source: [3, p. 177].

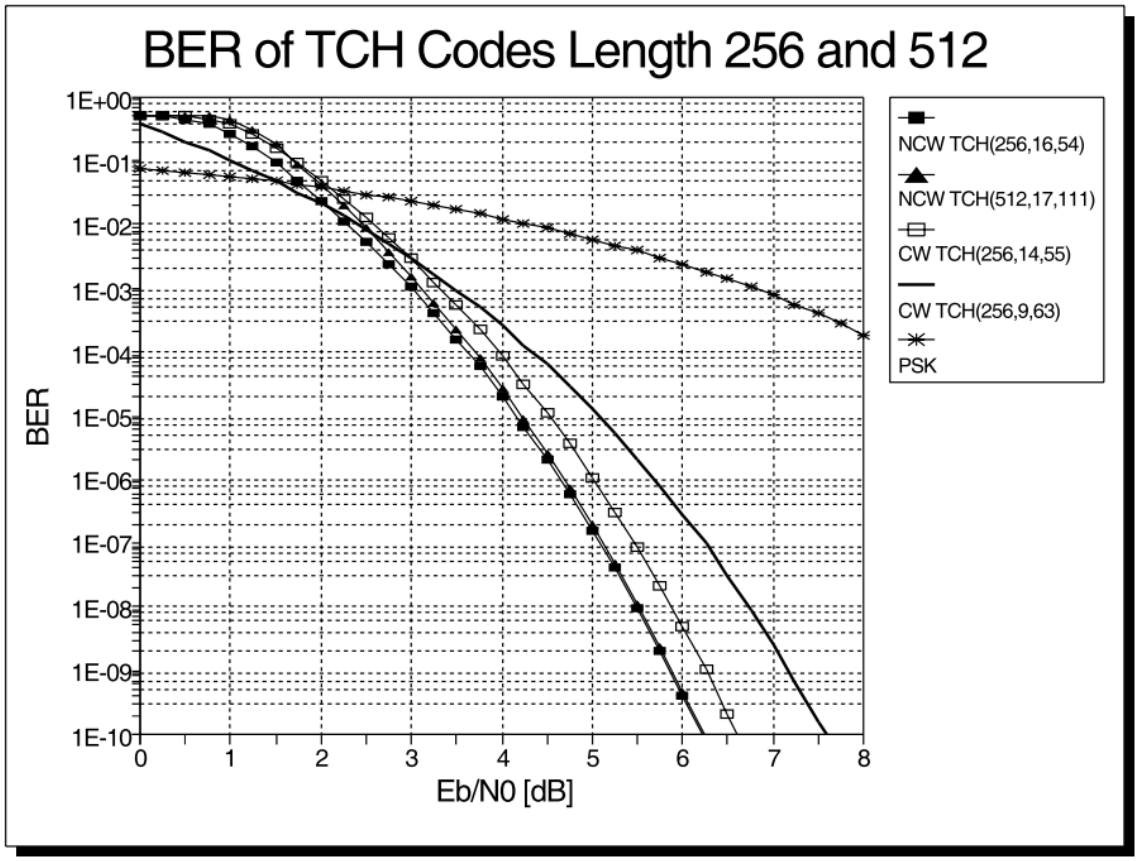

Figure 2.13 - BER of TCH codes length 256 and 512. Source: [3, p. 177].

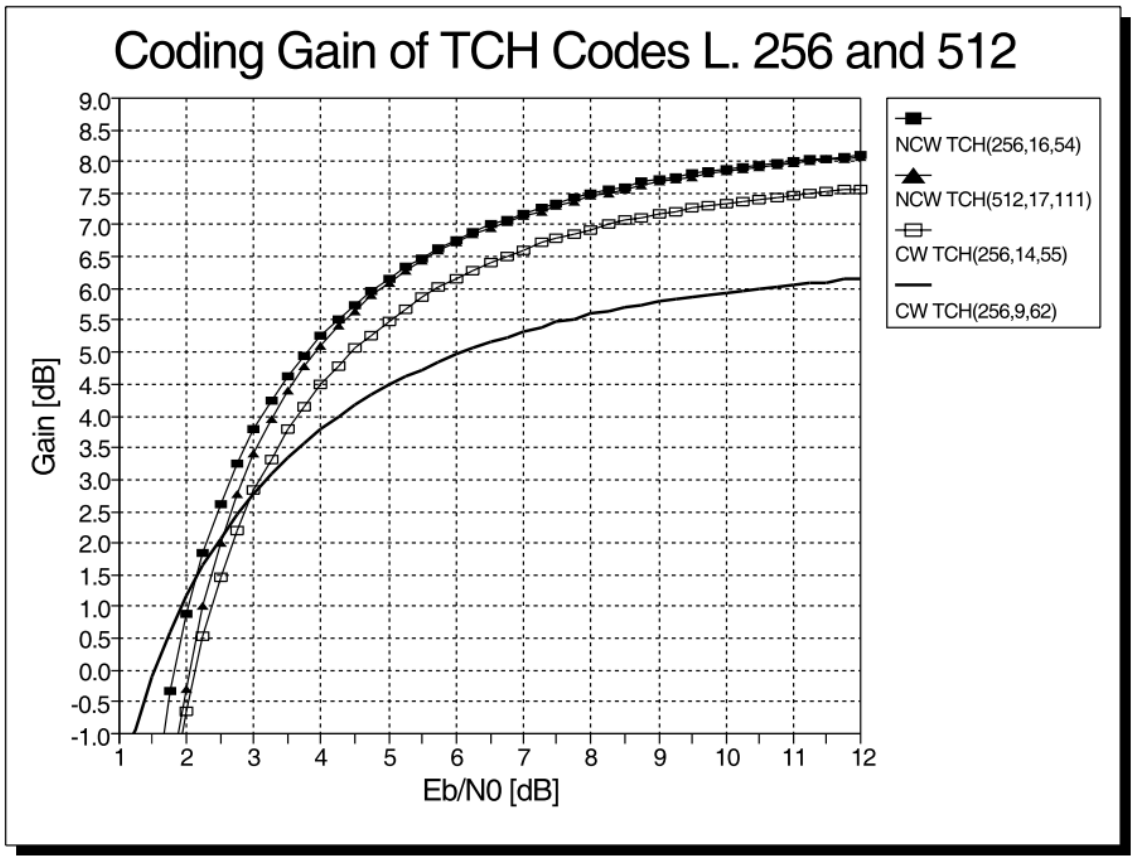

Figure 2.14 - Coding gain of TCH codes length 256 and 512. Source: [3, p. 178].

In Figures 2.5, 2.7, 2.9, 2.11 and 2.13, it is shown the resulting BER curves for TCH codes of different lengths as function of $\frac{E_b}{N_0}$, whereas in Figure 2.6, 2.8, 2.10, 2.12 and 2.14 it is represented the evolution of the resulting coding gains, also as function of $\frac{E_b}{N_0}$. It is relevant to mention that the modulation used in the obtention of these figures was uncoded Binary Phase-Shift Keying (BPSK), which is usually applied in satellite links due to the inherent simplicity of this modulation.

2.2.3. Conclusion

By observing all the aspects stated above, some final considerations can be made pertaining to its advantages:

- Through the implementation of TCH codes, the equivalent structure of an optimal receiver based on multiple correlators is achievable (implementation of a bank of correlators), each performing maximum likelihood decoding, using FFTs, all the while keeping their number to a minimum, in order to reduce complexity, power consumption and overall costs [3].
- Obtention of elevated coding gains whilst recurring to low SNR ratios, nonetheless, securing an adequate performance.
- Utilization of the inverses of the codewords to achieve reduction of the number of correlators.
- Implementation of Digital Signal Processing (DSP) techniques, such as FFT algorithms to evaluate the correlation properties in frequency domain more effectively. Adding to this point, the implementation of cyclic codes may lead to further improvements [3].
- Due to the TCH codes properties, mainly $n_{TCH} = 2^m$, and remembering the aforementioned factors, it is possible to further reduce the total number of correlators [3].
- While analyzing figures in 2.2.2, it can be noted the coding gain of the various codes increases with the SNR, as we should expect.

As for a particular disadvantage, it can be noted that B-TCH polynomials are limited for certain values of code length. It is possible, however, to apply different methods to extend them, but the assurance of the integrity of their properties and structure may be harmed.

2.3. Orthogonal Frequency Division Multiplexing

OFDM is part of a wider class of multicarrier modulation (MCM) in which the data is transmitted over several lower rate subcarriers. The greatest advantages of OFDM are its robustness against channel dispersion and simple phase and channel estimation in time-varying environments, but it also has its cons, like high peak-to-average power ratio (PAPR) and sensitivity to frequency and phase noise [5].

2.3.1. Mathematical Arrangement for an OFDM Signal

To understand the mathematic formulation of an OFDM signal, it is important to comprehend the structure behind it.

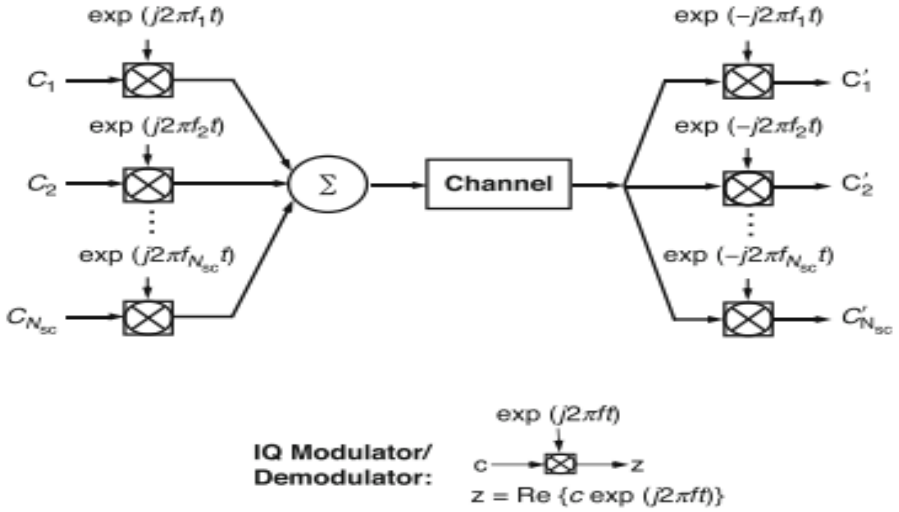

Figure 2.15 - Generic multicarrier modulation diagram. Source: [5, p. 33].

Considering *s(t)* as the MCM transmitted signal and considering the work present in [5], it can be represented as:

$$s(t)=\sum_{i=-\infty}^{+\infty}\sum_{k=1}^{N_{sc}} c_{ki}s_k\,(t-iT_s) \tag{2.17}$$

$$s_k(t)=\prod(t)e^{j2\pi f_k t} \tag{2.18}$$

$$\prod(t)=\begin{cases} 1, & (0<t\leq T_s) \\ 0, & (t\leq 0,\ t>T_s) \end{cases} \tag{2.19}$$

being c_{ki} the i^{th} information symbol at the k^{th} subcarrier, s_k the k^{th} subcarrier waveform, N_{sc} the number subcarriers, f_k the frequency of the subcarrier, T_s the symbol period and $\prod(t)$ the pulse shaping function. Each subcarrier makes use of a filter that matches its waveform or a correlator that matches with its own. This results in an information symbol, c'_{ik}, where

$$c'_{ik} = \frac{1}{T_s}\int_0^{T_s} r(t - iT_s)s_k^* \, dt = \frac{1}{T_s}\int_0^{T_s} r(t - iT_s)\, e^{-j2\pi f_k t} dt \tag{2.20}$$

and *r(t)* is the received time domain signal. [6] and [7] state that classical MCM uses nonoverlapped band-limited signals that can be implemented using a bank of many oscillators and filters both at transmission and reception. However, this proves to be unfavorable. To design filters and oscillators in a cost-effective way, the channel spacing must be a multiple of the symbol rate, this matter substantially degrades spectral efficiency, further leading to excessive bandwidth requirements.

Investigation made by [8] presents an approach to this matter through the employment of overlapped, orthogonal signal sets. This orthogonality is demonstrated by:

$$\delta_{ki} = \frac{1}{T_s}\int_0^{T_s} s_k s_l^* \, dt = \frac{1}{T_s} e^{(j2\pi(f_k - f_l)t)} dt = e^{(j\pi(f_k - f_l)T_s)} \frac{sin(\pi(f_k - f_l)T_s)}{\pi(f_k - f_l)T_s} \tag{2.21}$$

If,

$$f_k - f_l = m\frac{1}{T_s} \tag{2.22}$$

is satisfied, then two subcarriers are orthogonal to each other. This means that these orthogonal subcarrier sets, with channel spacing being a multiple to the inverse of symbol periods, can be recovered by using matched filters without intercarrier interference (ICI).

2.3.2. Implementation of the Discrete Fourier Transform in OFDM

The implementation of OFDM can be a challenge due to its large number of subcarriers.

This leads to overly complex architectures containing many oscillators and filters.

[9] demonstrates that OFDM modulation and demodulation can be achieved by using the inverse discrete Fourier transform (IDFT) and discrete Fourier transform (DFT).

According to [5], by re-denoting N_{sc} as N_{OFDM}, focusing on one OFDM symbol, and if *s(t)* is sampled at every $\frac{T_s}{N_{OFDM}}$ interval, it can be deduced that:

$$s_m = \sum_{k=1}^{N} c_k e^{j2\pi f_k \frac{(m-1)T_s}{N_{OFDM}}} \tag{2.23}$$

By using (2.22) and the convention that

$$f_k = \frac{k-1}{T_s} \tag{2.24}$$

And by merging (2.24) into (2.23), the result is

$$s_m = \sum_{k=1}^{N} c_k e^{j2\pi \frac{(k-1)(m-1)}{N_{OFDM}}} = \mathfrak{F}^{-1}\{c_k\} \tag{2.25}$$

where $\mathfrak{F}$ is the Fourier transform and $m \in [1, N_{OFDM}]$.

As for the receiving end,

$$c'_k = \mathfrak{F}\{r_m\} \tag{2.26}$$

with r_m being the received signal, sampled at every $\frac{T_s}{N_{OFDM}}$ interval.

It is critical to note the use of two devices for this implementation: a digital-to-analog converter (DAC) that converts the discrete values of the signal into continuous analog values, and an analog-to-digital converter (ADC) that does the opposite. DFT/IDFT implementations have two principal advantages: efficient IFFT/FFT algorithms that greatly reduce the number of complex multiplications [10] and many orthogonal subcarriers can be generated and demodulated without complex RF oscillators and filters, allowing a rather simple architecture.

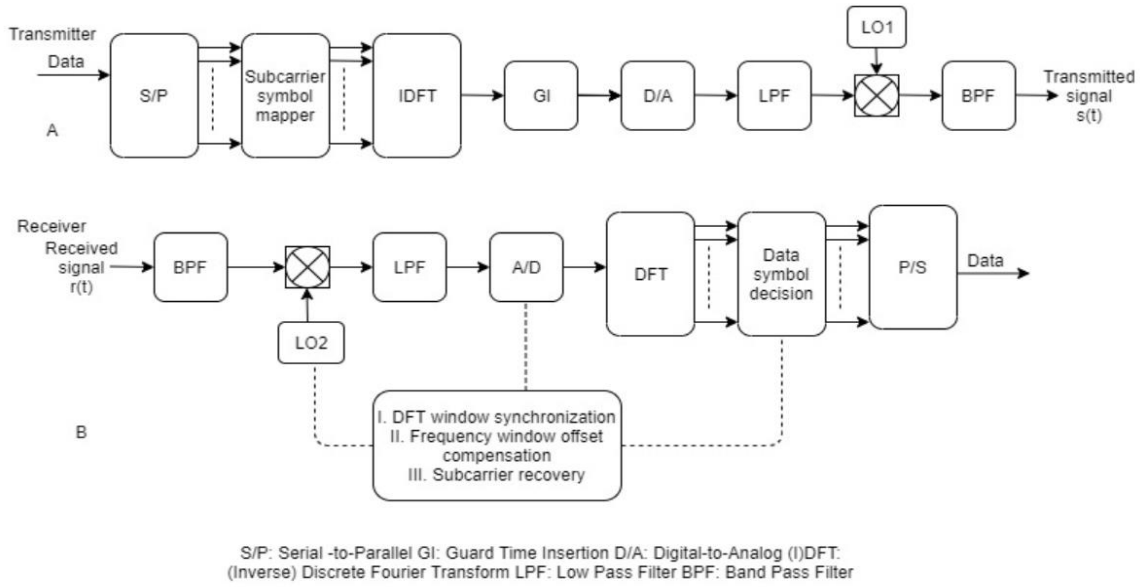

Figure 2.16 - OFDM transmitter (A) and Receiver (B) diagrams. Source: [5, p. 35].

[5] affirms that, at the transmitter end, the inputted bits are converted into several parallel data pipes, all mapped onto corresponding information symbols within one OFDM symbol, the digital time domain signal is obtained through IDFT and a guard interval is inserted to prevent inter-symbol interference (ISI) that may originate from channel dispersion. The baseband signal can then be upconverted to an RF passband using an In-phase/Quadrature (IQ) modulator. As for the receiving end, a similar process occurs but reversed, the signal is down converted to baseband with an IQ demodulator, sampled using an ADC and demodulated using DFT, thus recovering the transmitted data through signal processing.

2.3.3. Cyclic Prefix

The works of [11] and [12] defend that the insertion of a cyclic prefix is one of the techniques that make the implementation of OFDM systems feasible.

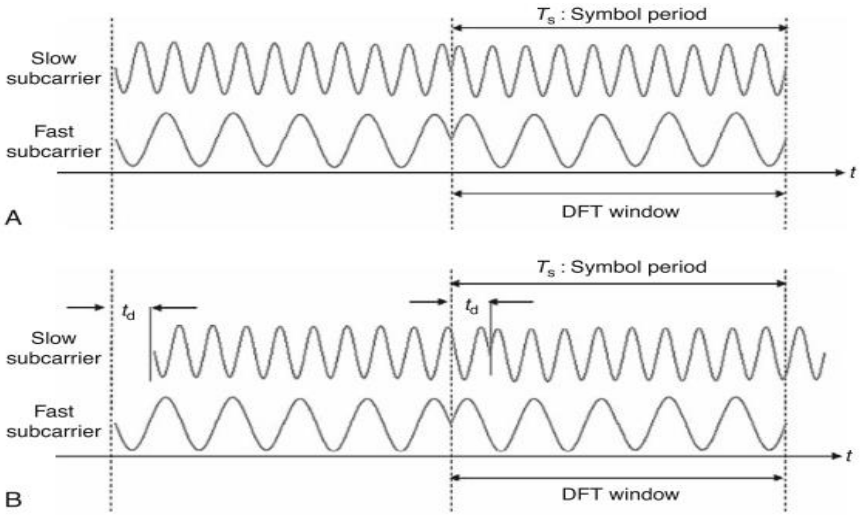

Figure 2.17 - OFDM signal without cyclic prefix at the transmitter (A) and the receiver (B). Source: [5, p. 37].

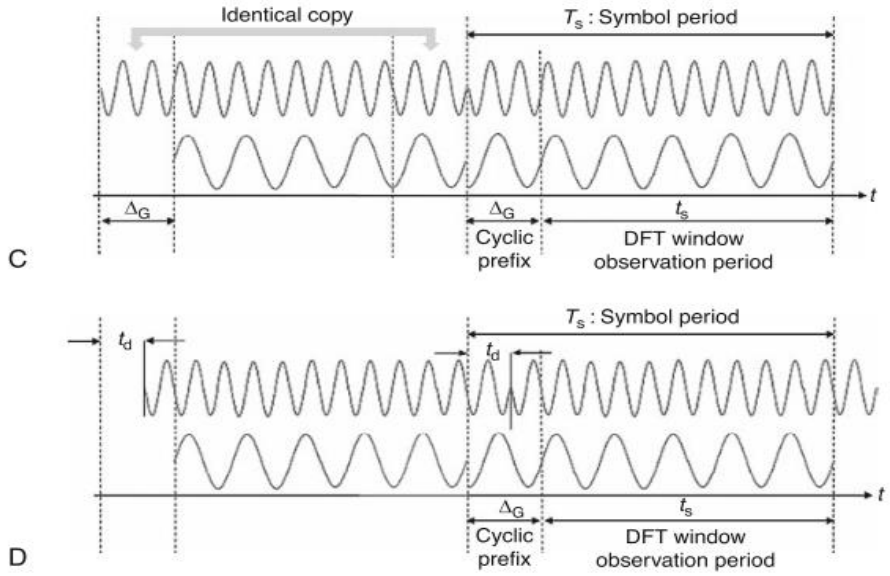

Figure 2.18 - OFDM signal with cyclic prefix at the transmitter (C) and the receiver (D). Source: [5, p. 37].

Considering two consecutive OFDM symbols undergoing a dispersive channel with delay spread of t_d, and if each symbol includes only two subcarriers with fast and slow delay spread, dubbing them as “fast subcarrier” and “slow subcarrier” respectively, in both Figure 2.17 and Figure 2.18, it is shown that in (A), the two subcarriers are aligned upon transmission, while in (B) the slow subcarrier is delayed by t_d, due to channel dispersion, consequently leading to ISI and ICI.

[11] suggested the use of cyclic prefix to resolve this issue and the results are shown in (C), where a guard interval Δ_G is introduced, whose waveform is an identical copy,

shifted forward by t_s. In (D), the same can be observed upon reception. By assuming that a signal subjected to a similar dispersive channel and DFT window containing a complete OFDM symbol for the fast subcarrier waveform, a similar symbol can be maintained in the subcarrier within the same conditions due to a portion of the cyclic prefix being shifted, replacing the identical part that has been shifted out. As for the slow subcarrier, the symbol is a quasi-identical copy of its waveform with an additional phase shift, this shift is therefore resolved through channel estimation and thus removed for symbol decision [5].

It is possible to determine the condition for ISI-free OFDM transmission, that condition being:

$$t_d < \Delta_G \tag{2.27}$$

There are two procedures required to properly recover OFDM symbols: an appropriate selection of the DFT window, in other words, DFT window synchronization, and channel estimation.

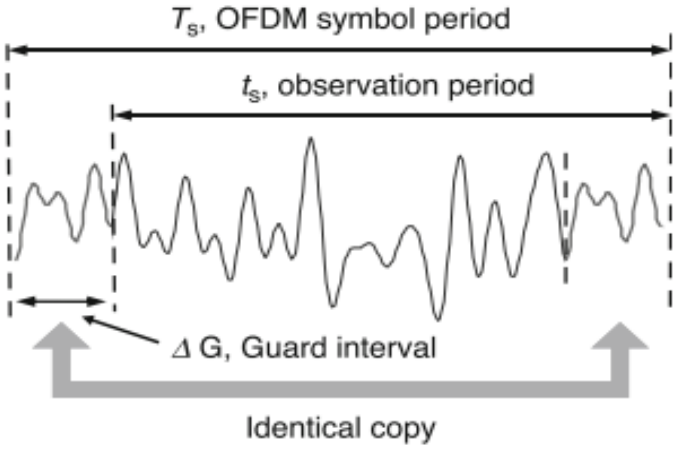

Figure 2.19 - Time domain representation of an OFDM symbol. Source: [5, p. 38].

To evaluate the cyclic prefix, it can be made use of (2.28) to describe the guard interval:

$$\prod(t) = \begin{cases} 1, (-\Delta_G < t \leq t_s) \\ 0, (t \leq -\Delta_G,\ t > t_s) \end{cases} \tag{2.28}$$

2.3.4. Conclusions

Just like in 2.2.3, some of the advantages for OFDM technology are noted, mainly:

- Permeability of usage throughout a wide array of wireless and telecommunication standards.
- Avoidance of ISI and ICI (through the introduction of the Cyclic Prefix).
- Robustness to dispersion, high spectral efficiency and improved channel estimation in time-varying environments. [5]
- Capability to attenuate problems that arise from multipath propagation [13] and [14].
- Lower costs of signal processing [15], [16] and [17].
- Orthogonality prevents interference from the overlapping sidebands from received carriers [18].
- Allows more efficient use of available spectrum for transmission by saving bandwidth [5].
- In similarity with TCH codes, it makes use of FFT, which leads to reduced computation complexity.

As well as the disadvantages:

- High PAPR with elevated frequency offset and phase noise sensitivity that can lead to ICI [5].
- High vulnerability to frequency synchronization problems [18].

The following figure depicts the BER results that are expected to be obtained when using OFDM modulation with various modulation indexes:

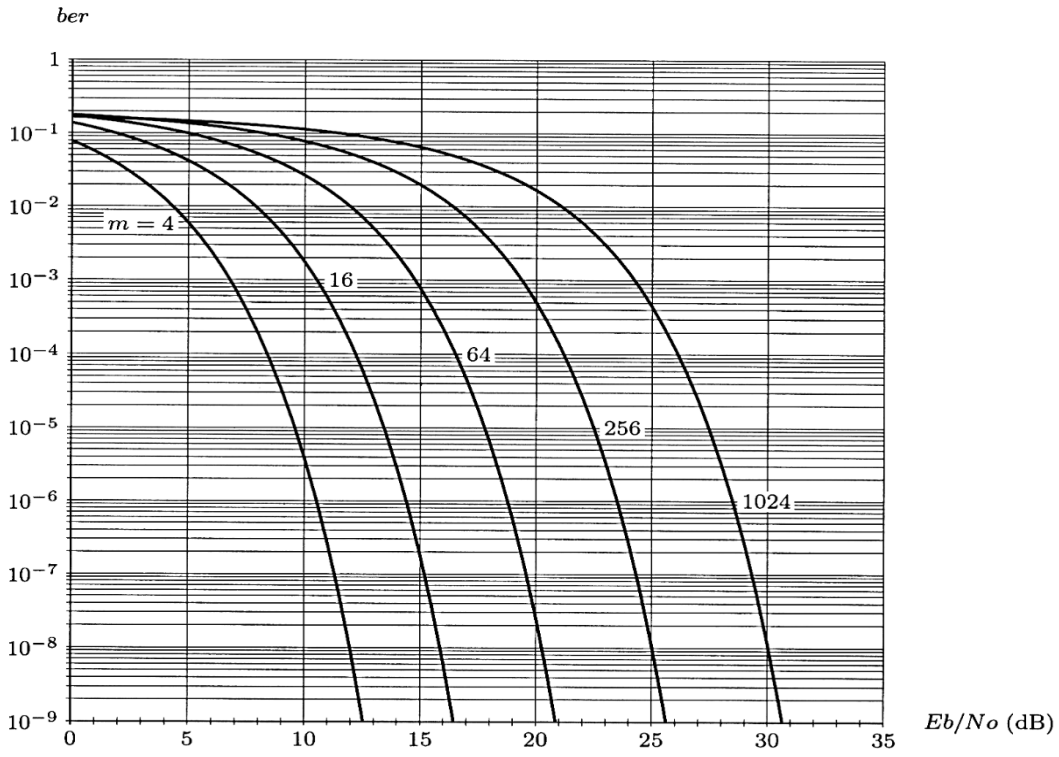

Figure 2.20 - BER variance in function of $\frac{E_b}{N_0}$ for the QAM modulation indexes M=4, 16, 64, 256 and 1024. Source: [19, p.320].

2.4. AWGN Channel and Channel Estimation

AWGN is a basic model that introduces random properties to a signal over the course it takes from the transmitting to the receiving end. It is considered additive because it introduces noise to the system, white because it has uniform power across the frequency band and gaussian since it has normal distribution in the time domain.

This is, in fact, a simple model since it does not consider many important factors such as: fading, nonlinearity and dispersion.

Once the channel is established, it is of utmost importance that there is a way to study some properties inherent to it. In this case, since AWGN channel is being considered, it is relevant to analyze the attenuation that results from it. According to [25] this analysis can be performed through channel estimation, aiming to achieve high data rates and reliability. In summation, this process is akin to the usage of mathematical models to describe physical alterations to the channel.

One way that is considered in this study to perform channel estimation is through Pilot Symbol Aided Modulation (PSAM) [20].

PSAM is a method used in channel estimation, used in various works, such as [21], [22] and [23] where the introduction of known symbols periodically in the transmitter is applied so that there is no change in the pulse shape nor in the PAPR. That said, the receiver must be capable of estimating the amplitude and phase rotations by interpolating the channel measurements provided by said symbols [18]. In Figure 2.21 it is possible to observe the structure of an OFDM signal where PSAM is being applied.

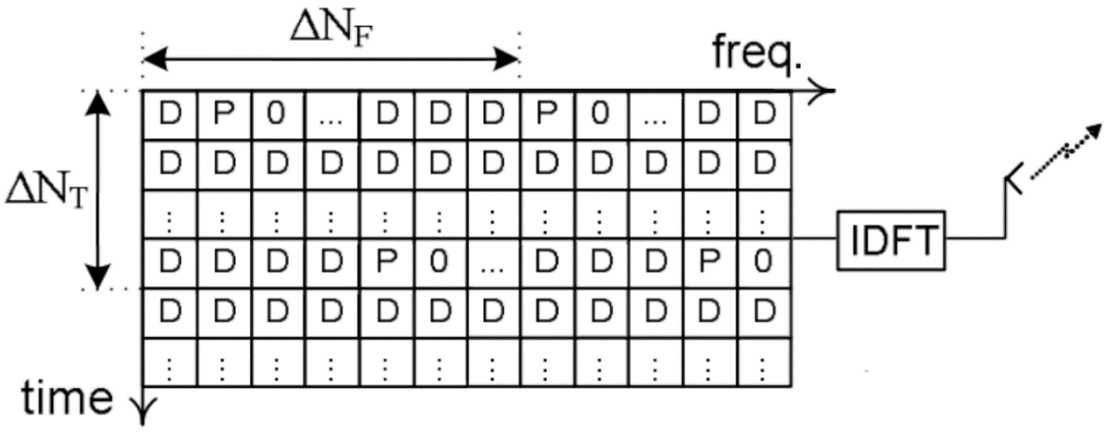

Figure 2.21 - Frame structure of an OFDM signal using PSAM. Source: [18, p. 13].

Some noteworthy parameters that can be found in Figure 2.21 are the spacings for frequency domain ΔN_F and time domain ΔN_T, the data *D* and pilot *P* symbols.

Taking into account OFDM characteristics, and according to [25], PSAM can be accomplished by adding more subcarriers to the system, or by utilizing some already existing ones.

The addition of these pilots must be in accordance with the Nyquist sampling theorem shown below:

$$f_s \geq 2B \tag{2.29}$$

denoting *B* as the maximum bandwidth of the signal and f_s as the frequency needed to sample the continuous-time signal, also known as Nyquist frequency. However, according to [25], this theorem assumes an infinite number of samples and noiseless channel, which is unrealizable in practicality. Therefore, the pilot insertion rate must be higher than the stated condition, all the while creating a channel behavior pattern, facilitating the estimation process. Later, the received pilots are interpolated with the original ones (because the pattern is known and shared by both transmitter and receiver).

Besides these aspects, it is also necessary the inclusion of equalization to successfully perform the channel estimation. Some of the most well-known equalizers are: Zero Forcing (ZF) and Minimum Mean-Square Error (MMSE) [25].

Giving special attention to the ZF equalizer, this one performs linear equalization by applying the inverse of the frequency response of the channel. If *H(f)* is the impulse response of a given channel, by applying the ZF method:

$$ZF(f) = \frac{1}{H(f)} \tag{2.30}$$

There are, however, disadvantages associated. ZF equalizers require a near infinite length depending on the frequency, if the received signal is weak, it may lead to a concerning surge in generated noise, which in turn reduces the overall SNR, affecting the estimation.

CHAPTER 3

Methodology

The aim of this chapter is to explain and describe the many processes that occur to a signal during simulation. In this study, the simulated signal is an OFDM waveform that is affected by such processes in a sequential manner. From transmission to reception, the course of the signal can be divided into blocks that, by themselves, represent major processes that are further analyzed in more detail:

- Transmission, in which occurs:
    - Coding.
    - Modulation.
- Wireless Channel Implementation.
- Reception, including:
    - Demodulation.
    - Channel Estimation.
    - Decoding.

The various figures present in this chapter that show the effects of the application of these modules were obtained using the MATLAB programming and numeric computing platform.

3.1. Transmitter

When realizing the transmitter, some aspects must be considered. Since this work aims to send a signal that goes through both coding and modulation, these are dissected and presented in detail.

Before considering the coding process, a signal must be created. The signal starts as a binary bitstream of zeros and ones generated randomly, given several bits N_{bits}, where the length of said bitstream can be managed by defining a desired multiplier, resulting in the total number of generated bits, $N_{bitstream}$.

3.1.1. TCH Coding

To encode the signal by means of TCH encoding, some inherent parameters are described. It is expected to realize the encoding by utilizing various code lengths, which means, different values of n_{TCH}, previously defined in 2.1.1. In this study, the values considered for the codeword length n_{TCH} are 16, 32, 64, 128 and 256.

Given these values, it is also required to define the polynomials that are used in the coding process. Even though [3] proposes a wide array of polynomials to define these codes, this study focuses on specific polynomials for a given length.

Table 3.1 presents, for the mentioned code lengths, the corresponding polynomials (written in hexadecimal notation), minimum distance between polynomials d_{min} and their designation.

Table 3.1 - TCH codes for various lengths and subsequent designation.

n_{TCH}	Polynomials (HEX)	d_{min}	Designation
16	B320 5861	6	TCH(16,6,2)
32	819A5D5E	14	TCH(32,6,6)
64	E257E6d0291574EC	28	TCH(64,7,13)
128	602B6274CF774B0EE1A5DDE65C8DA80C 96CA077DEB1707547C5CA1047EB25B1C	56	TCH(128,9,27)
256	BC208E6D36041F9AF8FF37959AC50ADCDC0BEC19F9735494195AEA73C648A2D0	126	TCH(256,9,62)

Recalling the TCH codes nomenclature, by observing the designations stated in Table 3.1, there is some information about these codes that can be retrieved, such as the codeword length n_{TCH}, the information block length with k_{TCH} bits, and the number of bits that the code can correct after decoding, t_{cap}, resulting in $TCH(n_{TCH}, k_{TCH}, t_{cap})$.

The purpose of this encoder based on TCH codes is to take blocks of k_{TCH} bits from the generated bitstream and convert them into codewords size n_{TCH}. To accomplish this, a polynomial is selected according to the intended codeword length, by using this polynomial, the number of circular shifts to be applied to a codeword is determined. These shifts also consider their negation, resulting in the coding capacity being doubled.

For the encoding process, the total number of output coded chips can be determined based on known values:

$$N_{coding} = \frac{n_{TCH}}{k_{TCH}} \times N_{bitstream} \quad (3.1)$$

3.1.2. OFDM Modulation

After coding the original bitstream into several codewords, the next step is the modulation process.

There is the need to define various parameters who not only are inherent to the modulation process but also important to define the signal. This includes the modulation index *M*, number of subcarriers/tones used in the transmission of one OFDM symbol N_{sc} and the number of bits within one Quadrature Amplitude Modulation (QAM) symbol $bits_{symbol}$. There are some other parameters that can be obtained, such as the number of chips present in the cyclic prefix

$$N_{CP} = N_{sc} \times 0{,}0695 \quad (3.2)$$

which in this study is 6,95% of the number of subcarriers [25] and the bit duration/information block length

$$T_0 = \frac{N_{sc}}{B} \quad (3.3)$$

that can be used to calculate the chip time

$$T_c = \frac{T_0}{N_{sc}} \quad (3.4)$$

By joining (3.2) with (3.4), the cyclic prefix duration is obtained:

$$T_P = T_c \times N_{CP} \quad (3.5)$$

It is also the possible to obtain both the symbol and bit rates:

$$R_s = \frac{N_{sc}}{T_0 + T_P} \quad (3.6)$$

$$R_b = R_s \times bits_{symbol} \quad (3.7)$$

where R_s represents the symbol rate, while R_b represents the bit rate.

Since a cyclic prefix is added to the signal to prevent interference and distortion, the overall number of subcarriers present in one OFDM symbol is given by the sum of the number of subcarriers within such symbol with the ones relative to the CP:

$$N_T = N_{sc} + N_{CP} \quad (3.8)$$

With all this information it becomes feasible to begin the modulation process, however, there still are some vital parameters to be defined to enable the representation of the signal both in time and frequency domain.

To understand the modulation process and the various blocks that represent various techniques exercised in it, it is important to reference Figure 2.16, more specifically, the modulator architecture it illustrates.

3.1.2.1. QAM Mapping and Sampling

To perform modulation, firstly QAM mapping is considered. After the obtention of the coded bitstream resulting from TCH encoding, this step takes said bitstream and creates groups of bits with length $bits_{symbol}$ to form QAM symbols with the purpose of accommodating higher transfer rates, typical in OFDM technologies.

The mapping technique employed in the modulator is QAM Gray coded symbol mapping. This technique deconstructs an inputted bitstream into several groupings of length $bits_{symbol}$ that are thereafter assigned a symbol designation. These symbols are mapped unto a constellation diagram that represents both in-phase and quadrature components where each symbol has a specific distance from the center of origin of the diagram, representing their amplitude. QAM mapping is intrinsically linked to the modulation index since the value of said index *M* determines the number of symbols contained within the constellation, therefore, when identifying the QAM mapping technique used, it is referred as a *M-QAM* mapping.

In this work, the modulation indexes studied and simulated are *M*=4, 16, 64 and 256, which means that the mapping techniques employed are *4*-QAM, *16*-QAM. *64*-QAM and *256*-QAM, who all share a quadratic symbol disposition in their constellations.

For this simulation, to realize the mapping of the symbols, it is calculated the number of OFDM symbols being transmitted. To obtain the desired constellation, there is the need to guarantee that all the positions in the In-Phase/Quadrature (IQ*)* matrix, that contains all the symbols, are filled. In case this condition is not verified, one way to work around this issue is by using zero-padding to fill in the gaps. In this simulation, however, the original random bitstream, when generated, considers this issue to guarantee that the

execution of padding is not necessary. To assure this property, special care is given when defining the number of initial bits randomly generated before encoding, N_{bits}, and the number of OFDM symbols being transmitted, N_b:

$$N_{bits} = bits_{symbol} \times k_{TCH} \tag{3.9}$$

$$N_b = \frac{N_{coding}}{N_{sc} \times bits_{symb}} \tag{3.10}$$

To guarantee the inexistence of gaps, N_b, the number of OFDM symbols/blocks, must be an integer, resulting in an *IQ* matrix with dimensions $N_b \times N_{sc}$.

Figure 3.1 exemplifies the constellations for the modulation indexes 16 and 64.

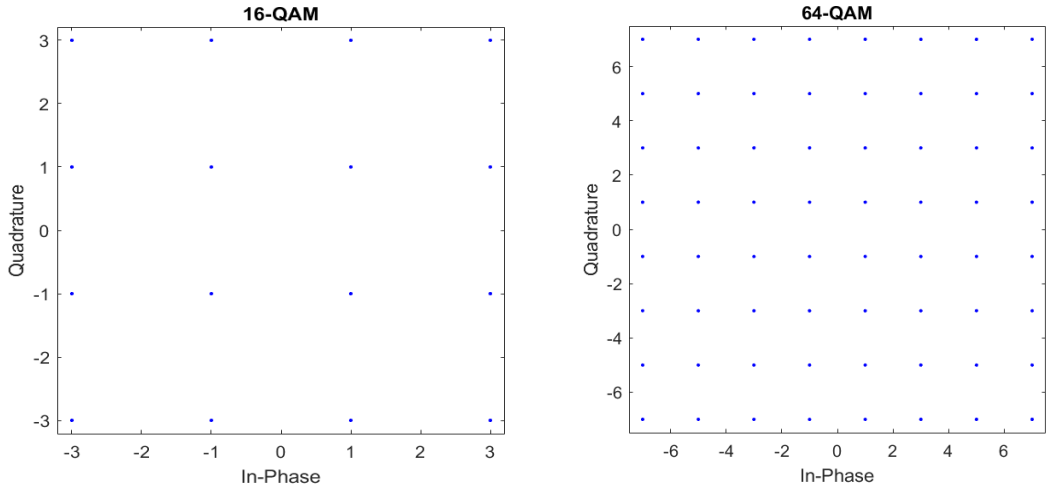

Figure 3.1 - Constellations for 16 and 64-QAM utilizing Gray mapping.

The next step to analyze is the introduction of samples. Sampling is a method that enables the reduction of the continuous-time signal to a discrete-time one, it serves has the interface between real and simulated systems. The aim of this method is to allow a reliable representation of a real signal after it is processed through different blocks. It is also noteworthy to mention that the kind of sampling method used in this simulation is Sample and Hold, which takes the voltage of a continuously varying analog signal and locks it at a constant level for a specific period.

To sample the signal, first and foremost, the number of samples per tone N_s must be defined. Since the signal varies with time, it is necessary to measure the value of the

continuous function every given interval, this interval is called the sampling interval/period. This interval can be obtained by making use of the chip time T_c:

$$T_{samp} = \frac{T_c}{N_s} \tag{3.11}$$

Inversely, the sampling frequency/rate can be determined, giving insight on the average number of samples obtained in one second:

$$f_s = \frac{1}{T_{samp}} \tag{3.12}$$

These aspects allow the computation of the number of samples representing one OFDM symbol

$$N_{s\_OFDM} = N_s \times N_T \tag{3.13}$$

and, by extension, it can be determined the total number of samples that represent the transmitted symbol:

$$N_{s\_total} = N_{s\_OFDM} \times N_b \tag{3.14}$$

In simulation terms, the total number of samples is essential to enable the formulation of both the time and frequency axes that serve as pillars for the representation of the signal.

3.1.2.2. OFDM Modulation Steps

This chapter explains the steps that affect the signal before its transmission. It is comprised of:

- Insertion of pilot symbols.
- Serial to parallel conversion and zero-padding.
- IFFT of the zero padded input.
- Insertion of the cyclic prefix.
- Digital to analog conversion.
- Filtering.
- Up-conversion.

These are illustrated in Figure 2.16, diagram A.

The importance of the insertion of pilot carriers resides in the aid of the channel estimation and is therefore explained in further detail in that chapter.

Having the pilot subcarriers established, the signal goes through a Serial to Parallel conversion where the contents are formatted into word size and then parallelly assigned to a carrier. After this process, to create some space between sampling-originated spectrum repetitions, zero padding is realized to introduce oversampling null carriers in the frequency domain. This is followed by the application of an IFFT to the signal since the remaining modulation steps occur in time domain [25].

The insertion of the cyclic prefix consists in the addition of a copy of the final part of the given OFDM symbol to the beginning of the said symbol. Figure 2.19 provides a simple illustration of this step.

This process is followed by a DAC, which is ruled by the same principles that are presented in the 3.1.2.1, when it comes to the use of sampling.

All these steps depicted in this chapter occur at the level of an OFDM symbol, meaning that this is an iterative process. After they are completed, Parallel to Serial Conversion is performed to restore the signal to the original format. The resulting Power Spectral Density (PSD) of the signal can be observed in Figure 3.2:

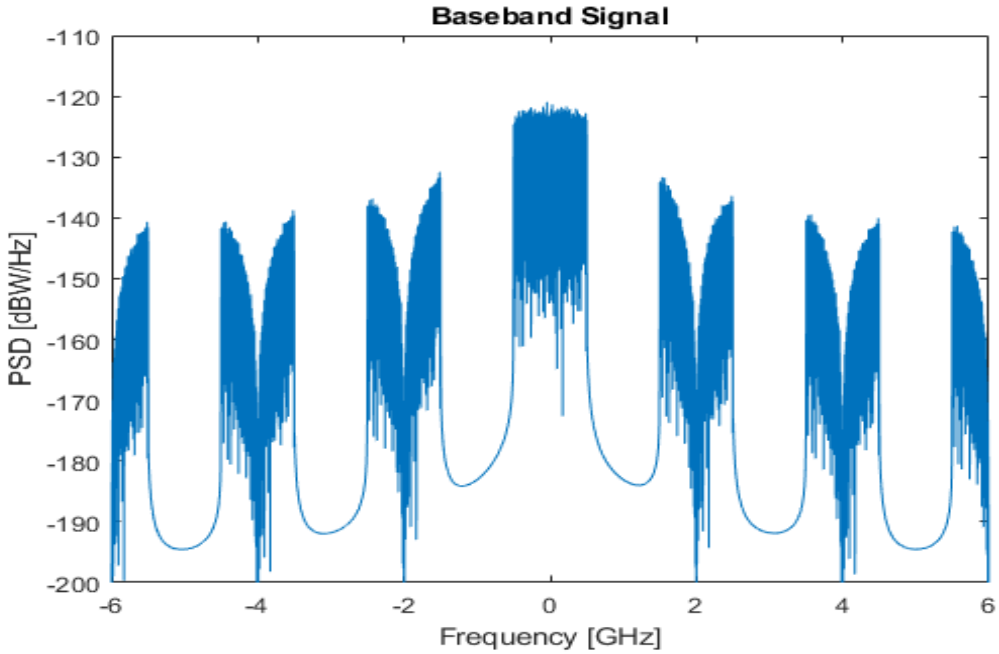

Figure 3.2 - Power spectral density of the signal after going through the modulation steps.

As can be seen, besides the main lobe that is represented in the center of Figure 3.2, it is accompanied by multiple symbol replicas that were generated from DAC. Since those are not desired for the signal transmission, there is the need to prune them away.

One way of suppressing the unwanted features in the signal is through usage of filters. Filters serve as a way of removing some components that manifest in certain frequency ranges, allowing the selection of a band that aligns with the goal of the simulation. In this work, the type of low pass filter (LPF) selected, which is a filter that allows the passage of frequencies lower than a given limiter called cutoff frequency, is an ideal rectangular filter, whose transfer function resembles the *rect* function in frequency domain. These types of filters can only be implemented in a simulated environment and are not realizable in practice. However, due to their ideal characteristics, allowing a perfect/near as perfect clearance of the aliasing components that lead to distortion of the signal, they reveal themselves as a powerful tool in simulation practices since they allow better visualization of signals, facilitating their study.

In a similar manner has is explained in [25] a range that defines which frequencies are allowed to pass and which are eliminated is established, since the entirety of the signal is wanted for transmission, the bandwidth of the filter is superior to the OFDM signal bandwidth. To realize filtering on the signal, it is required the obtention of the transfer function of the filter so it can be applied to the signal. This can be done through a convolution in time domain or a multiplication in frequency domain.

$$x_{LPF}(t)=IFFT(FFT(x_{DAC}(t))\times H_{rect}) \tag{3.15}$$

Since the filter is created in the frequency domain, and by obtaining its transfer function H_{rect}, to apply said function to the signal that is in time domain, x_{DAC}, which is the signal that resulted from the DAC process, a FFT is used to transfer it to frequency domain and, right after, an IFFT reverts the resulting filtered signal $x_{LPF}(t)$ back to time domain.

As seen in Figure 3.2, the signal is centered at 0 GHz, this means that, by defining a filter that has bandwidth B_{LPF} of 1 GHz, the filtered signal will be limited. These limits range from -B_{LPF} to B_{LPF}. In this range, the signal is untouched and keeps the same properties, while the remaining replicas are eliminated, as Figure 3.3 illustrates.

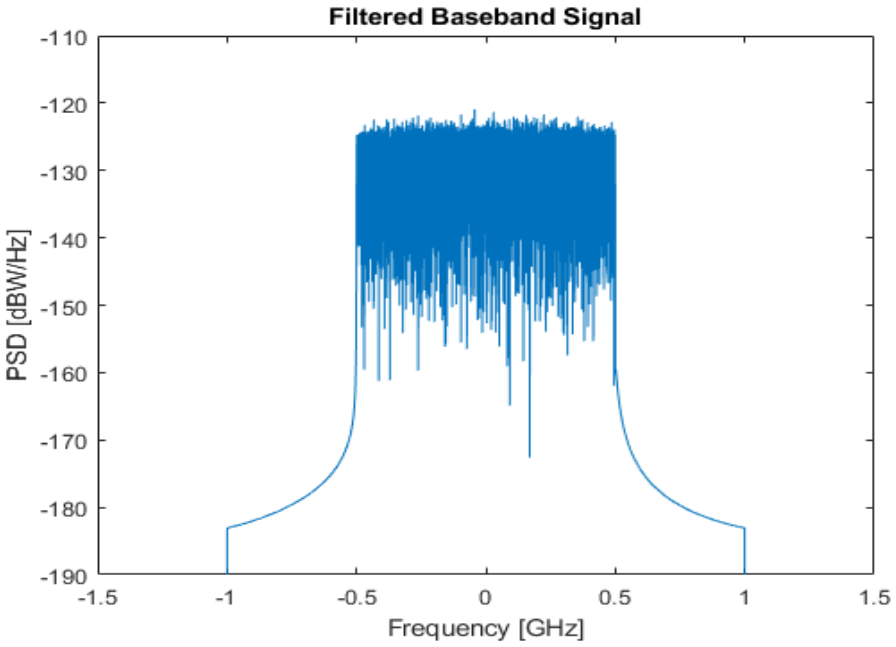

Figure 3.3 - Power spectral density of the signal after filtering with filter bandwidth B.

The final step that is fulfilled before transmission of the signal is the carrier up-conversion. Being a heterodyning technique, up-conversion is used to shift the frequency range of the signal into another. Since a LPF was used in this simulation and it is intended to shift the signal that resulted from that step, a low pass equivalent (LPE) representation is used. The aim of this representation is to translocate the current signal that is centered at 0 GHz in frequency domain to the nominal frequency f_p. This means that the signal is dislocated to the frequency ranges from $-f_p - B$ to $-f_p + B$ and from $f_p - B$ to $f_p + B$.

However, there is an important aspect to consider. To assure precision during the conversion process, the value of f_p needs to be accommodated:

$$N_p = max(t + T_s) \times f_p \tag{3.16}$$

$$f_{p\_up} = \frac{round(N_p)}{max(t + T_s)} \tag{3.17}$$

noting that N_p is the number of periods, t the time vector that represents the time domain and f_{p_up} is the resulting accommodated frequency that is used for upconverting the signal.

The next step to consider is carrier modulation. The information present in a low pass signal can be obtained as:

$$x_{LPE}(t)=A(t)e^{j\varphi(t)} \tag{3.18}$$

This formulation represents the LPE/complex envelope of the signal. To proceed with this process, the signal in (3.18) must be divided into real/in-phase (I) and imaginary/quadrature (Q) components.

$$x_{LPE}(t)=x_I(t)+jx_Q(t) \tag{3.19}$$

To perform these calculations to the simulated signal, these components can be calculated as:

$$S_{I\_up}(t)=I(t)cos(2\pi f_{p\_up}\, t) \tag{3.20}$$

$$S_{Q\_up}(t)=Q(t)sin(2\pi f_{p\_up}\, t) \tag{3.21}$$

being $S_{I\_up}(t)$ the real component of the upconverted signal and $S_{Q\_up}(t)$ the imaginary component.

To obtain the transmitted signal, equations (3.20) and (3.21) are recombined,

$$S_{tx}(t)=S_{I\_up}(t)-S_{Q\_up}(t) \tag{3.22}$$

In Figure 3.4, the upconverted signal PSD is illustrated.

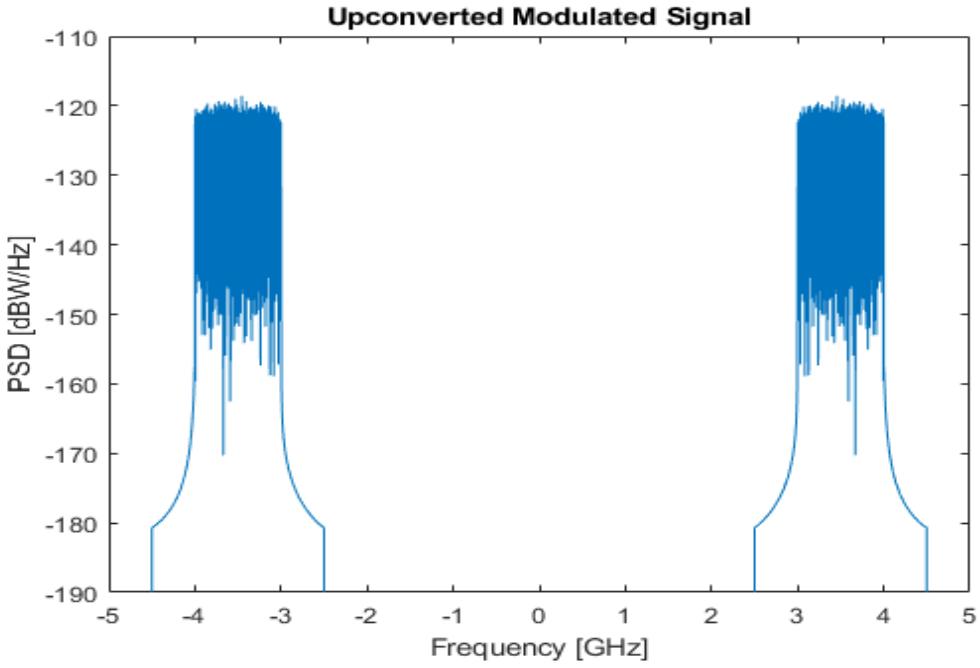

Figure 3.4 - Power spectral density of the signal after up-conversion.

In Figure 3.4 it can be observed that the signal has successfully been shifted in frequency according to the parameter f_{p_up} obtained in (3.17).

3.2. Wireless Channel

This chapter introduces the implementation of the wireless channel that is comprised in two major aspect: propagation model and channel type.

The studies of [26] and [27] present the free-space loss equation, the Friis formula. This formula (2.23) establishes a relation between power of two antennas, assuming ideal conditions for the transmission of a signal, whose use is recurrent in telecommunication systems.

$$\frac{P_r}{P_t} = D_t D_r \cdot 20 \log_{10}\left(\frac{\lambda}{4\pi d}\right) \tag{2.23}$$

The parameters involved in this formulation are the powers pertaining to the received signal P_r and the transmitted signal P_t, the directivities of both the transmitting antenna D_t, the receiving one D_r, the signal wavelength λ and the distance between antennas d.

If we assume that these antennas are isotropic, meaning that the intensity of the radiation emitted by them is omnidirectionally homogeneous, that translates as both having unitary gain. Knowing this, (2.23) can be simplified:

$$\frac{P_r}{P_t} = 20 \log_{10}\left(\frac{\lambda}{4\pi d}\right) \tag{2.24}$$

For this calculation, some parameters are required, such as the value of the distance d, that being arbitrary, and the wavelength of the signal, λ, that being:

$$\lambda = \frac{c}{f_p} \tag{3.25}$$

With these parameters, it is feasible to establish a function of the distance between antennas, derived from the (3.24):

$$f_{model}(d) = \frac{\lambda}{4\pi d} \tag{3.26}$$

As for the AWGN channel, its implementation translates into generating random gaussian coefficients with null mean and average power of 1 [25] that are added to the signal. These coefficients however are dependent on the unilateral noise PSD, N_0. To obtain this PSD through the signal to noise ratio, it can be deduced that,

$$snr = \frac{p_{signal}}{p_{noise}} = \frac{p_{signal}}{N_0 B_{en}} \tag{3.27}$$

since the PSD here represented is bilateral, then

$$N_0 = \frac{p_{signal}}{snr \times \frac{B_{en}}{2}} \tag{3.28}$$

being p_{signal} obtained by calculating the mean of the squared modulus of the baseband signal, *snr* the signal to noise ratio and B_{en} the equivalent noise band, calculated as

$$B_{en} = \int_0^{\infty} \left| \frac{H_{rect}(f)}{H_{rect}(0)} \right| df \tag{3.29}$$

The filter considered in the formulation of the B_{en} is usually the frequency response of the reception filter, however, in this simulation, the filter used for transmission of the signal is the same as the one used for reception, which is an ideal rectangular filter.

Having the noise PSD, a noise signal can now be created through generation of a vector of random coefficients $rand_{coeff}$, and by using the sampling frequency f_s, obtained in (3.12),

$$n_{AWGN}(t) = \sqrt{N_0 f_s} \times rand_{coeff} \tag{3.30}$$

as seen in Figure 3.5,

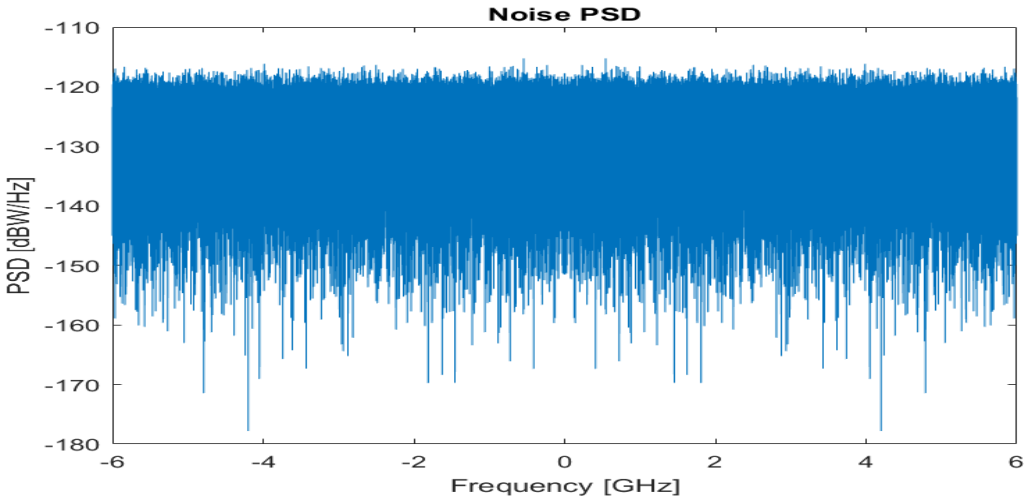

Figure 3.5 - AWGN power spectral density.

which is then added to the transmitted signal,

$$S_{AWGN}(t)=S_{tx}(t)+n_{AWGN}(t) \quad (3.31)$$

finally adding the function of propagation model, resulting in the received signal

$$S_d(t)=f_{model}(d)^2 \times S_{AWGN}(t) \quad (3.32)$$

whose PSD is illustrated in Figure 3.6.

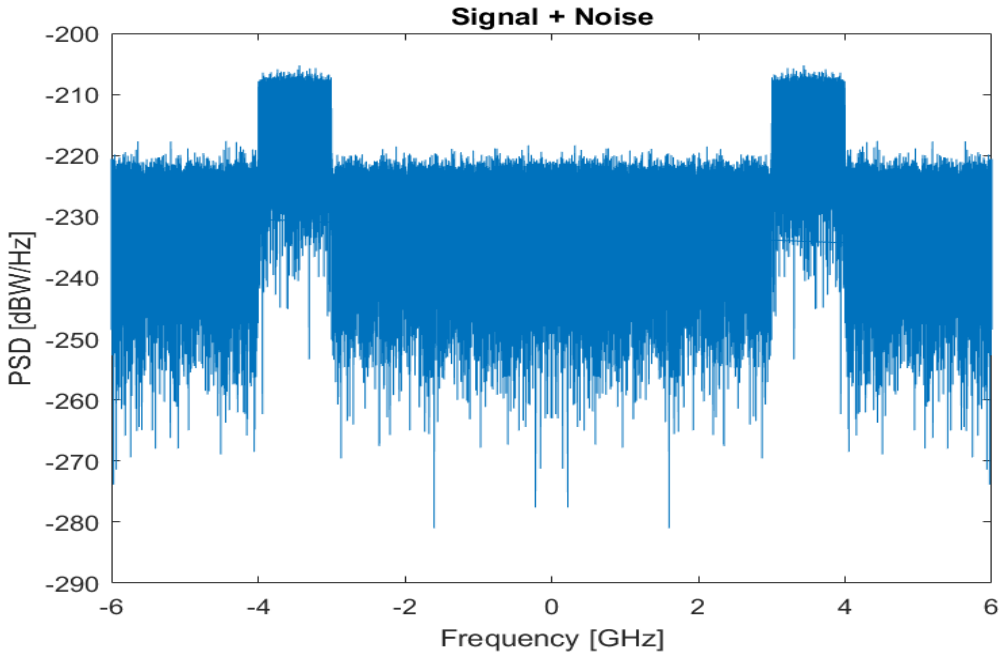

Figure 3.6 - Power spectral density of the signal after passing through the wireless channel.

In Figure 3.6, it is observable the addition of the AWGN noise shown in Figure 3.5 added to the modulated upconverted signal illustrated in Figure 3.4, which is the signal that is thereafter picked up by the receiver.

3.3. Receiver

In this chapter both the decoding, demodulation and symbol detection processes realized for the reception of the signal are explained in detail.

3.3.1. OFDM Demodulation

In contrast with the transmission, the receiver aims to recover the coded signal by applying the inverse methodology presented in the 3.2, in this section specifically, the methods presented revert the effects of the ones introduced in 3.1.2.2, such as:

- Down-conversion.
- Synchronism.

- Serial to parallel conversion.
- ADC.
- Cyclic prefix removal.
- FFT.
- Zero padding removal.

This happens so that the many alterations made to the signal are undone, while attempting to recover the signal through and through. To better understand this process, diagram B of Figure 2.16 can be referred.

3.3.1.1. OFDM Demodulation Steps

The process of down-conversion serves to relocate the received signal back into the baseband representation it previously had before the up-conversion. Like was the case with the up conversion, there is the need to divide the signal into real and imaginary components,

$$S_{I\_down}(t) = S_d(t) cos(2\pi f_{p\_up} t) \tag{3.33}$$

$$S_{Q\_down}(t) = S_d(t)(-sin(2\pi f_{p\_up} t)) \tag{3.34}$$

S_{I_down} is the real component of the down-converted signal while S_{Q_down} is the quadrature component.

To these components a rectangular filter, identical to the one presented in 3.1.2.2 is applied in the same way,

$$S_{I\_down\_filt}(t) = IFFT(FFT(S_{I\_down}(t)) \times H_{rect}) \tag{3.35}$$

$$S_{Q\_down\_filt}(t) = IFFT(FFT(S_{Q\_down}(t)) \times H_{rect}) \tag{3.36}$$

and finally, they are merged into the down-converted signal:

$$S_{rx}(t) = S_{I\_down\_filt}(t) + jS_{Q\_down\_filt}(t) \tag{3.37}$$

Given the possibility of the introduction of delays during the filtering process, to facilitate the analysis of the signal, a correlation function is used to synchronize the down-converted signal with the transmitted signal before filtering, $x_{DAC}(t)$.

After these steps, the PSD of the recovered signal is demonstrated in Figure 3.7:

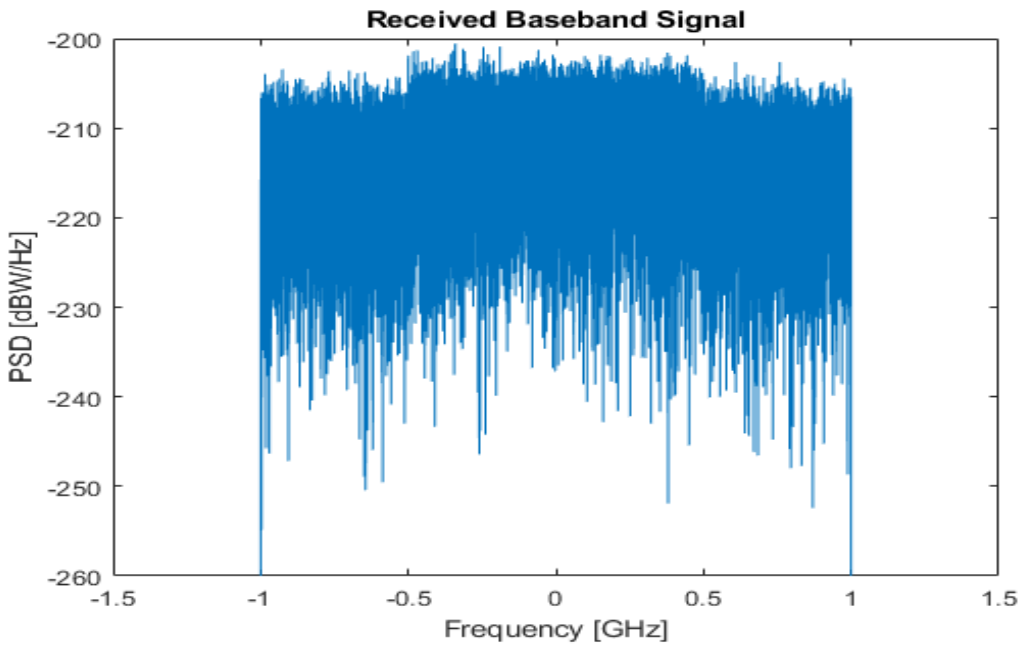

Figure 3.7 - Power spectral density of the down converted signal.

In Figure 3.7, as expected, the recovered signal corresponds to the transmitted modulated baseband signal, however, the recovered signal also has a noise component added to it due to the influence of the AWGN channel.

With the recovered baseband signal, it is possible to retrace the steps that it went through during modulation, but in this case, these are reversed so that the original coded bitstream that is being transmitted can be recovered.

The demodulation process, like the modulation one, intends to work at OFDM symbol/block level, meaning that the OFDM symbols are demodulated in a sequential manner. That said, the process begins with serial to parallel conversion.

After obtention of the OFDM symbols, ADC is realized by extracting the middle sample amidst the groups of samples in a chip.

This is followed by the removal of the CP, which consists in the elimination of the copy of the final part of the OFDM symbol that was inserted in the beginning of it, as was mentioned in 3.1.2.2.

Knowing that the remainder of the demodulation occurs in frequency domain, a FFT is realized.

To complete the demodulation, it is needed to remove the zero padding that was performed during modulation, which is the removal of the oversampling null carriers.

Hereupon, the current signal corresponds to the discrete-frequency OFDM symbols without samples [25]. Examples of demodulated constellations for the modulation index *M* of 4 and 16 are illustrated in Figure 3.8.

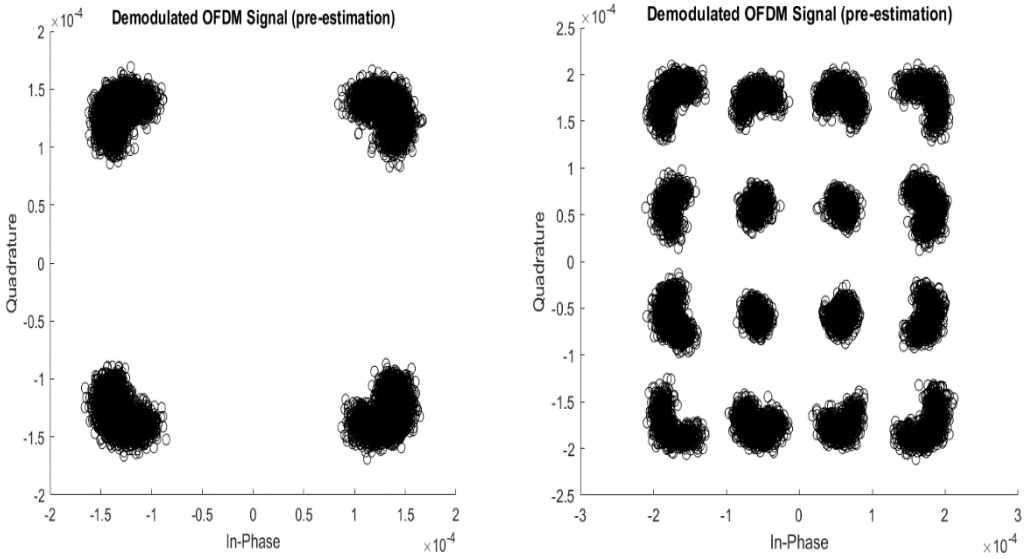

Figure 3.8 - Demodulated constellations for 4-QAM and 16-QAM before equalization.

However, the constellations presented in Figure 3.8 are still affected by the channels effects which are estimated and compensated after performing channel estimation.

By recovering the corresponding QAM symbols, the obtention of the coded bitstream is realized by demapping the constellation through the usage of a decision method.

Being the opposite of the symbol mapping presented 3.1.2.1, the demapping process consists in picking up the QAM symbols and revert them back to binary format. The decision method serves as a catalog of sorts that receives the demodulated QAM symbols and assigns them to a specified location of a given constellation. This means that, after decision, all symbols are placed under one of the original coordinates of the constellation that was initially formed in the mapping process. The method used in the simulation is hard decision, since the decision is made based on a fixed set of values (the original coordinates of the constellation).

After decision, it becomes possible to demap the QAM symbols by returning them to binary format based on their current value, resulting in the recovered coded bitstream.

3.3.1.2. Channel Estimation

Despite the demodulation, there is the need to estimate the effects of the channel and understand how they affect the signal to allow an elevated trust factor when recovering said signal.

This can be made by utilizing the pilots added in the modulation process.

As previously stated in 2.4, PSAM is used to define some already established subcarriers as pilot subcarriers. An interval between subcarriers of equivalent value is defined with the intent of determining which subcarriers will therefore be selected for the channel estimation to retrieve the original signal with as few errors as possible. It can be noted that some awareness may be required when adding/defining the pilots. It is important to guarantee that the pilots do not have the same value/do not represent the same symbol to avoid the occurrence of constructive interference in the time domain, leading to the appearance of peaks in power, subsequently rising the PAPR.

To determine the interval of values where the subcarriers in each OFDM symbol are assigned as pilots, the parameter $plt_{interval}$ is defined. Depending on the value of this parameter, subcarriers whose position is a multiple of that value are assigned as pilots. It is also important to note that, to facilitate the channel estimation, the first and final subcarriers should be assigned as pilots so that the entirety of an OFDM symbol is considered for the interpolation process.

To exemplify this aspect, knowing that in this work the total number of subcarriers in one OFDM symbol is 16000, and that $plt_{interval}$ is 8, this means that the total number of pilot subcarriers present in one symbol is $\frac{16000}{8}$=2000, plus one, since the first subcarrier is also assigned as a pilot, resulting in 2001 pilot subcarriers total. It is important to note this $plt_{interval}$ value is chosen in a way that guarantees that $N_{sc} mod(plt_{interval}) = 0$, so that there is only the need to assign the first subcarrier as a pilot, since this method assures that the final subcarrier is always assigned as a one. The value of $plt_{interval} = 8$, was selected for this work since it led to the best channel estimation results. When assigning the pilot subcarriers, it is best to use as few pilots as possible to optimize the effective data transfer rate [25], by having an interval of 8 subcarriers being assigned as pilots, this translates into having only 12,5% of the total subcarriers assigned as pilots.

The distribution of the pilot subcarriers is illustrated in Table 3.2.

Table 3.2 – Pilot subcarriers (yellow) distribution in each OFDM symbol throughout the totality of the information subcarriers (blue).

	Subcarriers												
OFDM Symbols	1	…	8	…	$\frac{N_{sc}}{2}-8$	…	$\frac{N_{sc}}{2}$	…	$\frac{N_{sc}}{2}+8$	…	$N_{sc}-8$	…	N_{sc}
	1	…	8	…	$\frac{N_{sc}}{2}-8$	…	$\frac{N_{sc}}{2}$	…	$\frac{N_{sc}}{2}+8$	…	$N_{sc}-8$	…	N_{sc}
	1	…	8	…	$\frac{N_{sc}}{2}-8$	…	$\frac{N_{sc}}{2}$	…	$\frac{N_{sc}}{2}+8$	…	$N_{sc}-8$	…	N_{sc}
	1	…	8	…	$\frac{N_{sc}}{2}-8$	…	$\frac{N_{sc}}{2}$	…	$\frac{N_{sc}}{2}+8$	…	$N_{sc}-8$	…	N_{sc}

As [25] states, the effects of pilot transmission are calculated through obtention of the quotient of both the amplitude and phase of the demodulated and original pilots. This process occurs for an established set of pilots, which are later used for interpolation and equalization purposes.

Assuming S_{pilots} as the entirety of the pilots that were defined during modulation, and S_{dem_pilots} as the very same pilots recovered after the demodulation, the transfer function of the channel can be obtained:

$$H_{ch}(f)=\frac{S_{pilots}}{S_{dem\_pilots}} \qquad (3.38)$$

Like is mentioned in 2.4, the equalization technique used in this simulation is the ZF method. Attending to the equation (2.31), to apply this equalizer, the inverse of the transfer function $H_{ZF}(f)$ is calculated,

$$H_{ZF}(f)=\frac{1}{H_{ch}(f)} \qquad (3.39)$$

Through this function, the amplitude and phase responses are obtained to be used in the interpolating process as a means of inferring the location of the QAM symbols. When done successfully, the obtention of both amplitude and phase responses of the equalized channel becomes feasible.

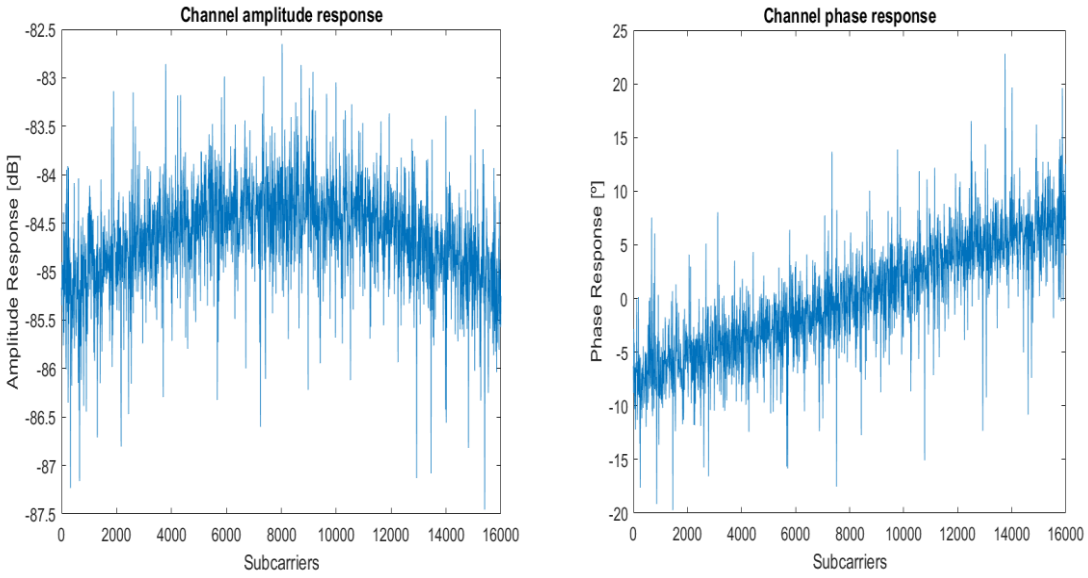

Figure 3.9 – Amplitude and phase responses of the channel.

Considering $H_{amplitude}(f)$ as the amplitude response of the equalized channel and $H_{phase}(f)$ as the phase response, those merges, forming the interpolated:

$$H_{interp}(f) = H_{amplitude}(f) \times e^{jH_{phase}(f)} \tag{3.40}$$

To realize the interpolation of these responses, an interpolating polynomial is calculated considering the position of the pilot subcarriers.

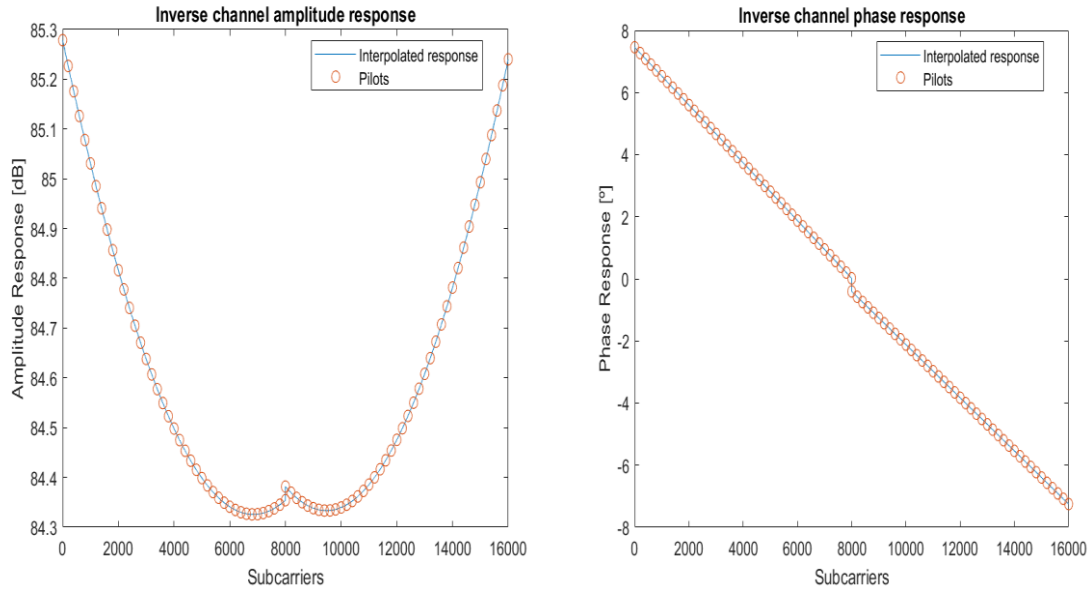

Figure 3.10 – Interpolated amplitude and phase responses of the inverse of the channel.

In Figure 3.10 the interpolated responses of the inverse of the channel are dictated by the positions of the pilots whose disposition can be determined by an interpolating

polynomial of degree two for the amplitude response and by a linear interpolating polynomial for the phase response.

Finally, the equalization is applied to the demodulated signal,

$$S_{final}=S_{dem}\times H_{interp}(f) \tag{3.41}$$

where S_{dem} represents the demodulated QAM symbols and S_{final} the estimated QAM symbols that are to be demapped and decoded on posterity.

Figure 3.11 demonstrates the recovered demodulated constellations for *4*-QAM and *16*-QAM after equalization.

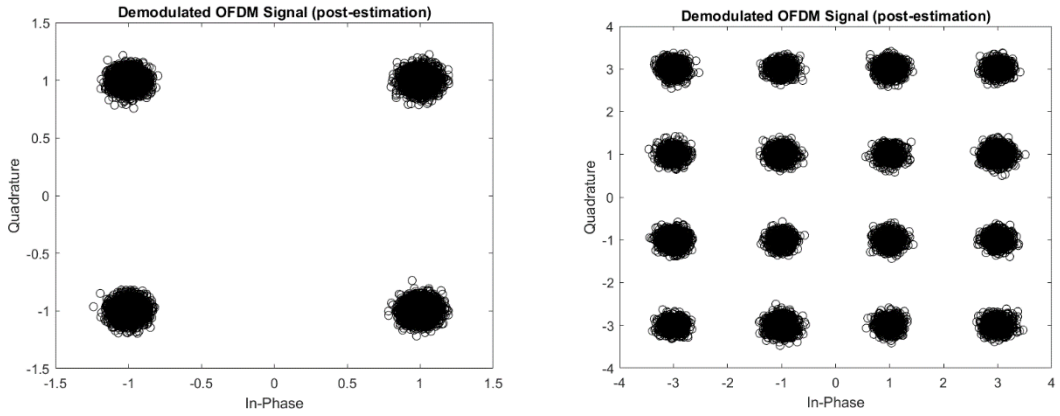

Figure 3.11 - Recovered demodulated constellations for 4-QAM and 16-QAM after equalization.

3.3.1.3. TCH Decoding

The last part of the recovery of the signal is the decoding process. By taking the result from the demodulation, all that is left is to turn the coded bitstream back into the original bitstream.

Like is explained in 2.2.1, and according to [3], the TCH decoding process is based on a bank of correlators that compare a received codeword length n_{TCH} with the various codewords of that TCH code. This comparison is made to the largest value and then decoded by implementing a straightforward conversion table containing the stored codewords complex conjugate of their spectra, making using of a FFT, a complex multiplication and an IFFT. This is exemplified in Figure 2.4.

To exemplify this process, the received coded bitstream is trimmed into codewords of length n_{TCH}. For each codeword being analyzed, a FFT is realized, followed by a

complex multiplication that makes use of the result and the spectra table, whose imaginary components are negated. An IFFT is applied to obtain values that are used for comparison in the peak and sign detector, these detected peaks are the most likely polynomial used for the integration of a given codeword, once identified, it is possible to apply the inverse method that was used in the encoding process and therefore determine the groups of information bits that created the codewords.

Figures 3.12 and 3.13 exemplify the detection of the number of shifts performed to a polynomial.

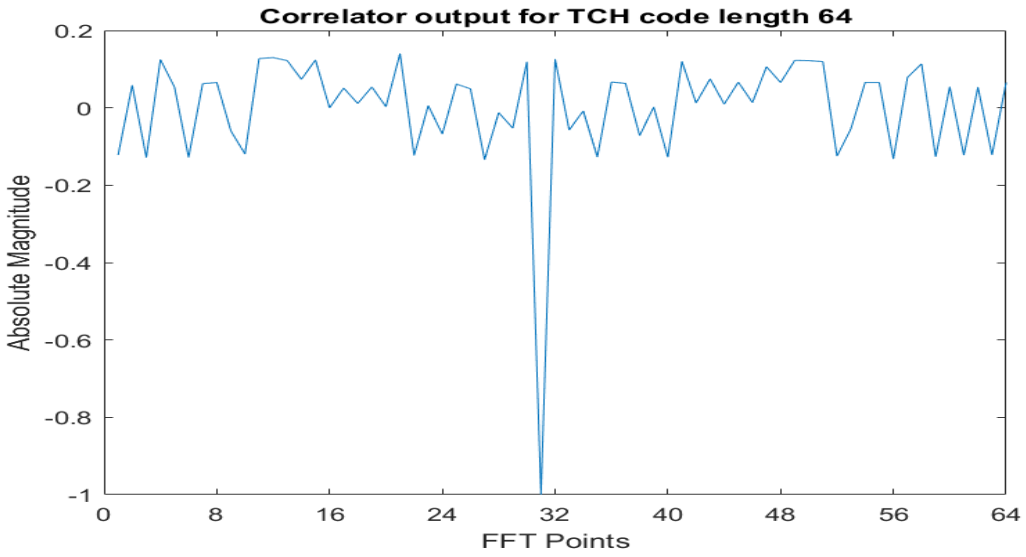

Figure 3.12 – Output of the FFT correlator for a TCH code length 64.

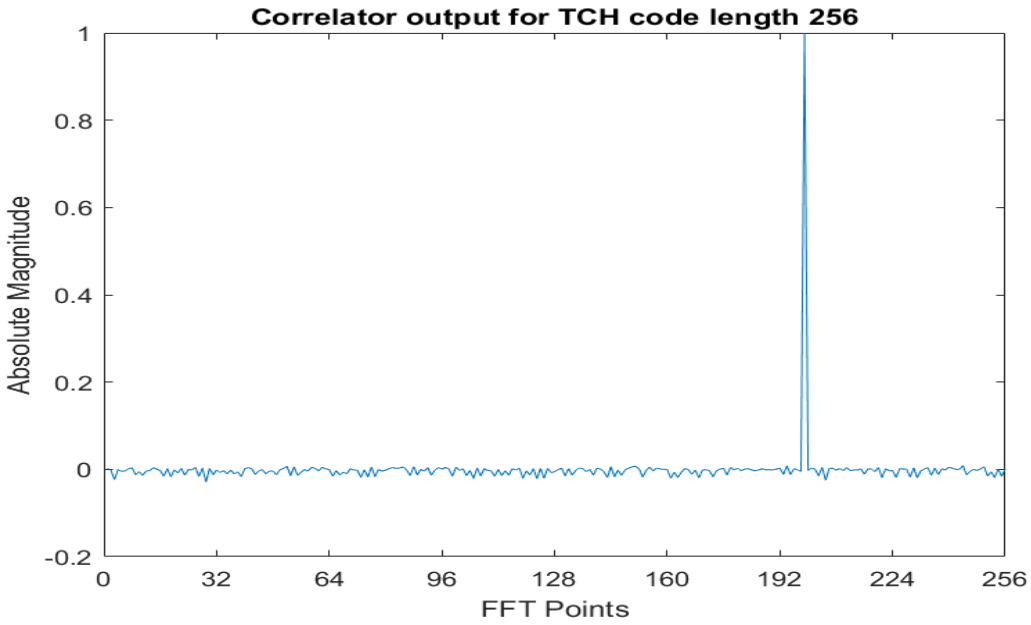

Figure 3.13 - Output of the FFT correlator for a TCH code length 256.

In these figures it can be observed that, if the correlation peak is positive, the transmitted codeword can be determined by shifting the correspondent polynomial a certain number of times equivalent to the number of FFT points that correspond to the detected peak and decode it using the spectra lookup table. Whereas for a negative correlation peak, said shifts are performed to the negation of the codeword, resulting in the total number of shifts being the FFT points for the detected peak plus the length of the code.

3.4. BER Estimation

Lastly, to evaluate the performance of the system being simulated, since the methodology used is a Monte Carlo simulation, the obtention of the BER is required.

By having recovered the bitstream, it is possible to compare it to the generated one. Since the implementation of a wireless channel that introduces noise components to the system, the occurrence of errors is to be expected. That said, the obtention of the BER ratio provides an adequate idea of the performance of the system since it weights the quantity of erred bits against the totality of the transmitted bits,

$$BER = \frac{N_{err}}{N_{tx}} \tag{3.42}$$

Since the quantity of errors obtained is dependent on the quality of the signal, meaning, the SNR, it can be assumed that, for low SNR values, the presence of noise is more notable, leading to more errors, and vice-versa, high SNR values lead to less errors. Therefore, there is the need to associate the performance of the system, the BER, to the strength/quality of the signal, making the BER a result in function of a SNR, or, in this study, in function of $\frac{E_b}{N_0}$. In [3] it is determined that:

$$\frac{E_b}{N_0} = snr \frac{B_{en}}{R_b} \tag{3.43}$$

Knowing the SNR and the code rate presented in equation (2.13), the quality of the link is formulated:

$$\frac{E_b}{N_0}[dB] = SNR[dB] + 10\log_{10}\left(\frac{B_{en}}{R_b}\right) \tag{3.44}$$

Even though this allows the obtention of $\frac{E_b}{N_0}$, there is the need to perform certain corrections:

$$\frac{E_b}{N_0}[dB]=SNR[dB]+10\,log_{10}\left(\frac{B_{en}}{R_b}\right)-10\,log_{10}(R_c)-3 \tag{3.45}$$

As for these corrections, the one made with the code rate is performed due to the encoding process that has been previously explained in 3.1.1. and the adjustment of -3 dB is due to the unilaterality of the noise component introduced in 3.2.

A common practice that enables the evaluation of the performance and accuracy of the simulation is the comparison of the simulated BER with the theoretical BER for an array of corresponding $\frac{E_b}{N_0}$ values. Since, in this case, there is not a theoretical formulation for the BER obtained from the coding process (there is, instead, an upper bound value), the theorical BER can only be obtained for the modulation process and is used for comparison with the simulated BER.

$$BER_{teo}=2\times\frac{1-\frac{1}{\sqrt{M}}}{log_2 M}\times erfc\left(\sqrt{\frac{3\times log_2\sqrt{M}}{M\text{-}1}}\times\frac{snr}{log_2 M}\right) \tag{3.46}$$

Having concluded the transmission and reception of the signal and having obtained all these parameters that allow the evaluation of the system, all conditions are reunited to perform the analysis of the results.

CHAPTER 4

Analysis and Discussion of the Results

This chapter contains the various results obtained after the realization of many simulations with varying parameters.

4.1. Simulation Parameters

Here are presented the parameters used for the simulation process and the results that come from it. These are thereafter analyzed in further detail and comparisons are established with previous similar works to verify their feasibility and seek validation.

The parameters pertaining to the simulation are displayed in Table 4.1.

Table 4.1 - Simulation Parameters.

Parameter	Value
Central frequency	3.5 GHz
Modulation Index	4, 16, 64, 256 QAM
Number of carriers/tones used for transmission	16000
Signal Bandwidth	1 GHz
Distance between antennas	1 m
Speed of light (in vacuum)	299792458 m/s
Number of samples per tone	12
Interval of symbols assigned as pilots	8
Imposed Power for transmission	0 dBm

Besides these, some other parameters can be mentioned since they define how the simulation runs.

The number of generated bits before reaching the encoder is presented in (3.9), however, to properly simulate a RF system, the amount of information being generated for the simulation must be in accordance with similar systems. This means that to correctly assess the performance of the simulation, an elevated number of bits is generated so that the resulting BER values are more accurate. Thus, a multiplier can be applied to the number of randomly generated bits, N_{bits}, to better simulate the intended scenario. Since the simulator is not optimized, the maximum multiplier that is used to determine

the length of the generated bitstream that allows the obtention of the best results is 2×10^5, meaning that the length of the generated bitstream is $N_{bits}\times2\times10^5$.

Being this a Monte Carlo simulation and since a direct-error counting (DEC) approach is considered, it can be said that this process is an iterative one, so, it will repeat itself, aiming to achieve new results each time a cycle is completed. Therefore, there is the need to define the iterations which these cycles go through. In this simulator, the SNR is the parameter that dictates the obtention of the BER values, so, to determine the range of the simulation results, an interval of SNR values is defined. This interval of SNR values varies in compliance with the usage of coding and/or modulation.

Knowing that the simulation in this work performs both coding and modulation of a given signal, these two major aspects can be analyzed individually before considering their joint effects to better understand their role and impact in the results of the simulation.

4.2. Coding Results

Here are presented the results obtained after realizing the encoding and decoding process by using TCH codes with different lengths in junction with BPSK modulation. In this scenario, OFDM modulation is not used.

The TCH codes used in the simulation can be consulted in Table 3.1. These codes are used in this simulation due to their simple implementation.

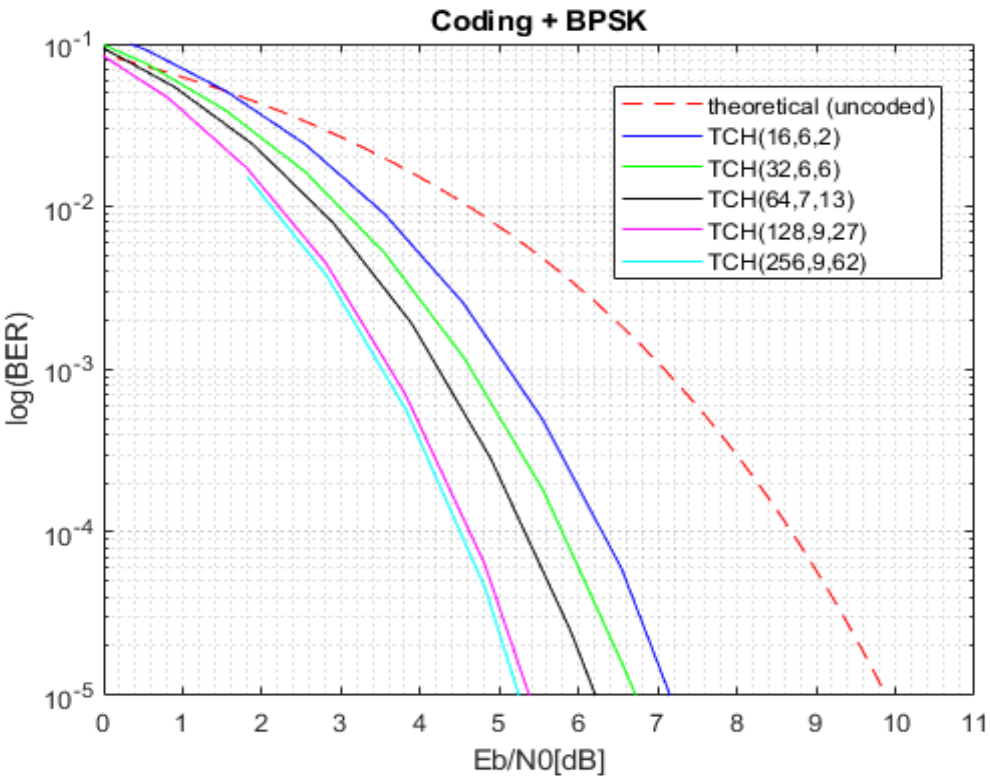

Figure 4.1 - BER results obtained from the coding process for various TCH codes.

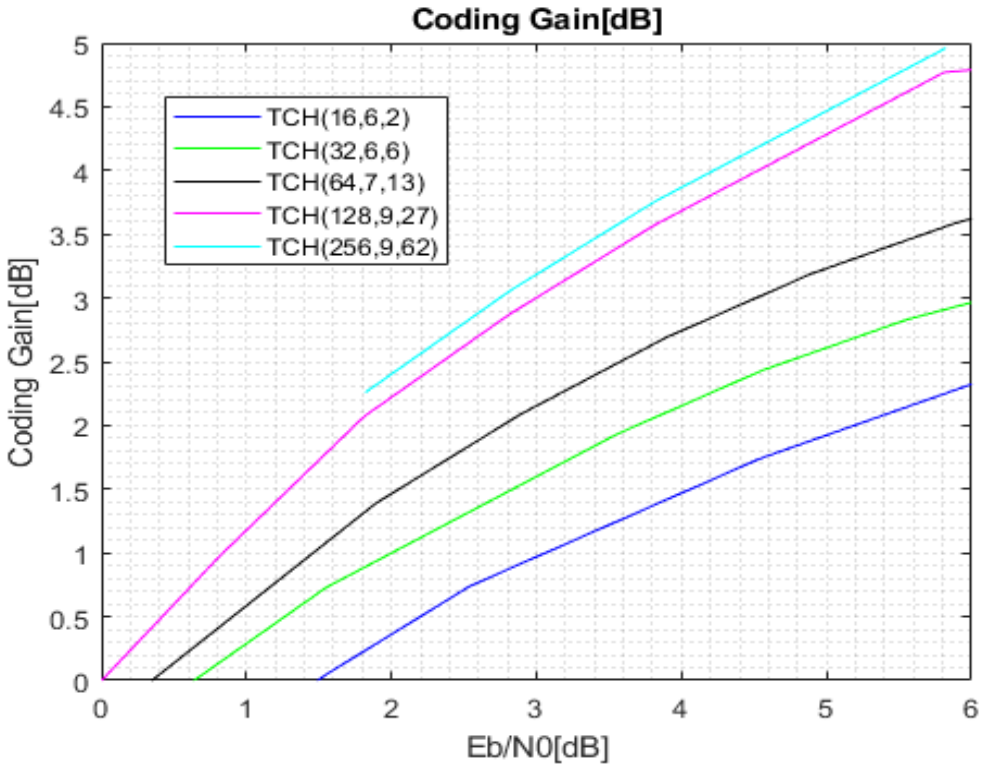

Figure 4.2 - Coding gains obtained from the coding process for various TCH codes.

In Figure 4.1 it is represented the BER curves that result from the coding process. These results include the theoretical BPSK uncoded BER and five different curves for the

resulting BER of each simulated TCH code length. In Figure 4.2 the coding gain of each code is calculated.

To obtain the results of the coding gain shown in Figure 4.2, the $\frac{E_b}{N_0}$ of the uncoded BER curve is compared to the $\frac{E_b}{N_0}$ obtained after the simulation for each code. This aspect is important to better understand how these codes compare to each other and how they improve the recovery of the signal.

By observing Figure 4.1 it can be noted that with the increase of the $\frac{E_b}{N_0}$ (or SNR) ratio, the quality of the signal over the noise effects improves, thus reducing the number of errors detected with each cycle, therefore reducing the value of the BER. It can also be noted that, for TCH codes of higher length, the obtained BER values decrease at a higher rate, allowing the obtention of the same BER for lesser $\frac{E_b}{N_0}$ values. This decrease is expected because even though the number of coded bits increases with the length n_{TCH} of the code, the correcting capacity also increases.

By taking this information into account, in Figure 4.2 it is shown that the increase of $\frac{E_b}{N_0}$ leads to higher coding gains which is also to be expected since a code with higher coding gain shows a faster decrease of BER values

Table 4.2 shows the approximate $\frac{E_b}{N_0}$ values simulated for the uncoded BPSK theoretical curve, and the TCH codes length 16, 32, 64, 128 and 256 and compares them with the ones obtained by [3] in 2.2.2.

Table 4.2 - $\frac{E_b}{N_0}$ values obtained for various n_{TCH} code lengths with BPSK modulation.

TCH Codes	**$\frac{E_b}{N_0}$[dB] $@log_{10} BER = 10^{-5}$ [3]**	**Coding gain@5.8 dB [3]**	**$\frac{E_b}{N_0}$[dB] $@log_{10} BER = 10^{-5}$ (simulated)**	**Coding gain@5.8 dB (simulated)**
TCH(16,6,2)	7.5	1.4	7.2	2.4
TCH(32,6,6)	6.8	2.4	6.8	2.8
TCH(64,7,13)	6.3	2.9	6.2	3.6
TCH(128,9,27)	5.5	4.2	5.4	4.8
TCH(256,9,62)	5.1	4.9	5.2	5.0

These results show some deviation from the ones obtained by [3] but seem to be fairly close. They allow a better understanding on how the coding affects the simulation. It can be observed that the use of various TCH code lengths affects the coding gain, enabling a way of improving the recovery of signal subjected to noise components, since the resulting signal will have reduced $\frac{E_b}{N_0}$ for the same BER in comparison with the uncoded counterpart, meaning that less power is required to achieve the same number of errors during transmission.

4.3. Modulation Results

To facilitate the analysis of the simulation results, besides coding, it is likewise important to understand how the modulation process affects them. The results here illustrated were obtained for the following modulation indexes *M*=4, 16, 64 and 256-QAM.

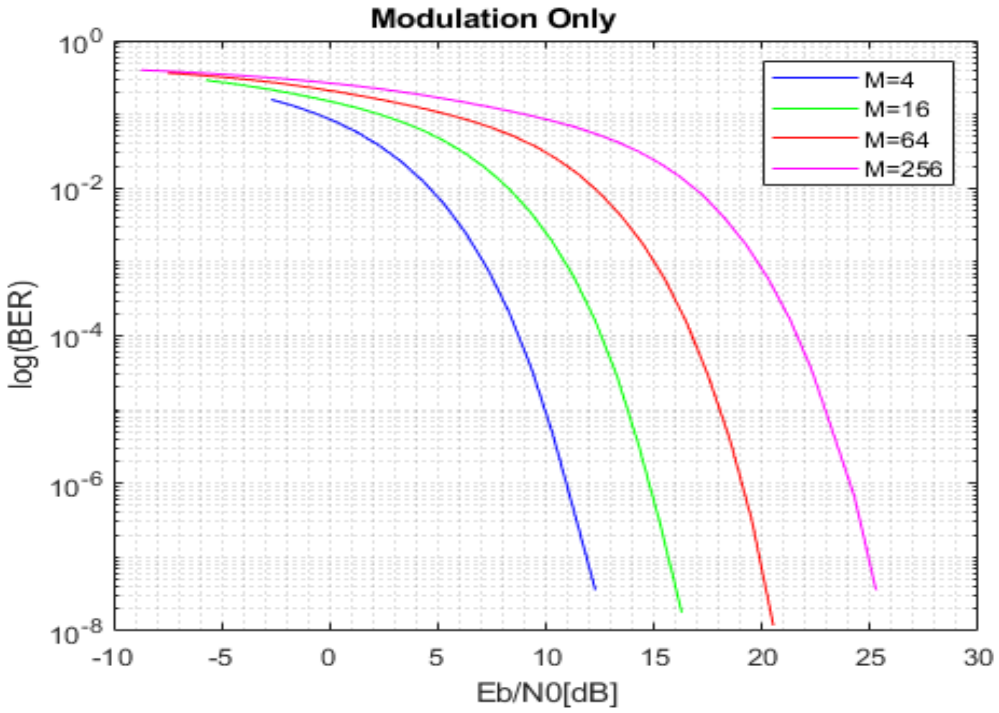

Figure 4.3 - BER results in function of $\frac{E_b}{N_0}$ for the QAM modulation indexes M=4, 16, 64 and 256.

To validate these results, a parallel to Figure 2.20 can be made. By making a side-by-side comparison of the $\frac{E_b}{N_0}$ values for a given $log_{10} BER$ in both figures, the similarities in them becomes noticeable.

Table 4.3 shows the simulated $\frac{E_b}{N_0}$ values for the modulation indexes displayed in Figure 4.3 for the value $log_{10} BER$ of 10^{-5}.

Table 4.3 - $\frac{E_b}{N_0}$ values obtained for various modulation indexes.

Modulation Index	$\frac{E_b}{N_0}$**[dB]** $@log_{10} BER = 10^{-5}$
4-QAM	10
16-QAM	14
64-QAM	18
256-QAM	23

By comparing these results to the ones shown in Figure 2.20 it can be assumed that the modulation process is being correctly simulated.

It is important to note that, alongside the increment of the modulation index, the range of $\frac{E_b}{N_0}$ values also increase. These happens because for higher modulation indexes, the distance between QAM symbols in the constellation becomes smaller, therefore there is a higher demand of energy to obtain the same error probability.

The curves in Figure 4.3 are expected to equate to their theoretical *M*-QAM counterpart, meaning that, when making use of the formula presented (3.46), the resulting simulated BER curves ought to be the same as the theoretical ones.

4.4. Coding and Modulation Results

Having the effects of the coding and the modulation processes analyzed individually, the results obtained from using both are hereby presented. Like in 4.2 and 4.3, these are simulated for various TCH code lengths and modulation indexes presented in them, however, due to an undetermined reason, the resulting curves for the TCH code length 16 do not show the results that are to be expected since they do not seem to behave like the other code lengths do.

The best results obtained through simulation, considering the length of the initial bitstream mentioned in 4.1, were for the modulation indexes of 16, 64 and 256-QAM, having the first index reach a value of $log_{10} BER = 10^{-4}$ and the other two reaching

$log_{10} BER = 10^{-5}$. The corresponding approximate $\frac{E_b}{N_0}$ values and coding gains are also presented.

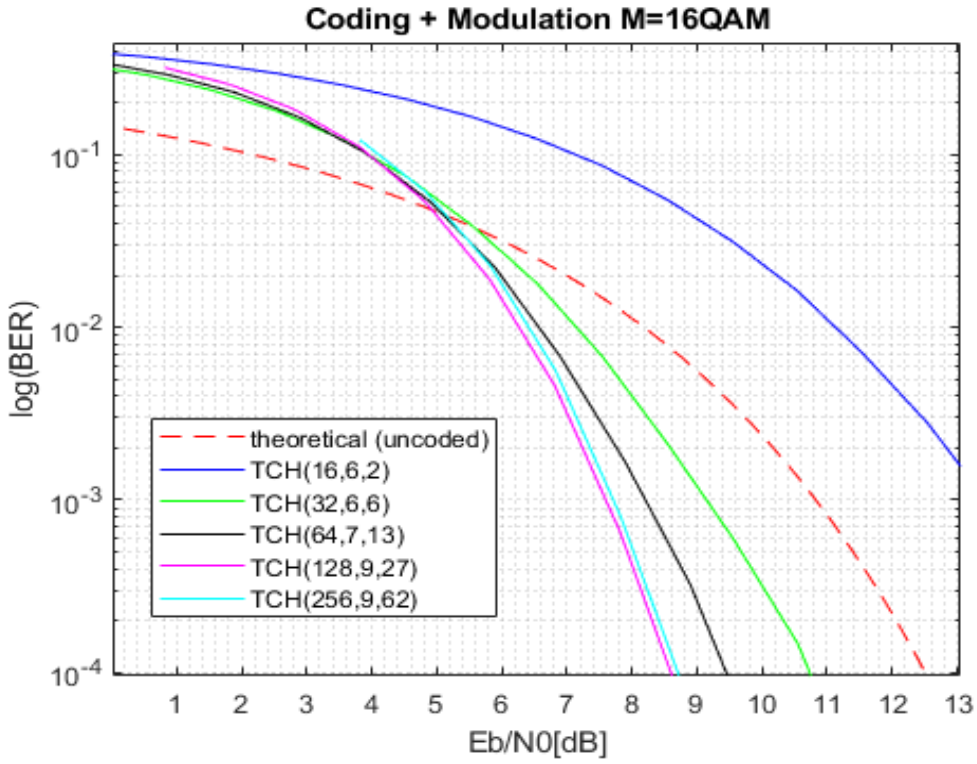

Figure 4.4 - BER results in function of $\frac{E_b}{N_0}$ for 16-QAM with TCH codes.

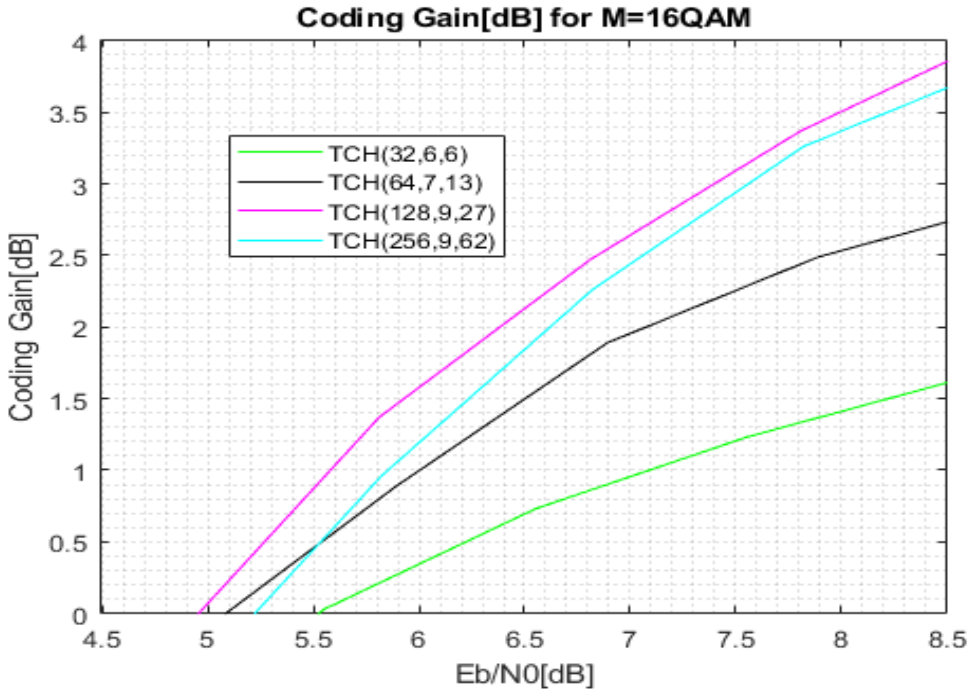

Figure 4.5 - Coding gain results in function of $\frac{E_b}{N_0}$ for 16-QAM with TCH codes.

Table 4.4 - Simulated coding gains for each TCH code length for 16-QAM.

TCH Codes	$\frac{E_b}{N_0}$**[dB]** $@log_{10} BER = 10^{-4}$	**Coding gain@8.5 dB**
TCH(32,6,6)	10.8	1.6
TCH(64,7,13)	9.5	2.7
TCH(128,9,27)	8.6	3.8
TCH(256,9,62)	8.7	3.7

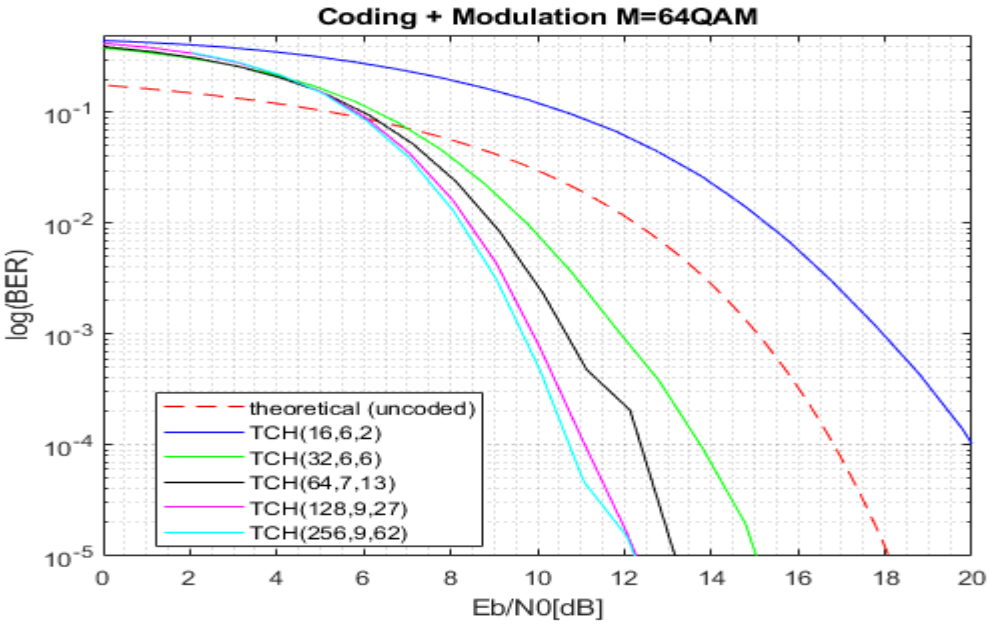

Figure 4.6 - BER results in function of $\frac{E_b}{N_0}$ *for 64-QAM with TCH codes.*

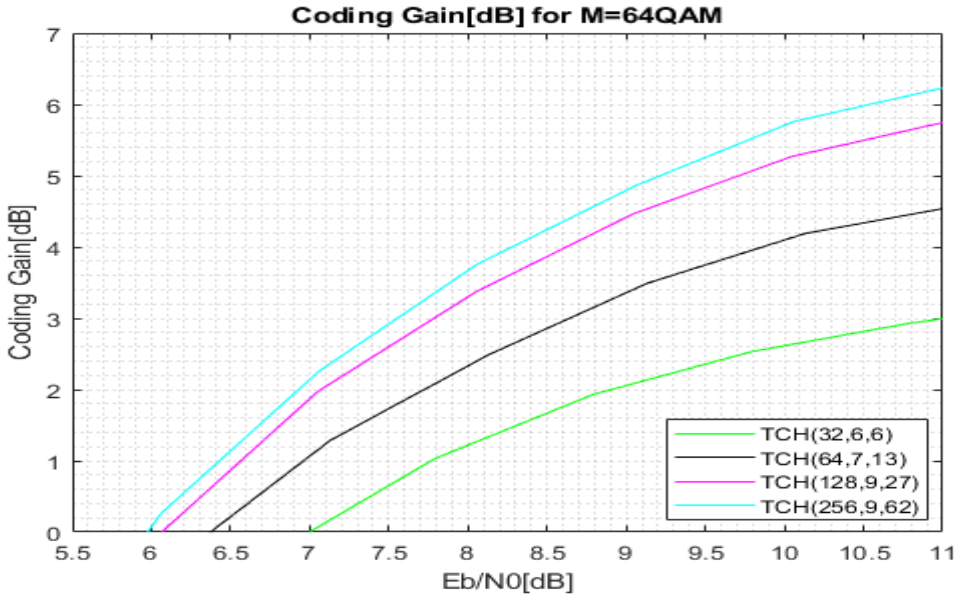

Figure 4.7 - Coding gain results in function of $\frac{E_b}{N_0}$ *for 64-QAM with TCH codes.*

Table 4.5 - Simulated coding gains for each TCH code length for 64-QAM.

TCH Codes	$\frac{E_b}{N_0}$**[dB]** $@log_{10} BER = 10^{-5}$	**Coding gain@11 dB**
TCH(32,6,6)	15.0	3.0
TCH(64,7,13)	13.0	4.5
TCH(128,9,27)	12.5	5.8
TCH(256,9,62)	12.5	6.2

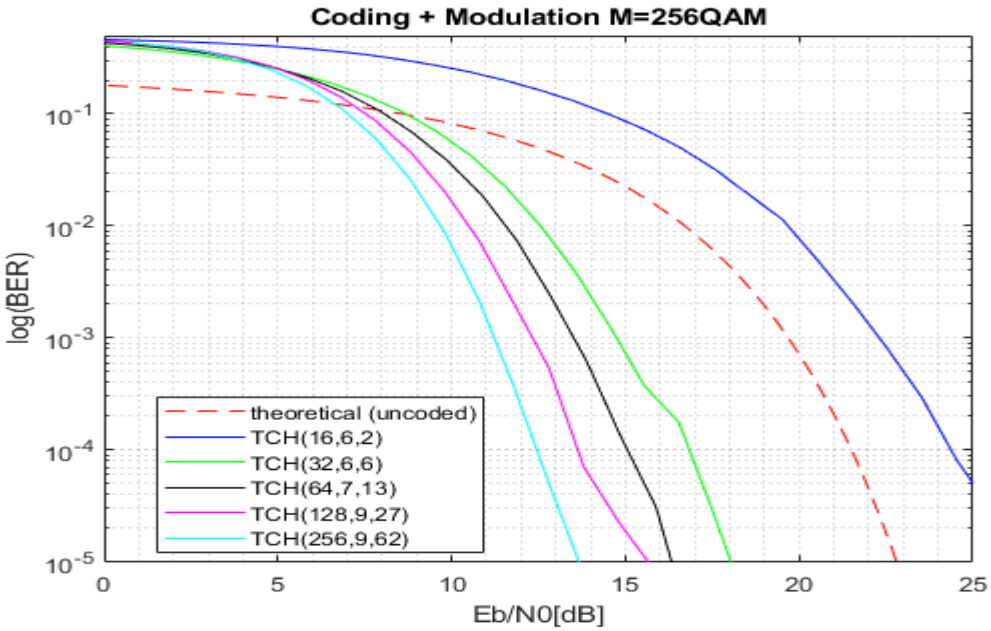

Figure 4.8 - BER results in function of $\frac{E_b}{N_0}$ *for 256-QAM with TCH codes.*

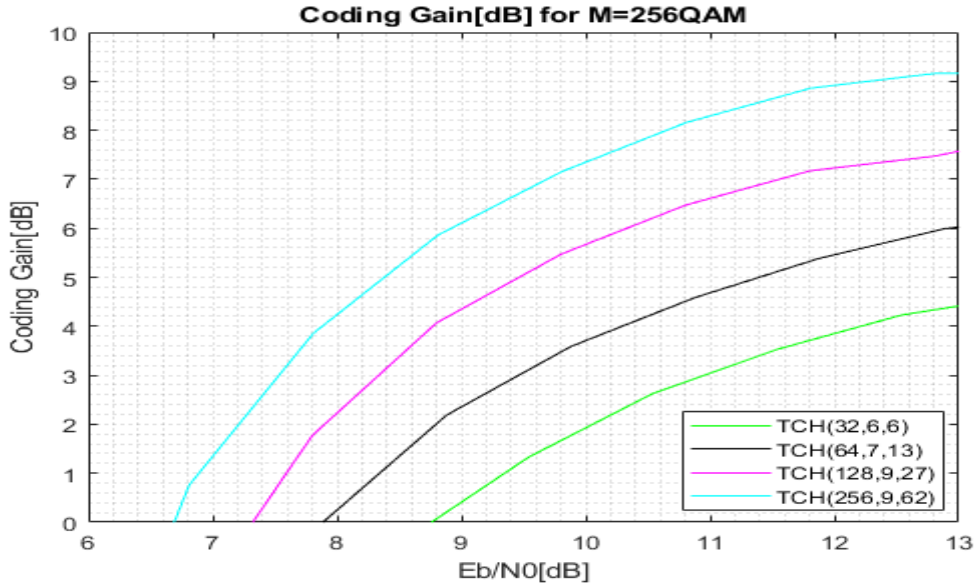

Figure 4.9 - Coding gain results in function of $\frac{E_b}{N_0}$ *for 256-QAM with TCH codes.*

Table 4.6 - Simulated coding gains for each TCH code length for 256-QAM.

TCH Codes	$\frac{E_b}{N_0}$**[dB] @**$log_{10} BER = 10^{-5}$	**Coding gain@13 dB**
TCH(32,6,6)	18.0	4.6
TCH(64,7,13)	16.5	6.0
TCH(128,9,27)	16.0	7.6
TCH(256,9,62)	13.5	9.2

Figure 4.4, 4.6 and 4.8 illustrate the resulting BER curves in function of the SNR while in Figure 4.5, 4.7 and 4.9 illustrate the coding gains for each code length. Tables 4.4, 4.5 and 4.6 reveal the estimated $\frac{E_b}{N_0}$ results for a given BER and coding gain for each code length and modulation index.

It can be observed that, as expected, by applying the TCH codes to an OFDM signal, to obtain a certain $log_{10} BER$, the higher the code length, the lesser are the required $\frac{E_b}{N_0}$ values. This aspect may not be verified in its entirety for the 16-QAM results due to the reduced number of bits being simulated for that scenario.

CHAPTER 5

Conclusions

This final chapter presents the conclusions of the realized study considering aspects mentioned in earlier chapters and using them to further analyze and criticize the results obtained in 4. The limitations that surged while performing the study and proposals for future work are also presented.

5.1. Main conclusions

The main objective of this work is to simulate and implement a RF communications system using TCH codes of different lengths to study the benefits and limitations of a receiver by performing channel estimation. To that end, an OFDM signal was generated and various TCH codes were applied to it.

To make sure that the simulation was working properly, the coding and modulation processes were analyzed separately, so that their role could be better understood.

It was tested how the use of these codes improve the overall system given their correcting capability. This aspect was observed in chapter 4, since the number of recovered errors seems to decrease in accordance with the code length.

Through analysis of the results, it can be inferred that the application of TCH codes to an OFDM signal, especially to higher modulation indexes, seems to be a viable way of improving the reception of the signal. Since higher modulation indexes generate more symbols, these, when grouped and placed in accordance with their corresponding constellation mapping, the spacing between them is reduced, leading to a higher occurrence of erred recovered bits. This means that the implementation of TCH codes is a viable solution to reduce the BER, especially when applying codes of increased length since these have higher correcting capacities, therefore leading to higher coding gains, minding that lower $\frac{E_b}{N_0}$ values are required to obtain the same $log_{10} BER$.

With this information, it is concluded that the employment of TCH codes on RF signals, more specifically, paired with OFDM modulation used in broadband communications, is a good method of improving the quality of the received signal. This

aspect leads to the belief that the use of TCH codes appears to be advantageous in similar applications and IoT environments.

5.2. Limitations of the study

Originally, besides the implementation of a simulation, the realization of an experimental study was also intended for the sake of comparison of the simulated results with realistic ones to determine the true performance of the developed system. However, due to time limitations, this step was disregarded for this study.

This chapter intends to present some of the major predicaments and limitations that were found:

- The QAM-mapping process, even though it allows the realization of some of the most common *M*-QAM modulations, it does not allow the implementation of some modulation indexes, such as 2-QAM/BPSK and 128-QAM. This may be the case since the implemented QAM-mapping technique is optimized for the creation of constellations with a quadratic pattern (meaning that the disposition of the constellation is squared).
- As can be seen in in 4.4, the results for the TCH code length 16 do not show the expected behavior compared to the other codes, even though this curve is subjected to the same processes as the others are. The reason of this abnormality was undetected.
- The way the simulator was implemented is not optimized. Due to its structure, the consumption of memory is aggravated, not allowing the generation of more than $N_{bits} \times 2 \times 10^5$, as mentioned in 4.1. Specifically, the modulation process may be poorer optimized compared to the coding one since some key variables used throughout this process already have an exceedingly high memory consumption. This can be observed, for instance, in the results obtained for 16-QAM especially for the code length 256, due to the reduced number of bits being generated in that scenario, the resulting BER curves and respective coding gains do not have a behavior as consistent as the others that were obtained for higher modulation indexes.

5.3. Proposals for future investigation

To further improve on the work presented in this study some suggestions are made:

- Reconstruct the simulator in favor of improving the structure. Discern what may be the best way to optimize the consumption of memory so that the number of bits being generated can be increased, therefore leading to better and more accurate results.
- Optimize the QAM-mapping so that more mapping architypes can be implemented and, possibly, study other types of OFDM technologies.
- Realize an experimental study of this system so that the simulated work can be further scrutinized, its true performance can be truly comprehended and assort the feasibility of the implementation of said system in present-day RF communications and IoT environments.

Bibliography

[1] A. Ijaz *et al.*, "Enabling Massive IoT in 5G and beyond Systems: PHY Radio Frame Design Considerations," *IEEE Access*, vol. 4, pp. 3322–3339, 2016.

[2] M. S. Alouini, "Paving the way towards 5G wireless communication networks," pp. 1–1, 2018.

[3] F. A. B. Cercas, "A new family of codes for simple receiver implementation," Ph. D. Thesis, Technical University of Lisbon, Instituto Superior Técnico, Lisbon, 1996.

[4] C. E. Shannon, "A Mathematical Theory of Communication", Bell Syst. Tech. J., 27, pp. 379-423(Part I), 623-656(Part II), July 1948.

[5] W. Shieh and I. Djordjevic, Orthogonal Frequency Division Multiplexing for Optical Communications. Elsevier Science Publishing Co Inc, 2010.

[6] R. R. Mosier and R. G. Clabaugh, Kineplex, a bandwidth-efficient binary transmission system. AIEE Trans 1958;76:723–8.

[7] M. S. Zimmerman and A. L. Kirsch, AN/GSC-10 (KATHRYN) variable rate data modem for HF radio. AIEE Trans 1960;79:248–55.

[8] J. M. Tang , P. M. Lane and K. A. Shore, High-speed transmission of adaptively modulated optical OFDM signals over multimode fibers using directly modulated DFBs. J Lightwave Technol 2006;24:429–41.

[9] S. B. Weinsten and P. M. Ebert, Data transmission by frequency-division multiplexing using the discrete Fourier transform. IEEE Trans Commun 1971;19:628–34.

[10] P. Duhamel and H. Hollmann, Split-radix FFT algorithm. IET Elect Lett 1984;20:14–6.

[11] S. Hara and R. Prasad, Multicarrier Techniques for 4G Mobile Communications. Boston: Artech House; 2003.

[12] L. Hanzo, et al., OFDM and MC-CDMA for Broadband Multi-User Communications, WLANs and Broadcasting. New York: Wiley; 2003.

[13] B. Saltzberg. Performance of an efficient parallel data transmission system. IEEE Transactions on Communication Technology, 15(6):805–811, 1967.

[14] C. K. Ho, B. F. Boroujeny and F. Chin, Added pilot semi-blind channel estimation scheme for OFDM in fading channels. In Global Telecommunications Conference, 2001. GLOBECOM'01. IEEE, volume 5, pages 3075–3079. IEEE, 2001.

[15] R. V. Nee *et al.*, New high-rate wireless LAN standards. IEEE Communications Magazine, 37(12):82–88, 1999.

[16] R. V. Nee and R. Prasad, OFDM for Wireless Multimedia Communications. Artech House, Inc., Norwood, MA, USA, 1st edition, 2000.

[17] R. V. Nee, A New OFDM Standard for High Rate Wireless Lan in the 5 GHz Band. Signal Processing, pages 258–262, 1999.

[18] B. Miguel and D. C. Lopes, “Channel Estimation with TCH Codes for Machine-Type Communications”. October, 2017.

[19] C. Salema, Feixes Hertzianos, 4th ed. – Lisboa: IST Press, 2019, p. 320.

[20] X. Ma, G.B. Giannakis and S. Ohno, Optimal training for block transmissions over doubly selective wireless fading channels. IEEE Transactions on Signal Processing, 51(5):1351–1366, 2003.

[21] Y. Li, Pilot-symbol-aided channel estimation for OFDM in wireless systems. IEEE transactions on vehicular technology, 49(4):1207–1215, 2000.

[22] C. T. Lam *et al.*, Channel estimation for SC-FDE systems using frequency domain multiplexed pilots. In Vehicular Technology Conference, 2006. VTC-2006 Fall. 2006 IEEE 64th, pages 1–5. IEEE, 2006.

[23] Y. Zeng and T. Sang, Pilot cyclic prefixed single carrier communication: Channel estimation and equalization. IEEE Signal Processing Letters, 12(1):56–59, 2005.

[24] M. M. Silva et al., Transmission techniques for emergent multicast and broadcast systems. CRC Press, 2010.

[25] D. Mendes, “Study and Implementation of an Advanced Transceiver for 5G”. October, 2019.

[26] O. Landron *et al.*, A Comparison of Theoretical and Empirical Reflection Coefficients for Typical Exterior Wall Surfaces in a Mobile Radio Environment. 44(3), 1996.

[27] C. Sommer, S. Joerer and F. Dressler, On the Applicability of Two-Ray Path Loss Models for Vehicular Network Simulation. 2012 IEEE Vehicular Networking Conference (VNC), pages 64-69, 2012.

Appendix A

This section contains a paper that summarizes the work realized in this dissertation. Some of the contents from the literature review and methodology are highlighted and the results obtained through simulation are depicted.

Study and implementation of a low complexity receiver using TCH Codes

João Oliveira, Francisco Cercas, Tiago Alves
ISCTE-IUL
Av. das Forças Armadas, Lisboa,
Portugal
jacoa@iscte-iul.pt,
francisco.cercas@iscte-iul.pt,
tiago.manuel.alves@iscte-iul.pt

***Abstract*— In this paper an investigation on the usage of TCH codes, their properties, advantages, and disadvantages are presented. To test these properties, the simulation of an OFDM signal is realized, being subjected to noise components introduced by a wireless AWGN channel, considering a free path propagation model. By performing channel estimation, the BER and coding gains resulting from the application of various TCH codes are analyzed. Results were obtained for the modulation indexes of 16, 64 and 256 QAM.**

Keywords*— *TCH codes, OFDM, AWGN, channel estimation, BER, QAM.

I. INTRODUCTION

In order to provide better services, equipment and infrastructures, modern wireless communication systems, such as Fifth Generation (5G), were developed in order to cope with several challenges imposed by many aspects such as services, device classes, deployment types, environments and mobility levels, proposing some improvements in capacity/user-rates, latency, reliability, coverage, mobility, massive number of devices and cost/energy consumption [1], focusing mainly on the Internet of Things (IoT), an environment that features "(…) small data packets, massive connections of devices with limited power source, and delay tolerant communication." [1, p. 3323]

In short, modern wireless communication networks fulfill several pre-requisites, such as higher data rates, lower latency and massive connectivity that address various problems related to radiofrequency (RF) spectrum exhaustion. This leads to the development of new techniques such as massive multiple input multiple output (MIMO) systems in order to improve spectral efficiency at the link and network layers and to better utilize the unregulated bandwidth [2].

Considering this, the simulation of an Orthogonal Frequency Division Multiplexing (OFDM) signal is depicted, using Tomlinson, Cercas and Hughes (TCH) codes to determine the performance of the system and whether it is a viable solution for broadband applications and IoT environments. Various TCH codes with different sizes are implemented to study the advantages and limitations of the receiver by analyzing its performance after performing channel estimation and obtention of the Bit Error Rate (BER).

This paper is divided in: Section I that provides context to the theme of the study and explains it is approached, Section II explains the generation of TCH Sequences and their main properties, Section III presents the mathematical arrangement of an OFDM signal and some important inherent aspects, Section IV portrays the steps involved in the simulation, Section V shows the results of the simulation and lastly, Section VI, contains the main conclusions made through observation and analysis of these results.

II. TCH CODES

TCH codes provide a performance like other existing codes, however they have lesser complexity on the receiver. Due to their correlation properties and good coding gain, the same code words can be used to simultaneously correct errors in the channel, perform its estimation and to warrant synchronism. These codes seek to improve performance through a simplified structure to aid the development of robust applications with low latency in various domains, such as IoT and modern networks. Some of the characteristics of these codes are appropriateness for communications, mainly when those are performed in environments with unfavorable conditions, such as Doppler effects and reflections; nonlinear, non-systematic cyclic properties; use of transform techniques like Fast Fourier Transform (FFT); solid sizes, correcting and correlation performance [3].

TCH codes are a class of block codes with length n_{TCH}, where $n_{TCH}=2^m$, with $m \in \mathbb{N}$, that were found based on finite field theory. These codes have the advantage of being easy to implement on the receiver by using maximum-likelihood decoders with banks of correlators that use transform techniques like FFT, while attempting to maintain a low quantity of correlators. These codes are also nonlinear, since the linear addition modulo 2 of two codewords does not necessarily creates a valid result, and each of these is a block code undergoing continuous cyclic shifts, excluding the all-zero codeword [3].

In [3], TCH codes are defined by Base Polynomials $P_i(x)$, with input blocks with a given number of data bits, k_{TCH}, and a correcting capacity, t_{cap},

$$TCH(n_{TCH},k_{TCH},t_{cap}) = \sum_{i=1}^{h} Pi(x) \quad (1)$$

$$k_{TCH} = m + \log_2 h + 1 \quad (2)$$

The coding error correcting capacity, t_{cap}, is dependent on the minimum distance of a code, d_{min}, between any two polynomials, and H_d the Hamming distance between two polynomials:

$$d_{min} \geq 2t_{cap}+1 \quad (3)$$

$$d_{min} \leq H_d[P_i(x), \{P_j(x)^r\} \bmod n_{code}] \leq n_{code} - d_{min} \quad (4)$$

In order to generate TCH codes it is required to find polynomials $P_i(x)$ with length n_{TCH} whose coefficients a_i, $i=0, 1, \ldots, n_{TCH}-1$, are from a Galois Field, GF(2). Finite field theory allege that polynomials of degree n_{code} and coefficients of a Galois Field GF(q), where q is related to a prime number p through the equation, $q = p^{kTCH}$, being x a positive integer, can be field elements of GF(q) [3] by restricting the coefficients to GF(2). B-TCH polynomials can be created for all prime numbers p that obey:

$$p=n_{TCH}+1=2^m+1 \quad (5)$$

[3] also states that basic TCH polynomials can be described as:

$$P_i(x)= \sum_{i=0}^{\left(\frac{p-1}{2}\right)-1} a_i x^{K_i} \quad (6)$$

The exponent values of K_i verify that:

$$\alpha^{K_i}=1+\alpha^{2i+1},\ i=0,1,\ldots,\ \left(\frac{p-1}{2}\right)-1 \quad (7)$$

for any primitive root α of GF(q). Each of the existing α generates a different polynomial with $2n_{TCH}$ codewords, being the foundation for new TCH codes.

To obtain a better understanding on the use of TCH codes, it is important to make use of Fermat numbers. Fermat numbers are prime numbers that fulfill the condition in (8):

$$F_i=2^{2^i}+1,\ i \in \mathbb{N} \quad (8)$$

leading to a total of five values:

TABLE I

FERMAT NUMBERS FOR GENERATING TCH CODES

i	p	n_{TCH}
0	3	2
1	5	4
2	17	16
3	257	256
4	65537	65536

Source: [3 p. 54].

These values represent the five possible lengths of TCH Polynomials that can be created using the generator equation (8). These polynomials were named Basic TCH Base Polynomials (B-TCH).

[3] explains that TCH codes originated from B-TCH polynomials have good cross and auto-correlation. This proves to be a great advantage when using TCH codes of great size. When using such elevated code lengths, the correlation between sequences tends to resemble a Dirac impulse for larger values of n_{TCH}.

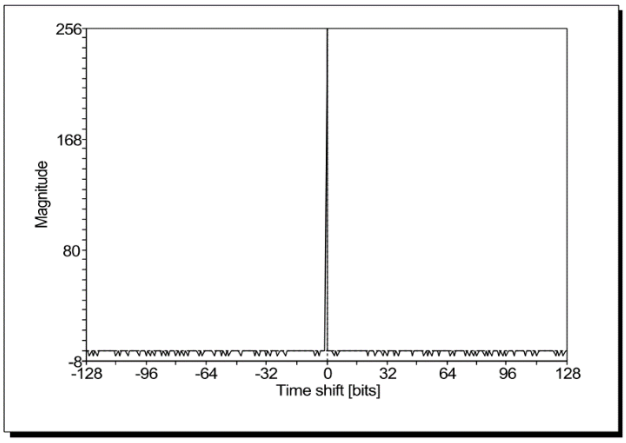

Fig. 1. Autocorrelation of B-TCH Polynomial of length n_{TCH}=256. Source: : [3, p. 71]).

While not exclusive to these codes, it is conceivable the determination of the code rate:

$$R_c=\frac{k_{TCH}}{n_{TCH}} \quad (9)$$

In [3], TCH codes have been used in a simple receiver implementation, based on a group of correlators, each of them comparing the received codeword. In a TCH (n_{TCH},k_{TCH}) code, the total number of codewords is $2^{k_{TCH}}=2n_{TCH}\cdot h$, where h is the number of correlators that can be implemented to verify the maximum likelihood. The sequence with higher correlation is the selected one.

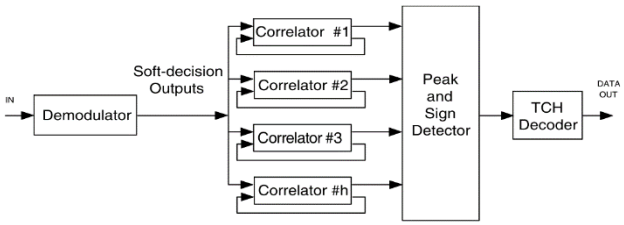

Fig. 2. TCH receiver simple implementation. Source: [3, p. 198].

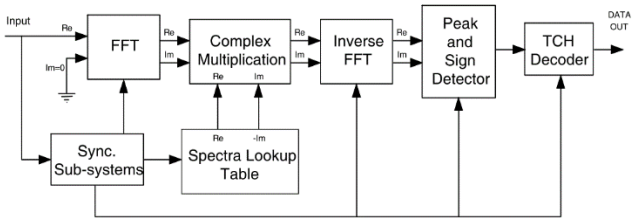

Fig. 3. Simple TCH decoder of maximum likelihood. Source: [3, p. 204].

III. ORTHOGONAL FREQUENCY DIVISION MULTIPLEXING

OFDM is part of a wider class of multicarrier modulation (MCM) in which the data is transmitted over several lower rate subcarriers. The greatest advantages of OFDM are its robustness against channel dispersion and simple phase and channel estimation in time-varying environments, but it also has its cons, like high peak-to-average power ratio (PAPR) and sensitivity to frequency and phase noise [4].

Considering *s(t)* as the MCM transmitted signal and considering the work in [4], it can be represented as:

$$s(t)=\sum_{i=-\infty}^{+\infty}\sum_{k=1}^{N_{sc}} c_{ki}s_k(t-iT_s) \quad (10)$$

$$s_k(t)=\prod(t)e^{j2\pi f_k t} \quad (11)$$

$$\prod(t)=\begin{cases}1, (0<t\leq T_s)\\ 0, (t\leq 0,\ t>T_s)\end{cases} \quad (12)$$

being c_{ki} the i^{th} information symbol at the k^{th} subcarrier, s_k the k^{th} subcarrier waveform, N_{sc} the number subcarriers, f_k the subcarrier's frequency, T_s the symbol period and $\prod(t)$ the pulse shaping function. Each subcarrier makes use of a filter that matches its waveform or a correlator that matches with its own. This results in an information symbol, c'_{ik}, where

$$c'_{ik}=\frac{1}{T_s}\int_0^{T_s} r(t-iT_s)s_k^* dt=\frac{1}{T_s}\int_0^{T_s} r(t-iT_s)\,e^{-j2\pi f_k t}dt \quad (13)$$

and $r(t)$ is the received time domain signal.

In [5] usage of overlapped orthogonal signal sets is employed to alleviate the bandwidth requirements. This orthogonality is demonstrated by:

$$\delta_{ki}=\frac{1}{T_s}\int_0^{T_s} s_k s_l^* dt=\frac{1}{T_s}e^{(j2\pi(f_k-f_l)t)}dt=$$
$$e^{(j\pi(f_k-f_l)T_s)}\frac{\sin(\pi(f_k-f_l)T_s)}{\pi(f_k-f_l)T_s} \quad (14)$$

If,

$$f_k-f_l=m\frac{1}{T_s} \quad (15)$$

is satisfied, then two subcarriers are orthogonal to each other. This means that these orthogonal subcarrier sets, with channel spacing being a multiple to the inverse of symbol periods, can be recovered by using matched filters without intercarrier interference (ICI).

According to [4], by re-denoting N_{sc} as N_{OFDM}, focusing on one OFDM symbol, and if $s(t)$ is sampled at every $\frac{T_s}{N_{OFDM}}$ interval, it can be deduced that:

$$s_m=\sum_{k=1}^{N} c_k\, e^{j2\pi f_k\frac{(m-1)T_s}{N_{OFDM}}} \quad (16)$$

By using (15) and the convention that

$$f_k=\frac{k-1}{T_s} \quad (17)$$

And by merging (17) into (16), the result is

$$s_m=\sum_{k=1}^{N} c_k\, e^{j2\pi\frac{(k-1)(m-1)}{N_{OFDM}}}=\mathfrak{F}^{-1}\{c_k\} \quad (18)$$

where $\mathfrak{F}$ is the Fourier transform and $m\in[1,N_{OFDM}]$.

As for the receiving end,

$$c'_k=\mathfrak{F}\{r_m\} \quad (19)$$

with r_m being the received signal, sampled at every $\frac{T_s}{N_{OFDM}}$ interval.

Through the implementation of both a digital-to-analog converter (DAC) and an analog-to-digital converter (ADC) and Discrete Fourier Transform/Inverse Discrete Fourier Transform (DFT/IDFT), it is feasible to greatly reduce the number of complex multiplications [6] and generate a high quantity of orthogonal subcarriers, allowing for simpler architectures.

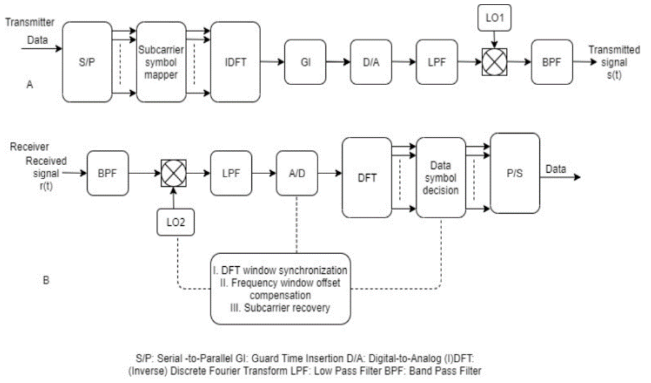

Fig. 4. OFDM transmitter (A) and Receiver (B) diagrams. Source: [5, p.35].

[5] affirms that, at the transmitter end, the inputted bits are converted into several parallel data pipes, all mapped onto corresponding information symbols within one OFDM symbol, the digital time domain signal is obtained through IDFT and the insertion of a guard interval is realized to prevent inter-symbol interference (ISI) that may originate from channel dispersion. The baseband signal can then be upconverted to an RF passband using an In-phase/Quadrature (IQ) modulator. As for the receiving end, a similar process occurs but reversed, the signal is down converted to baseband with an IQ demodulator, sampled using an ADC and demodulated using DFT, thus recovering the transmitted data through signal processing.

Another important aspect related to this technology is the insertion of a cyclic prefix (CP). Intending to solve delay related issues associated with the transmission of OFDM signals undergoing dispersive channels, [7] suggested the implementation of a cyclic prefix, defining a guard interval, Δ_G, whose waveform is an identical copy.

It is possible to determine the condition for ISI-free OFDM transmission, that condition being:

$$t_d<\Delta_G \quad (20)$$

with t_d being a delay spread for a given dispersive channel.

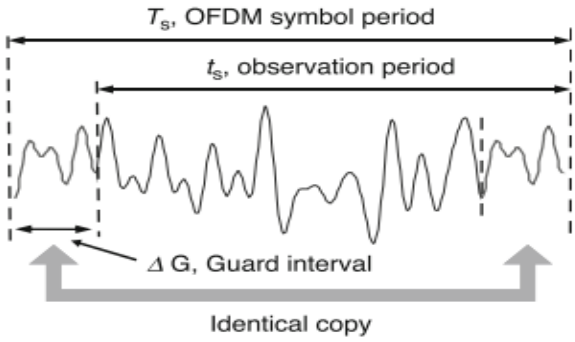

Fig. 5 Time domain representation of an OFDM symbol. Source: [5, p. 38].

To evaluate the cyclic prefix, it can be made use of (21) to describe the guard interval:

$$\prod(t)=\begin{cases} 1, (-\Delta_G<t\leq t_s) \\ 0, (t\leq-\Delta_G,\ t>t_s) \end{cases} \quad (21)$$

IV. System Model

This section explains and describes the processes that occur to a signal during the simulation.

A. Transmitter

To encode the signal by means of TCH encoding, some inherent parameters must be described. It is expected to realize the encoding by utilizing various code lengths, which means different values of n_{TCH}. The values considered for the codeword length n_{TCH} are 16, 32, 64, 128 and 256, each having corresponding polynomials. The codes used in the simulation are:

- TCH(16,6,2)
- TCH(32,6,6)
- TCH(64,7,13)
- TCH(128,9,27)
- TCH(256,9,62)

The purpose of the encoder based on TCH codes is to take groups of k_{TCH} bits from the generated bitstream and convert them into codewords size n_{TCH}. To accomplish this, a polynomial is selected according to the intended codeword length, by using this polynomial, the number of circular shifts to be applied to a codeword is determined.

After coding the original bitstream into several codewords, the next step is the modulation process. To perform modulation, firstly QAM mapping is considered. After the obtention of the coded bitstream resulting from TCH encoding, this step takes said bitstream and creates groups of bits to form QAM symbols with the purpose of accommodating higher transfer rates, typical in OFDM technologies.

The next step to analyze is the introduction of samples. Sampling is a method that enables the reduction of the continuous-time signal to a discrete-time one, it serves has the interface between real and simulated systems. The aim of this method is to allow a reliable representation of a real signal after it is processed through different blocks.

Pilot Symbol Aided Modulation (PSAM) is used in to define some already established subcarriers as pilot subcarriers. An interval between subcarriers of equivalent value is defined with the intent of determining which subcarriers will therefore be selected for the channel estimation to retrieve the original signal with as few errors as possible. After the pilots are established, the signal goes through a Serial to Parallel conversion where the contents are formatted into word size and then parallelly assigned to a carrier. To create some space between sampling-originated spectrum repetitions, zero padding is realized to introduce oversampling null carriers in the frequency domain. This is followed by the application of an IFFT to the signal because the remaining modulation steps occur in the time domain [8]. Then, the insertion of the cyclic prefix follows. The insertion of the cyclic prefix is, in fact, the addition of a copy of the final part of the given OFDM symbol to the beginning of said symbol. This process is followed by a DAC.

Fig. 6 illustrates the resulting Power Spectral Density (PSD) of the signal after Parallel to Serial Conversion.

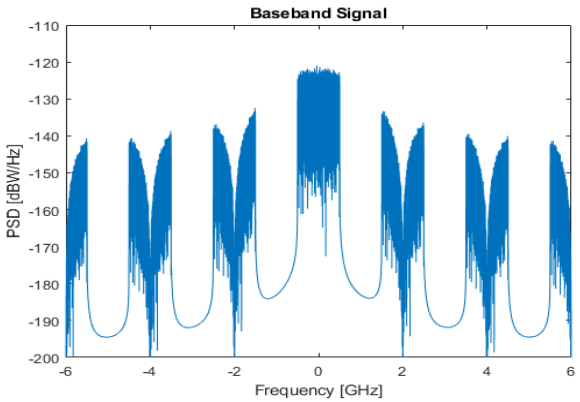

Fig. 6 Power spectral density of the signal after going through the modulation steps.

One way of suppressing the unwanted features in the signal is through usage of filters. Filters serve as a way of removing some components that manifest in certain frequency ranges, allowing the selection of a band that aligns with the goal of the simulation. In this work, the type of low pass filter (LPF) selected, which is a filter that allows the passage of frequencies lower than a given limiter called cutoff frequency, is an ideal rectangular filter. To realize filtering on the signal, it is required the obtention of the transfer function of the filter to be applied to the signal, this can be done through a convolution in time domain or a multiplication in frequency domain.

$$x_{LPF}(t)=IFFT(FFT(x_{DAC}(t))\times H_{rect}) \quad (22)$$

Since the filter is created in the frequency domain, and by obtaining the transfer function H_{rect}, to apply said function to the signal that is in time domain x_{DAC}, which is the signal that resulted from previous steps, a FFT is used to transfer it to frequency domain and, right after, an IFFT reverts the resulting filtered signal $x_{LPF}(t)$ back to time domain.

By defining a filter that has bandwidth B_{LPF} of 1 GHz, the filtered signal will be limited ranging from $-B_{LPF}$ to B_{LPF}.

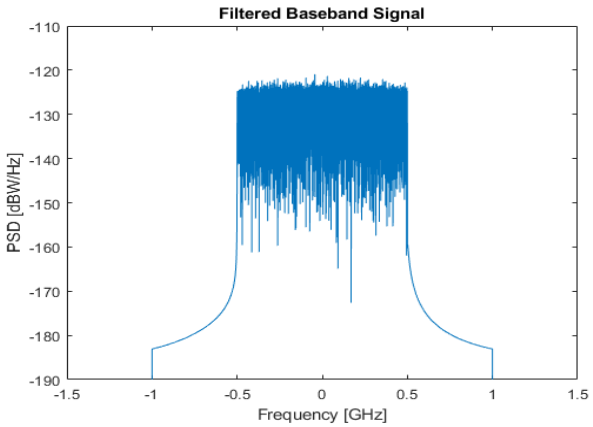

Fig. 7 Power spectral density of the signal after filtering with filter bandwidth *B*.

The final step that is fulfilled before transmission of the signal is the carrier up conversion. Being a heterodyning technique, up conversion is used to shift the frequency range of the signal into another. Since a LPF was used in this simulation and it is intended to shift the signal that resulted from that step, a low pass equivalent (LPE) representation is used. The aim of this representation is to translocate the current signal that is centered at 0 GHz in frequency domain to the nominal frequency f_p. This means that the signal is dislocated to the frequency ranges $-f_p - B$ to $-f_p + B$ and $f_p - B$ to $f_p + B$.

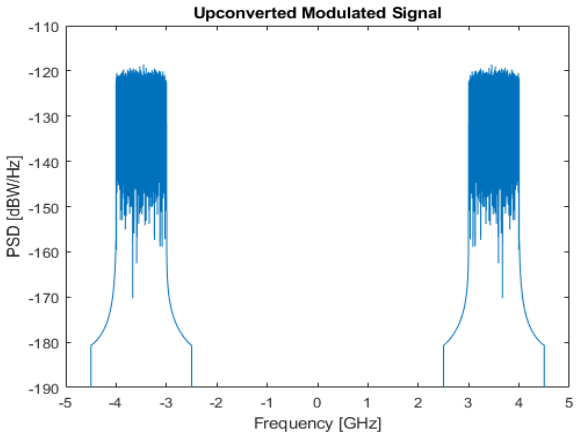

Fig. 8 Power spectral density of the signal after up-conversion.

B. Wireless Channel

The implementation of an AWGN channel translates into generating random gaussian coefficients with null mean and average power of 1 [8] that are later added to the signal. These coefficients however are dependent on the unilateral noise PSD, N_0. To obtain this PSD through the signal to noise ratio, it can be deduced that,

$$snr = \frac{p_{signal}}{p_{noise}} = \frac{p_{signal}}{N_0 B_{en}} \tag{23}$$

since the PSD here represented is bilateral, then

$$N_0 = \frac{p_{signal}}{snr \times \frac{B_{en}}{2}} \tag{24}$$

being p_{signal} the mean power of the baseband signal, *snr* the signal to noise ratio and B_{en} the equivalent noise band.

The noise signal is created through generation of a vector of random coefficients $rand_{coeff}$, and by using the sampling frequency f_s,

$$n_{AWGN}(t) = \sqrt{N_0 f_s} \times rand_{coeff} \tag{25}$$

Resulting in,

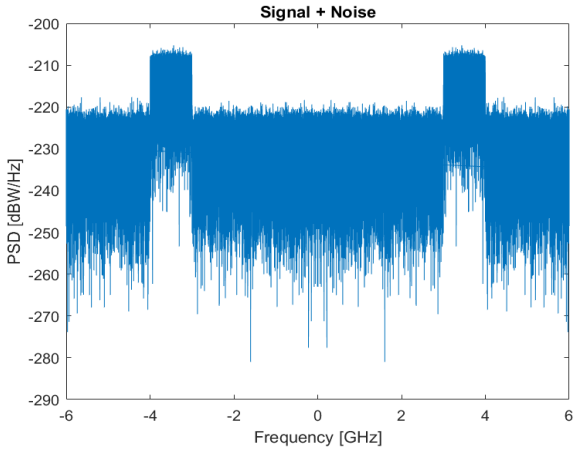

Fig. 9 Power spectral density of the signal after passing through the wireless channel.

C. Receiver

In contrast with the transmission, the receiver aims to recover the original generated signal by applying the inverse methodology. By using down conversion, the received signal, is restored back into baseband form. After this process and synchronizing the signal, the result is shown in Fig. 10.

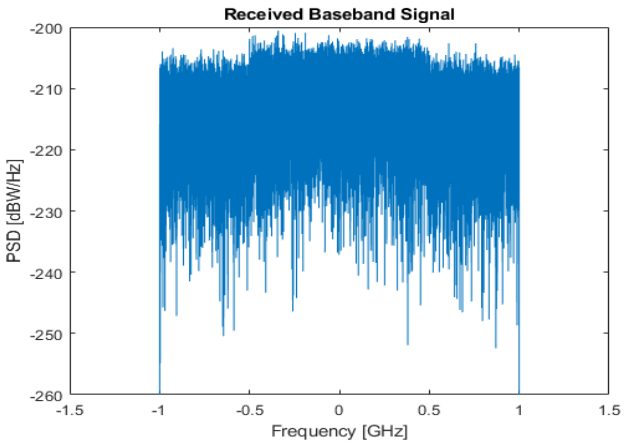

Fig. 10 Power spectral density of the down converted signal

This corresponds to the transmitted modulated baseband signal; however, the recovered signal also has a noise component added to it due to the influence of the wireless AWGN channel.

The demodulation process, like the modulation one, intends to work at OFDM symbol/block level, meaning that the OFDM symbols are demodulated in a sequential manner. That said, the process begins with serial to parallel conversion. After obtention of the OFDM symbols, ADC is realized by extracting the middle sample amidst the groups of samples in a chip. This is followed by the removal of the CP, which consists in the elimination of the copy of the final part of the OFDM symbol that was inserted in the beginning of it.

To complete the demodulation, it is needed to remove the zero padding that was performed during modulation, which is the removal of the oversampling null carriers.

There is also the need to estimate the effects of the channel to allow an elevated trust factor when recovering the signal. This can be made by utilizing the pilots added in the modulation process. As [8] states, the effects of pilot transmission are calculated through obtention of the quotient of both the amplitude and phase of the received and original pilots.

The equalization technique used in this simulation is the Zero-Forcing (ZF) method, which is the inverse of the transfer function of the channel $H_{ch}(f)$:

$$H_{ZF}(f) = \frac{1}{H_{ch}(f)} \tag{26}$$

Through this function, the amplitude and phase responses are obtained to be used in the interpolating process as a means of inferring the location of the QAM symbols. After their obtention, hard decision is employed to demap the symbols back into their binary counterpart.

The last part of the recovery of the signal is the decoding process. By taking the result from the demodulation, all that is left is to turn the coded bitstream back into the original bitstream. The TCH decoding process is based on a bank of correlators that compare a received codeword length n_{TCH} with the various codewords that result from shifting cyclically a single TCH polynomial and its inverse. The output is compared to the largest value and then decoded by implementing a straightforward conversion table containing the stored codewords complex conjugate of their spectra, use of a FFT, a complex multiplication and an IFFT.

V. Results

The best results obtained through simulation were for the modulation indexes of 16, 64 and 256-QAM. However, due to an undetermined reason, the resulting curves for the TCH code length 16 do not show the expected behavior.

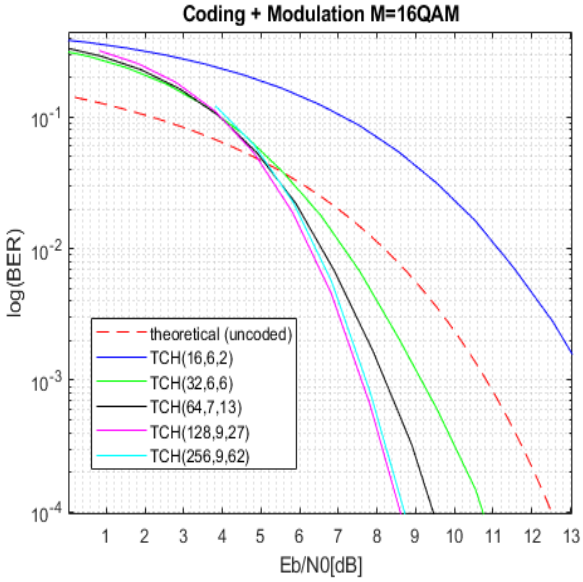

Fig. 11 BER results in function of $\frac{E_b}{N_0}$ for the 16-QAM with TCH codes.

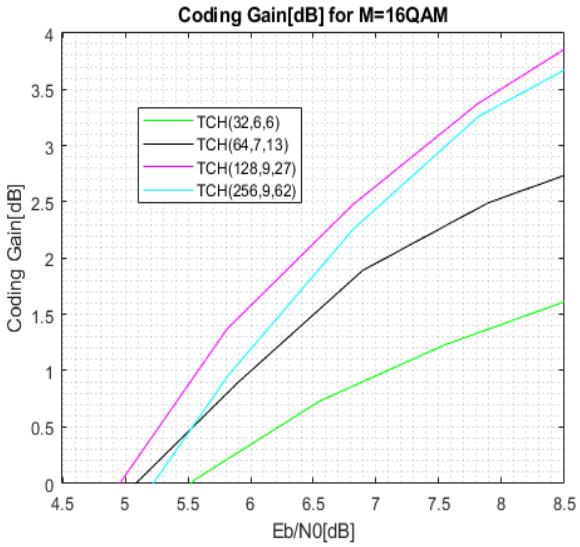

Fig. 12 Coding gain results in function of $\frac{E_b}{N_0}$ for the 16-QAM with TCH codes.

TABLE II

SIMULATED CODING GAINS FOR EACH TCH CODE LENGTH FOR 16-QAM

TCH Codes	$\frac{E_b}{N_0}$**[dB]** **@**$\log_{10} BER = 10^{-4}$	**Coding gain@8.5 dB**
TCH(32,6,6)	10.8	1.6
TCH(64,7,13)	9.5	2.7
TCH(128,9,27)	8.6	3.8
TCH(256,9,62)	8.7	3.7

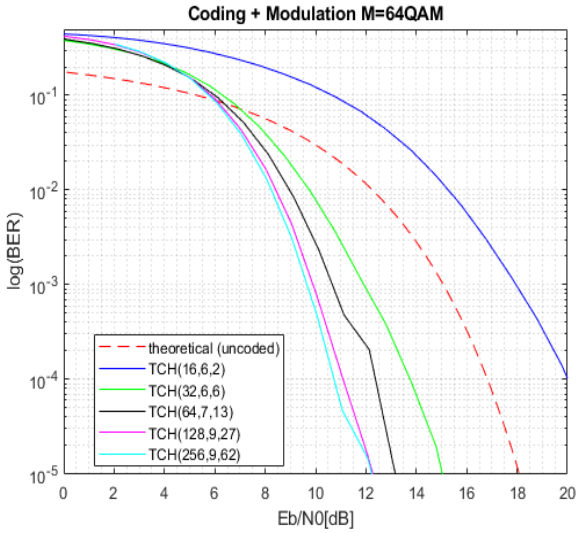

Fig. 13 BER results in function of $\frac{E_b}{N_0}$ for the 64-QAM with TCH codes.

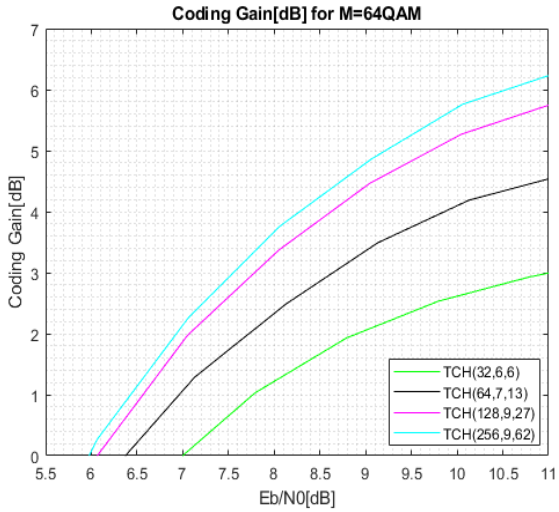

Fig. 14 Coding gain results in function of $\frac{E_b}{N_0}$ for the 64-QAM with TCH codes.

TABLE III

SIMULATED CODING GAINS FOR EACH TCH CODE LENGTH FOR 64-QAM

TCH Codes	$\frac{E_b}{N_0}$**[dB]** $@\log_{10} BER = 10^{-5}$	**Coding gain@11 dB**
TCH(32,6,6)	15.0	3.0
TCH(64,7,13)	13.0	4.5
TCH(128,9,27)	12.5	5.8
TCH(256,9,62)	12.5	6.2

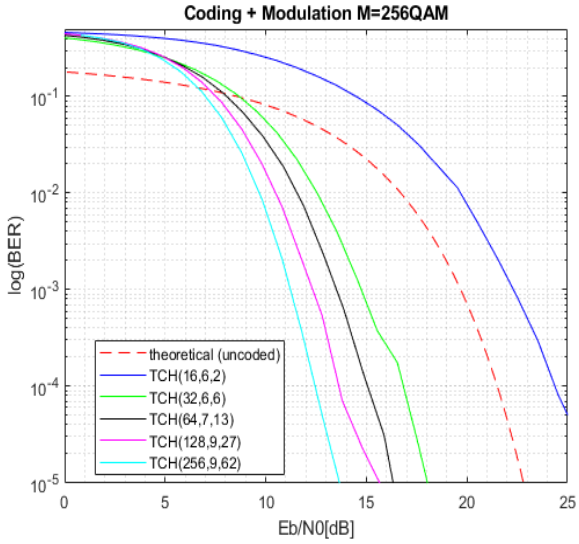

Fig. 15 BER results in function of $\frac{E_b}{N_0}$ for the 256-QAM with TCH codes.

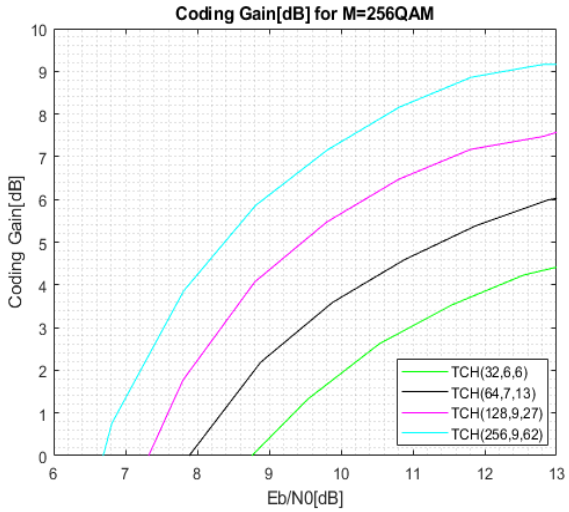

Fig. 16 Coding gain results in function of $\frac{E_b}{N_0}$ for the 256-QAM with TCH codes.

TABLE IV

SIMULATED CODING GAINS FOR EACH TCH CODE LENGTH FOR 256-QAM

TCH Codes	$\frac{E_b}{N_0}$**[dB]** $@\log_{10} BER = 10^{-5}$	**Coding gain@13 dB**
TCH(32,6,6)	18.0	4.6
TCH(64,7,13)	16.5	6.0
TCH(128,9,27)	16.0	7.6
TCH(256,9,62)	13.5	9.2

VI. CONCLUSIONS

Through analysis of the results, it can be inferred that the application of TCH codes to an OFDM signal, especially to higher modulation indexes, seems to be a viable way of improving the reception of said signal. Since higher modulation indexes generate more symbols, these, when grouped and placed in accordance with their corresponding constellation mapping, the spacing between them is reduced, leading to a higher occurrence of erred bits recovered. This means that the implementation of the TCH codes is a viable solution to reduce the erred bits recover rate, especially when applying codes of increased length since these have higher correcting capacities, therefore leading to higher coding gains, minding that lower $\frac{E_b}{N_0}$ values are required to obtain the same $log_{10} BER$.

It is concluded that the employment of TCH codes on RF signals, more specifically, paired with OFDM signals used in broadband communications, is a good method of improving the quality of the received signal. This aspect leads to the belief that the use of TCH codes appears to be advantageous in similar applications and IoT environments.

REFERENCES

[1] A. Ijaz et al., “Enabling Massive IoT in 5G and beyond Systems: PHY Radio Frame Design Considerations,” IEEE Access, vol. 4, pp. 3322–3339, 2016.

[2] M. S. Alouini, “Paving the way towards 5G wireless communication networks,” pp. 1–1, 2018.

[3] F. A. B. Cercas, “A new family of codes for simple receiver implementation,” Ph. D. Thesis, Technical University of Lisbon, Instituto Superior Técnico, Lisbon, 1996.

[4] W. Shieh and I. Djordjevic, Orthogonal Frequency Division Multiplexing for Optical Communications. Elsevier Science Publishing Co Inc, 2010.

[5] J. M. Tang , P. M. Lane and K. A. Shore, High-speed transmission of adaptively modulated optical OFDM signals over multimode fibers using directly modulated DFBs. J Lightwave Technol 2006;24:429–41.

[6] P. Duhamel and H. Hollmann, Split-radix FFT algorithm. IET Elect Lett 1984;20:14–6.

[7] S. Hara and R. Prasad, Multicarrier Techniques for 4G Mobile Communications. Boston: Artech House; 2003.

[8] D. Mendes, “Study and Implementation of an Advanced Transceiver for 5G”. October, 2019.